An Investigation of the Mechanical and Physical Properties of Copper-Silver Alloys and the Use of These Alloys in Pre-Columbian America

by

Shannon L. Taylor

Submitted to the
Department of Materials Science and Engineering
in Partial Fulfillment of the Requirements
for the Degree of

Bachelor of Science

at the

Massachusetts Institute of Technology

June 2013

Signature of Author: _____
Department of Materials Science and Engineering
May 3, 2013

Certified by: _____
Heather Lechtman
Professor of Archaeology and Ancient Technology
Thesis Supervisor

Accepted by: _____
Jeffrey Grossman
Carl Richard Soderberg Associate Professor of Power Engineering
Chair, Undergraduate Committee

An Investigation of the Mechanical and Physical Properties of Copper-Silver Alloys and the Use of These Alloys in Pre-Columbian America

by

Shannon L. Taylor

Submitted to the Department of Materials Science and Engineering
on May 3, 2013 in Partial Fulfillment of the Requirements
for the Degree of Bachelor of Science in
Archaeology and Materials

ABSTRACT

In both the Andean zone of South America and in Mesoamerica, copper-silver alloys were important in the production of thin, silver-colored sheet metal artifacts. This thesis examines the mechanical and physical properties of the copper-silver alloy system that are important to understanding why copper-silver alloys became central to the metallurgies that developed among prehistoric societies of the Andean zone and Western Mexico. These properties include their range of malleability, the microstructures behind their toughness, and the recrystallization and annealing behaviors that led to their development of silver-enriched surfaces.

To determine these properties, a series of cold rolling, cold hammering, and annealing experiments were performed on five Cu-Ag alloys and pure copper. Results of the cold rolling and cold hammering experiments reported here indicate that over the copper-silver alloy compositional range studied, the alloys can be cold rolled without annealing to over 90% reduction in thickness. Similar reductions in thickness were also achieved in two alloys (95 wt% Cu – 5 wt% Ag and 30 wt% Cu – 70 wt% Ag) by cold hammering. The rate of work hardening and the Vickers Hardness Number, as functions of the percent reduction in thickness, are similar for alloy compositions containing between 30 wt% and 80 wt% Cu. This suggests that ancient metalsmiths likely annealed the copper-silver alloy artifacts intentionally to produce the desired silver surface color rather than for any improvement in malleability. The silver surface colors were important for their cultural associations. The recrystallization temperature for the copper-silver alloys tested (70 wt% Cu – 30 wt% Ag and 30 wt% Cu – 70 wt% Ag) is determined to be 500ºC given a 30 minute anneal time.

Thesis Supervisor: Professor Heather Lechtman
Title: Professor of Archaeology and Ancient Technology

Table of Contents

1 List of Figures

2 List of Tables

3 Introduction

This thesis determines the mechanical and physical properties of the copper-silver alloy system that are important to understanding why copper-silver alloys became central to the metallurgies that developed among prehistoric societies of the Andean zone of South America and western Mexico. These properties include their range of malleability, the microstructures behind their toughness, and the recrystallization and annealing behaviors that led to their development of silver-enriched surfaces.

Metallurgy has played an important role in the cultural, economic, and political development of civilizations throughout the world. Two metallurgical centers or heartlands of metallurgy developed independently of each other, one in the Old World, in Southwest Asia (the Near East), the other in the New World, the Andean zone of South America (Lechtman in press). Figure 1 shows what anthropologists refer to as the Andean culture area, which is coincident with the territory that comprised the Inka empire in the early decades of the 16th century. The Andean zone, located on the western edge of the South American continent, covers regions occupied by the modern nations of Colombia, Ecuador, Peru, Bolivia, Chile and Argentina. The Andean heartland of metallurgy is considered to have developed in the northern reaches of what is today Peru.

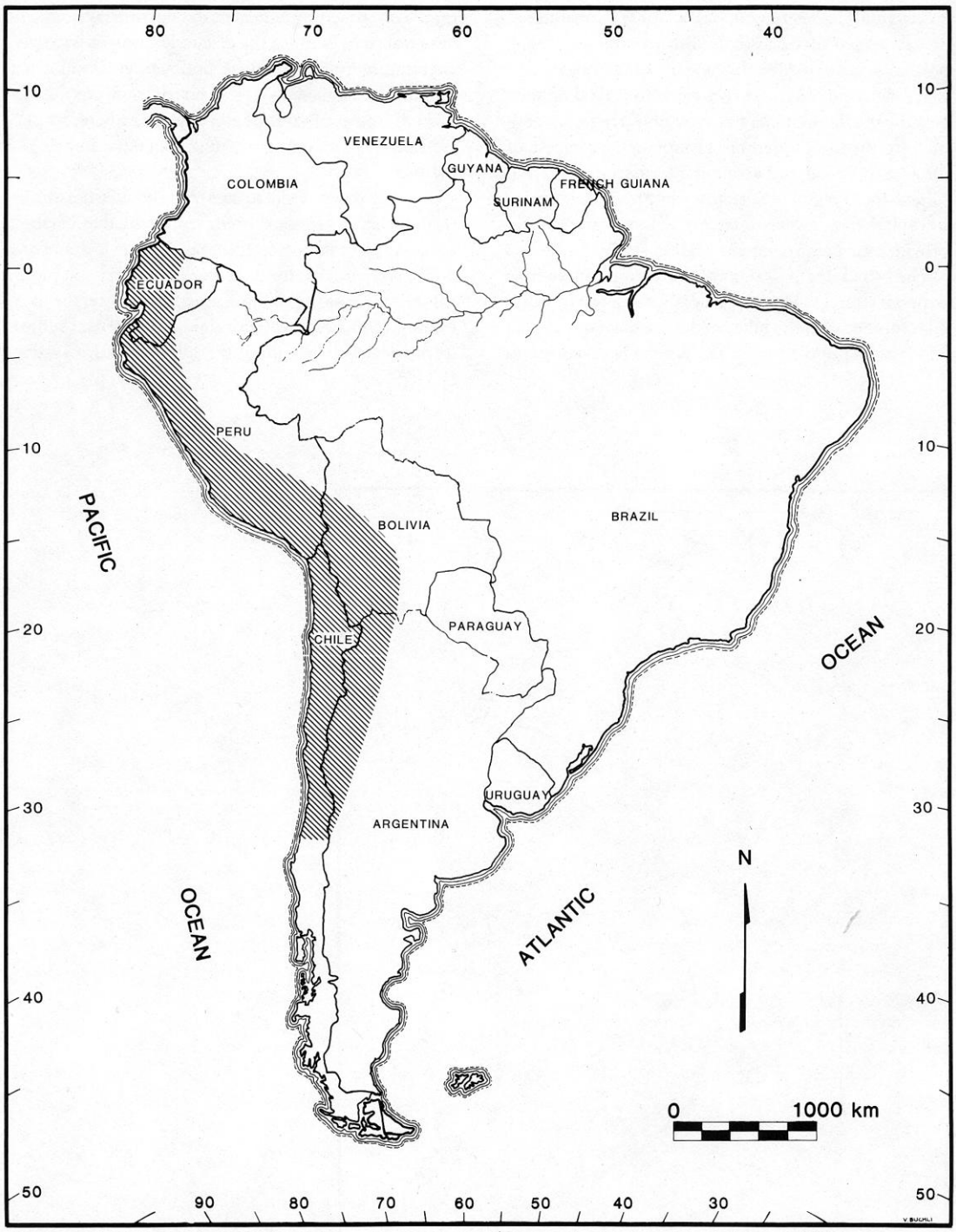

Figure 1. Map of South America. The Andean culture area, coincident with the maximum extent of the Inka empire (hatched region on map) is located on the western edge of South America and covers territory occupied by the modern nations of Colombia, Ecuador, Peru, Bolivia, Chile and Argentina. (after D'Altroy 1992: Figure 1.1)

From the Andean zone, the metallurgical tradition spread, via a maritime route as indicated in Figure 2, to the region anthropologists refer to as Mesoamerica, which encompasses central and southern Mexico, Guatemala, Belize, western Honduras, and El Salvador (Dewan and Hosler 2008; Hosler 1994). This transfer of technological knowledge led to the development of a copper-based metallurgical tradition in western Mexico between A.D. 800 and the 16th century when the Spaniards invaded and conquered the Aztec state (Hosler 1988, 1994). Figure 3 locates the metalworking zone of western Mexico.

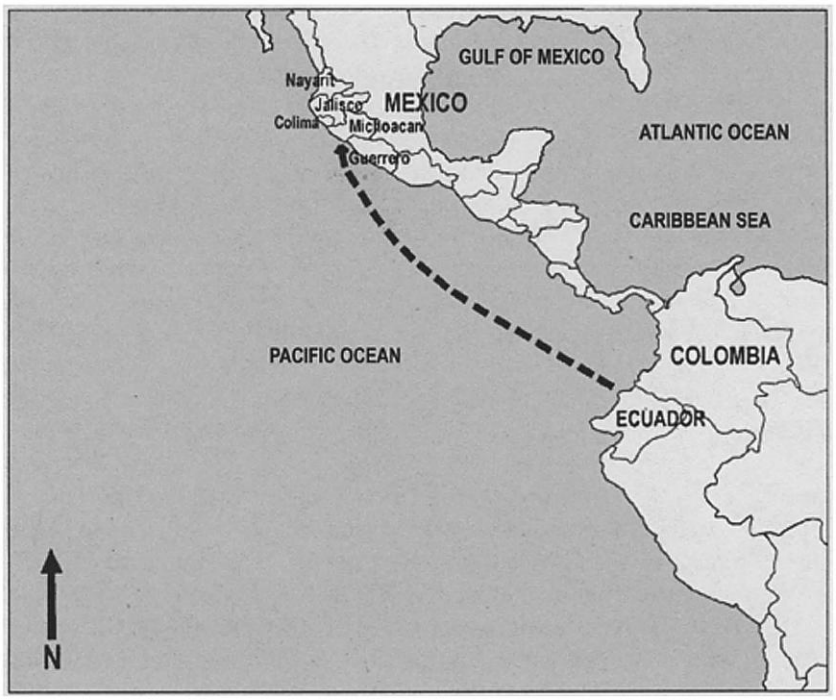

Figure 2. Possible maritime transmission route of metallurgical technology from the Andean zone to West Mexico, via balsa raft. (after Dewan and Hosler 2008: Figure 1)

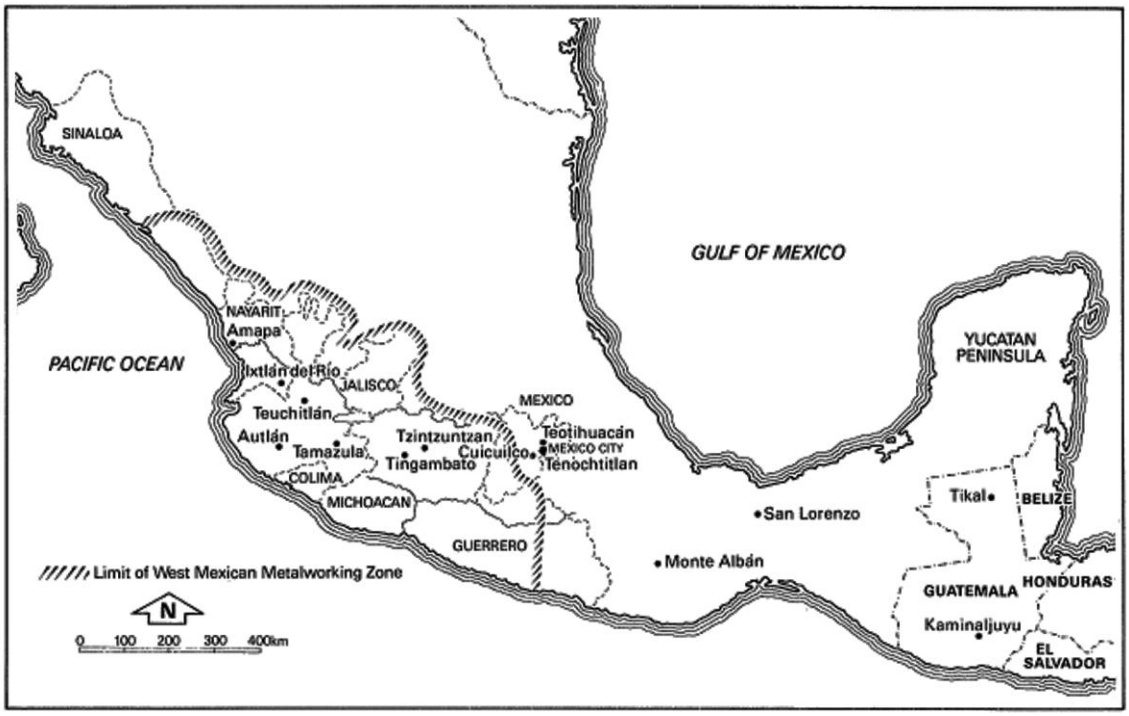

Figure 3. Map of Mesoamerica showing archaeological sites, the state boundaries within Western Mexico, and the limits of the West Mexican metal-working zone. (after Hosler 1995: Figure 1)

In western Mexico, metal was managed in the liquid state in order to shape it, and most objects were cast to achieve their final shapes. Some hammered metal artifacts have been found in West Mexico and include sheet metal objects made of copper-silver alloys (Hosler 1994, 1988). In the Andes, metal was managed in the solid state, and most objects were plastically deformed by hammering to achieve their final shapes (Lechtman 1988). At Chan Chan, a large urban site on the north coast of Peru (ca. A.D. 1100 – 1470), a set of metalworker's tools, shown in Figure 4, made from fine-grained metamorphic rock, was excavated by John Topic (John Topic, personal communication). Objects made of pure elements, such as native copper, silver, or gold, as well as alloys of two or more of these metals have been found in the archaeological record in both the Andes and Mesoamerica.

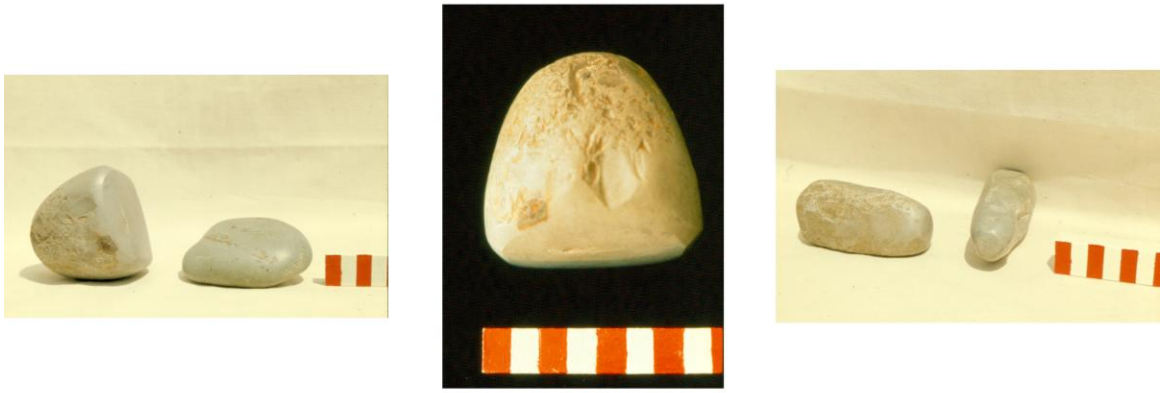

Figure 4. A set of stone metalsmithing tools made of fine-grained metamorphic rock excavated at Chan Chan, Peru: (a) anvil with flat planishing stone, (b) large, heavy stone hammer, (c) two small stone hammers, highly polished. (courtesy of Heather Lechtman and John Topic)

The earliest known alloy developed in the Andes is that of copper and silver (Lechtman 1979b, 1984a, 1984b). The copper-silver alloy was utilized for its unusually high degree of malleability and its toughness, developed during hammering. Equally important to the Andean metalsmiths were the silver-enriched surfaces that developed on the alloy surfaces after hammering and annealing (Lechtman 1984a, 1984b, 1988, 2007). The high malleability and subsequent toughening of copper-silver alloys during hammering allowed metalsmiths to produce objects made from very thin sheet metal such as the copper-silver plaques shown in Figure 5.

Figure 5. Two copper-silver alloy plaques from the north coast of Peru. The holes may have been used to attach the plaques to a wall as sheathing. (after Lothrop, Foshag and Mahler 1959: Plate CXXXIX)

The earliest copper-silver object found thus far in the Andean zone is a small bead (see Figure 6) from Malpaso, a coastal site in the Lurín Valley of Peru dating to about 1000 B.C. (Lechtman 1979b).

Figure 6. Bead made of hammered copper-silver alloy sheet from Malpaso, Lurín Valley, Peru. The bead measures approximately 20 mm in length with a maximum diameter of 6 mm. The sheet metal is about 0.15 mm thick. The chemical composition of the bead is about 41 wt% Cu – 45 wt% Ag (given approximately a 15% loss of metal due to corrosion). (after Lechtman 1979b: Figure 6)

In addition to flat sheet metal objects made from copper-silver alloys, Andean metalsmiths produced more complex geometries from one or more pieces of sheet that were joined by mechanical or metallurgical means (i.e. soldering or welding). Figure 7 shows a silver-colored Chimú (ca. 13th century A.D.) cup made of copper-silver alloy sheet. The cup was formed by crimping together two shaped pieces of copper-silver sheet: the sheet that forms the bottom of the cup and the sheet that forms the cylindrical wall of the cup (see Figure 8).

Figure 7. Cup made of copper-silver alloy sheet from the Chimú culture, Peru (Late Intermediate Period: A.D. 1000 to 1476). The cup is silver in color and was formed by mechanically crimping the edges of a circular sheet that formed the vessel bottom over and onto the circular perimeter of the base of the cylindrical vessel wall (see Figure 8). (after Lechtman 1988: Figure 30.21)

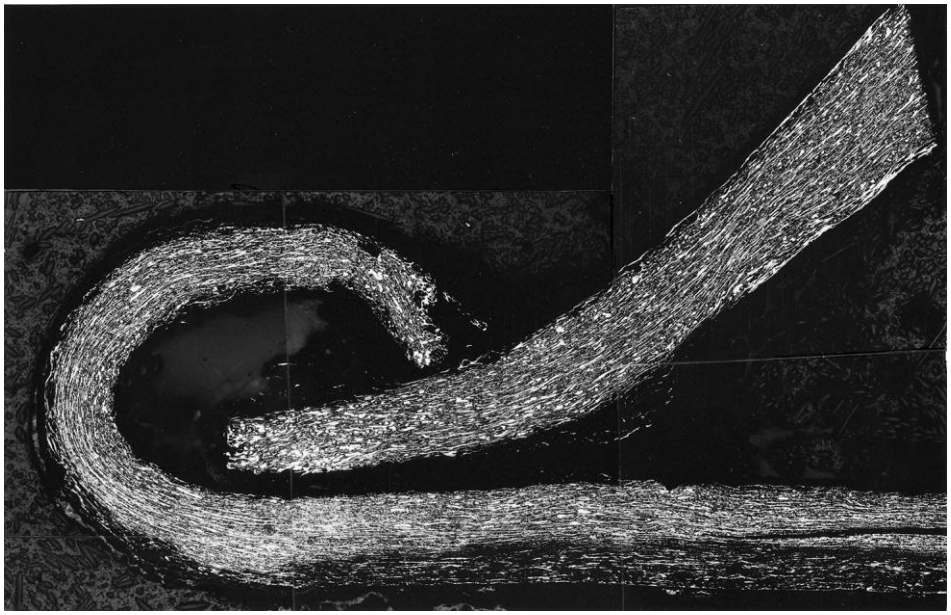

Figure 8. Photomicrograph of a cross section removed from the bottom and lower vessel wall of the copper-silver cup shown in Figure 7. The two sheets of metal were mechanically joined by crimping. In the upper right corner, the silver-enriched surfaces of the cylindrical vessel wall are visible along both edges of the sheet. MAG: 50; Etchant: Potassium dichromate and hydrochloric acid. (courtesy of Heather Lechtman)

A 1975 study by Lechtman, Parsons and Young provides evidence of the use of copper-silver alloys as solders in the assembly of thin, hammered gold sheets to produce small, hollow jaguar figurines. These early solder alloys were developed by Moche metalsmiths working at north coast Peruvian centers at about A.D 300 to 500.

4 Previous Research

4.1 Properties of Cu-Ag Alloys Based on Analysis of Andean Archaeological Artifacts

4.1.1 Composition of Cu-Ag Alloy Artifacts

The artifacts found in both the Andes and Mesoamerica made from Cu-Ag alloys span a wide range of chemical compositions. A compilation of many of the known Cu-Ag alloy artifacts whose compositions have been determined can be found in Appendix A.

A 1949 study by William Root classifies south coast, Late Intermediate Period (ca. A.D. 1100 – 1450) Peruvian artifacts made from copper-silver alloys into two categories: artifacts containing less than 20 wt% Cu (Type A) and artifacts containing more than 20 wt% Cu (Type B). Of the 67 Cu-Ag alloy artifacts analyzed in Root's study 55 are Type A and 12 are Type B. The Type B artifacts generally belong to the later Ica and Chincha cultures. The Ica culture occupied the Ica Valley on the southern coast of Peru from about A.D. 900 to 1476 (Silverman 1993). The Chincha culture also occupied the southern coast of Peru, but was farther north than the Ica, from about A.D. 1150 to 1476 (Menzel 1976). The Inka conquered the southern coast of Peru in A.D. 1476 (Menzel 1976).

Based on Root's work it appears that metalsmiths of the southern coast of Peru may have had a preference for high-silver content alloys, while the work of several other Andean scholars presents a broader compositional range of artifacts from northern Peru and Ecuador (Gordon and Knopf 2007; Hörz and Kallfass 2000; Lechtman 1979, 1988, 2007). For example, at the imperial Inka site Machu Picchu, the most commonly used copper-silver alloys contained 25-30 wt% silver (Gordon and Knopf 2007). A recent (2009) study carried out at the Center for Materials

Research in Archaeology and Ethnology (CMRAE) at MIT examined 16 metal artifacts from a cache excavated at an Inka fortress in the Pambamarca mountains, north of Quito, Ecuador. The fortress was built by the Inka in the early 1500s A.D. as they expanded their northern frontier into the territory of the Cayambe peoples in Ecuador. Of eleven artifacts analyzed for their composition, four are made of Cu-Ag alloys. One of these four utilizes a Cu-Ag alloy solder to join two copper members. The alloy compositions are presented in Table 1.

Table 1. Compositions of Four Metal Artifacts from Pambamarca, Ecuador (Analyses courtesy of Heather Lechtman)

Artifact	**MIT ID No.**	**Composition (wt%)**		
		Cu	**Ag**	**Sn**
tumi knife (?)	5433	96.2	3.8	–
bent rod with conical sheet	5435	99.7	–	–
solder between rod and cone	5435	59	41	–
MIT 5430 pouring sprue and runners	5430	65.7	29.8	4.5
sheet disc	5431	76	24	–

It seems clear that by the era of the Inka empire, high-copper Cu-Ag alloys were in common use by north Andean metalsmiths and by smiths in the service of the Inka state.

In Mesoamerica, the work of Dorothy Hosler provides the majority of the chemical analyses determined for Cu-Ag artifacts in this region (1994). Of the 36 Cu-Ag artifacts analyzed, nine would be classified as Type A and 27 would be classified as Type B. Eleven

artifacts contain between 70 and 80 wt% Cu. Based on these data it appears that Mesoamerican metalsmiths may have had a preference for high-copper content Cu-Ag alloys.

4.1.2 Microstructure of Cu-Ag Alloy Artifacts

Depending on the initial composition of the molten metal the cast ingot or object will exhibit one of three possible microstructures: primary Ag-rich α-phase dendrites surrounded by the eutectic microconstituent, primary Cu-rich β-phase dendrites surrounded by the eutectic microconstituent, or grains comprised of 100% eutectic microconstituent. Figure 9 shows the Cu-Ag phase diagram and the compositional ranges for which these three different microstructures are present.

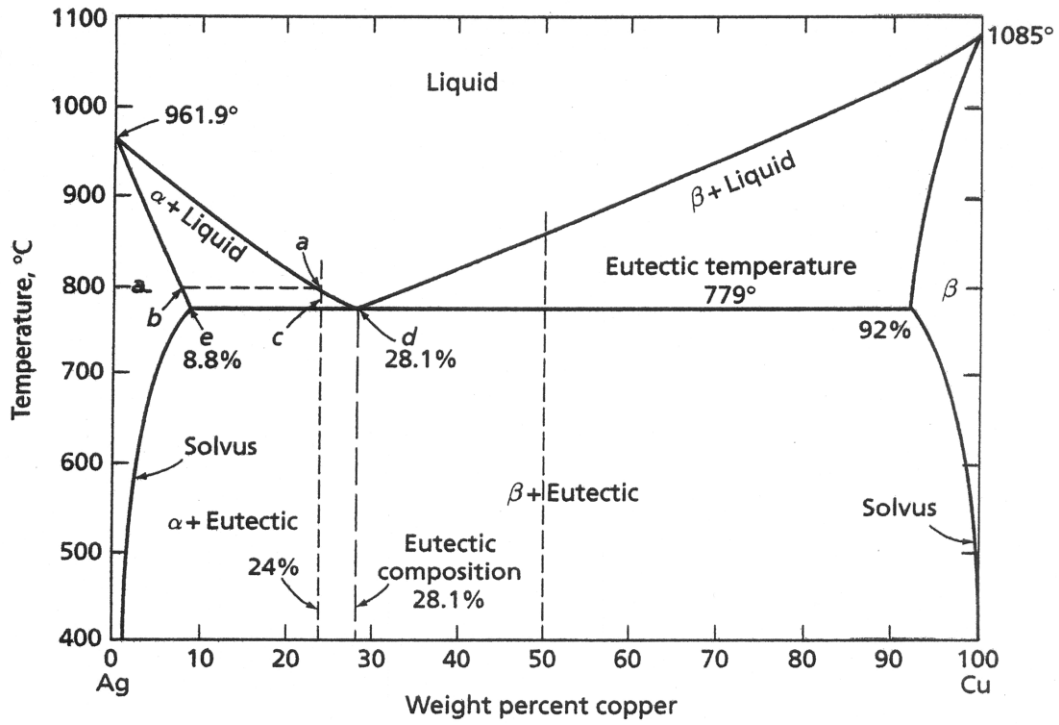

Figure 9. Cu-Ag Phase Diagram. The eutectic composition is 28.1 wt% Cu - 71.9 wt% Ag and the solid solubility limit of silver in copper is 8 wt% Ag (after Hansen and Anderko 1958: 18)

After smelting copper and silver from their respective ores, the ancient metalsmiths mixed alloy constituents in the desired ratios and melted them. The molten alloy was then poured into a mold and allowed to solidify. Figure 10 illustrates the cast Cu-Ag-Sn alloy sprue and runners from Pambamarca, Ecuador whose composition appears in Table 1 (MIT 5430).

Figure 10. Cast metal that solidified within a pouring sprue and runners excavated at Pambamarca, Ecuador. The concave upper surface, a result of the shrinkage of the molten metal upon solidification, and the two runners at the base indicate this artifact was the last metal to solidify when molten alloy was poured through a pouring sprue into a mold. The scale bar is in centimeters. (courtesy Heather Lechtman)

The molten alloy passed from the casting sprue through the runners into the mold. Upon solidification, the solid metal sprue and runners were cut from the mold but were not discarded. The alloy was precious enough to be saved and included in the cache of 16 artifacts buried at the Pambamarca fortress.

By the establishment of the Inka empire in the Andes at about A.D. 1450, the alloy of copper and silver had been used widely, including in Ecuadorian metallurgy, for approximately two millennia. The fact that 4.5 wt% tin was added to the alloy analyzed in the sprue-and-runner certifies that the alloy was produced among the Cayambe peoples after the Inka invasion of Ecuador. The single source of tin (cassiterite: SnO_2) in South America occurs in a rich and dense

ore field that runs from Bolivia through northwest Argentina. The Inka state controlled this vast tin source and disseminated tin or Cu-Sn bronze artifacts throughout the empire (Lechtman 1979b). The Ecuadorian metalsmiths likely added small amounts of tin, a new material for them, to their existing alloys not necessarily for any advantage to the alloy's properties but perhaps because tin was an imperial metal (Heather Lechtman, personal communication).

Figure 11 shows a photomicrograph of the cast microstructure of a section removed from one of the runners attached to the pouring sprue shown in Figure 10.

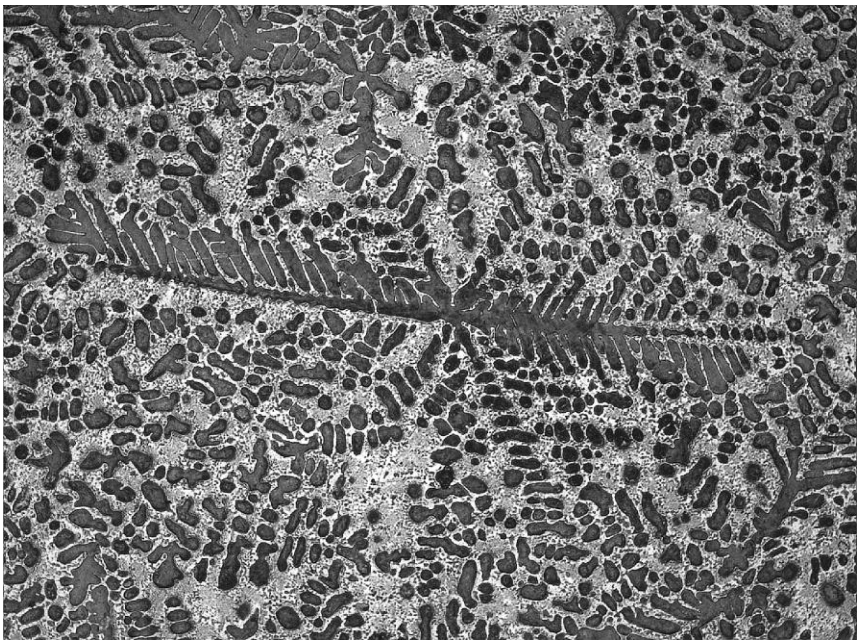

Figure 11. Etched photomicrograph of a section removed from a runner on the Ecuadorian casting shown in Figure 10. The Cu-rich β-phase dendrites are surrounded by eutectic microconstituent. MAG: 100; Etchant: 1:9 dilute potassium dichromate (courtesy Heather Lechtman)

Upon plastic deformation during hammering, the cast microstructure eventually develops thin, elongated lamellae of Ag-rich α-phase and Cu-rich β-phase material in which neither the original eutectic microconstituent nor the primary dendrites is discernible. The photomicrograph

in Figure 12 shows the heavily deformed microstructure of a cross section of metal removed from the copper-silver bead illustrated in Figure 6. Both the Ag-rich α-phase and Cu-rich β-phase lamellae are thin and highly elongated. This same heavy deformation and elongation of both the Ag-rich α-phase and Cu-rich β-phase lamellae is also visible in the thin sheet metal of the Chimú cup (see Figure 13).

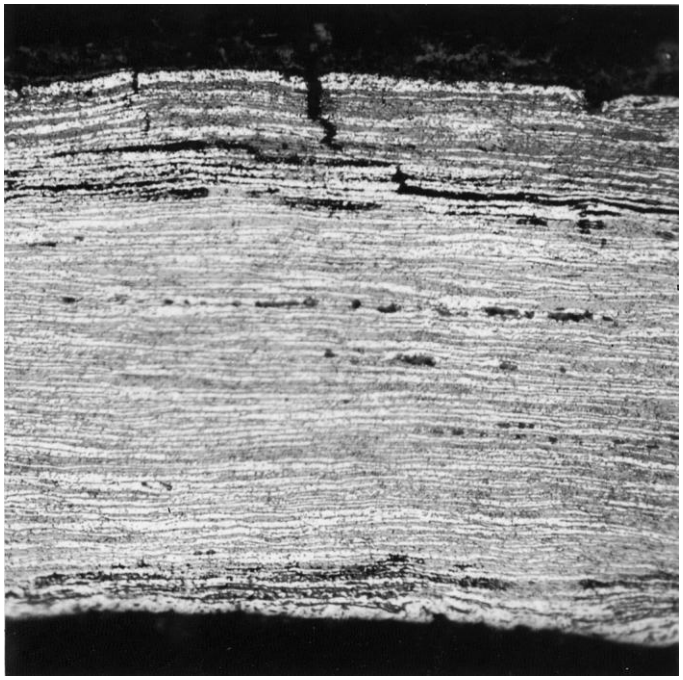

Figure 12. Photomicrograph of a cross section of metal removed from the copper-silver bead shown in Figure 6. Both the copper-rich β-phase (dark areas) and the silver-rich α-phase (light areas) have elongated in the direction of metal flow upon hammering. Both the upper and lower surfaces of the metal sheet exhibit silver enrichment. The cracks at the upper surface have been prevented from propagating through the sheet because of the presence of alternating lamellae. MAG: 500; Etchant: 0.2% $H_2Cr_2O_7$ + 0.2% H_2SO_4. (after Lechtman 1979b: Figure 7)

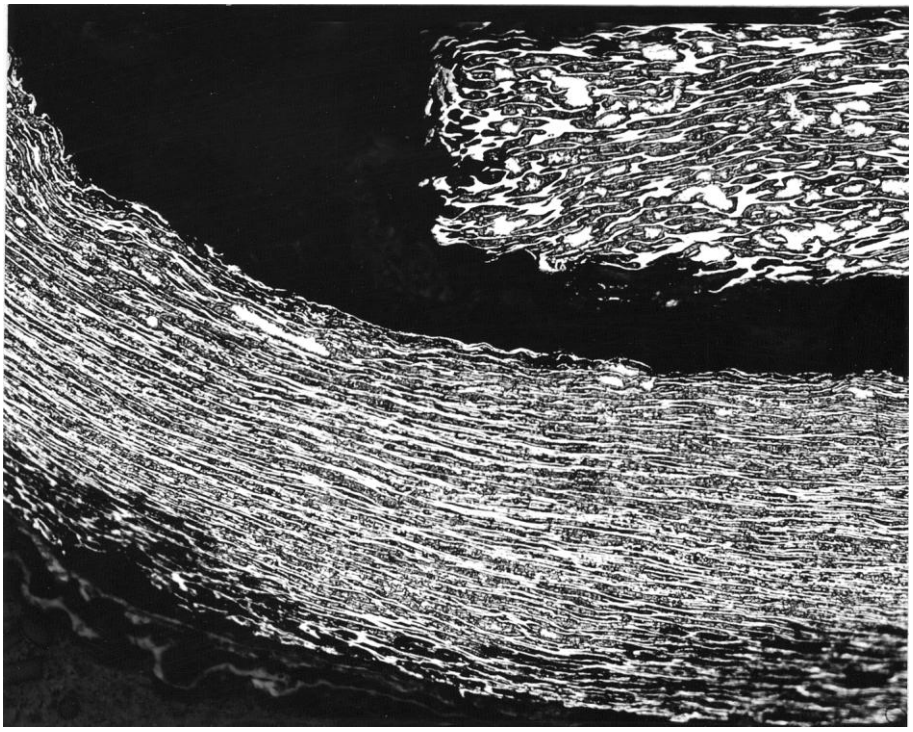

Figure 13. Higher magnification photomicrograph of the mechanical join between the two copper-silver alloy sheets in the Chimú cup shown in Figure 8. Etching reveals the heavily deformed lamellar microstructure of a worked copper-silver alloy. The dark areas are the copper-rich β-phase and the lighter regions are the silver-rich α-phase. Both phases are highly elongated in the direction of working as a result of the extensive deformation from cold hammering. This elongation is more pronounced in the bottom sheet than in the top sheet indicating that the bottom sheet was more heavily worked than the top one. MAG: 200; Etchant: Potassium dichromate and hydrochloric acid. (after Lechtman 1988: Figure 30.23)

4.1.3 Toughness of Cu-Ag Alloys

The high toughness of the deformed Cu-Ag alloy sheets is a result of their microstructures. They are essentially composite materials, because they are comprised of alternating lamellae of two different materials: a Ag-rich α-phase and a Cu-rich β-phase. When a transverse crack develops in a Cu-Ag alloy sheet, the alternating lamellae prevent the crack from propagating through the entire thickness of the sheet which would result in catastrophic failure by brittle fracture. This is evident in Figure 12 where the transverse surface cracks in the

corroded surface zones of the bead sheet metal have been deflected laterally by the presence of lamellar planes of solid solution material, and they stop. The corrosion products (oxides) are much more brittle than the intact Cu-Ag metal.

4.1.4 Development of Enriched Silver Surfaces

4.1.4.1 Annealing and Recrystallization Process

During the process of hammering these copper-silver alloy objects, the metalsmiths annealed them in order to relieve some of the stress and work hardening produced by the cold hammering and to restore the malleability of the alloy sheet. When work-hardened materials are annealed, the deformed grains recover, recrystallize, and grow. During recovery, the internal residual stresses introduced by working the material are relieved. The strength and hardness of the material do not change significantly. At higher temperatures, during the recrystallization phase, new strain-free grains nucleate at the grain boundaries and within the old, deformed grains (see Figure 14).

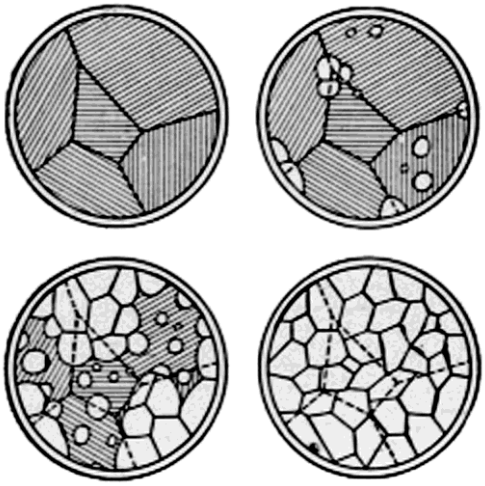

Figure 14. Recrystallization and growth of grains in metals. The new, strain-free grains nucleate at the grain boundaries of the older, strained grains and grow until all they replace the old grains. (courtesy of Heather Lechtman)

The temperature at which recrystallization occurs depends on the time of annealing and the extent of work hardening. After the new grains have nucleated, they grow larger, eventually replacing the old grains if the temperature is high enough and the time of annealing is long enough (Abbaschian et al. 2009). During recrystallization and growth, the strength and hardness of the material decrease as shown in Figure 15.

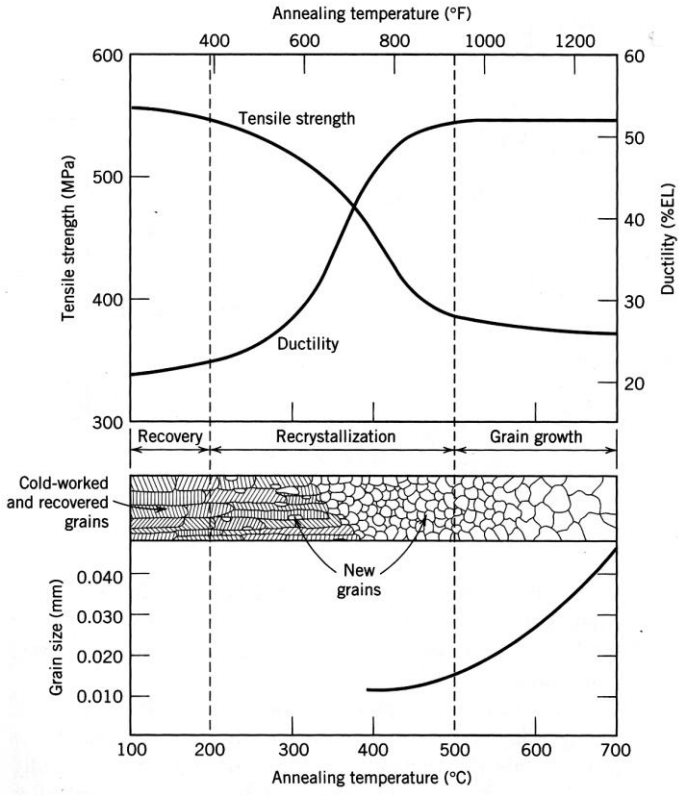

Figure 15. The effects of annealing temperature on the tensile strength and ductility of a brass alloy. As the grains begin to recrystallize, the tensile strength decreases and the ductility increases. (after Callister 2003: Figure 7.20)

The recrystallization temperature is typically reported as the temperature at which 50% of the grains in a worked piece of metal have recrystallized after 30 minutes of annealing, and it can be determined from a graph of hardness vs. annealing temperature. This thesis reports annealing experiments performed to determine the recrystallization temperature for two of the five Cu-Ag alloys (70 wt% Cu – 30 wt% Ag and 30 wt% Cu – 70 wt% Ag).

Literature values for the recrystallization temperature of pure Cu range from 100°C to 150°C, depending on the amount of cold work and length of the anneal time. Currently there are no values reported in the literature for the recrystallization temperatures of the Cu-Ag alloy compositions tested in this thesis. However, the addition of 0.05 wt% Ag to pure Cu has been

found to increase the recrystallization temperature from 140°C to about 330°C (Davis 2001). Thus, the recrystallization temperatures for compositions containing between 5 wt% Ag and 70 wt% Ag should be between 330°C and 779°C, the eutectic temperature for the Cu-Ag alloy system.

4.1.4.2 Enriched Silver Surfaces in Artifacts

When copper-silver alloys containing more than about 10 wt% Ag (Lechtman 1988) are annealed after hammering, the copper at the surface oxidizes preferentially, forming a copper oxide scale. If the copper oxide scale is removed, the surface layer becomes depleted in copper and enriched in silver. The copper oxide can be removed by pickling the object in an acidic or basic solution, imparting the finished object with a silver color (Lechtman 1971, 1984b). After etching a polished cross section sample removed from the bead shown in Figure 12, the silver-enriched surfaces of the thin metal sheet are visible. Figure 8 shows the silver-enriched surfaces of the Chimú cup.

A recent study by Gordon and Knopf (2007) on the mechanical properties of several copper-silver alloy compositions determined analytically from Inka artifacts at Machu Picchu suggests that the annealing exhibited in the artifact microstructures was carried out intentionally by the smiths in order to develop enriched silver-colored surfaces. The authors determined this by cold rolling and cold hammering copper-silver alloy samples and measuring their mechanical properties. None of the plastically deformed material developed enriched silver surfaces. Some samples were also annealed, however, and they did develop the silver-enriched surfaces. The

alloy compositions were chosen based on the compositions of several copper-silver artifacts from the Machu Picchu collection.

4.2 Engineering Research on Properties of Cu-Ag Alloys

Today, Cu-Ag alloys are used to make jewelry, coins, silverware, electrodes, and solders for circuit boards. In jewelry and silverware the most commonly used alloy is sterling silver (92.5 wt% Cu – 7.5 wt% Ag) and in coins a popular alloy is coin silver (90 wt% Cu – 10 wt% Ag) which was used to produce American silver coins prior to 1964 and is used for commemorative coins today. The properties of these high-silver content alloys are well known (ASM International 2002a, 2002b). A few studies have measured the mechanical and electrical properties of other compositions in the Cu-Ag alloy system (Broniewski 1938; Broniewski and Koslacz 1932; Butts 1975). Many of the materials properties, including the Brinell Hardness determined by Broniewski and Koslacz and shown in Figure 16, exhibit a plateau between about 30 wt% Cu and 80 wt% Cu. Over a large compositional range, the mechanical properties of copper-silver alloys are quite similar. That is to say, there is no single composition for which the mechanical properties of a copper-silver alloy are significantly improved. This thesis investigates this finding with respect to the malleability of the alloys over a large compositional range.

The extraordinary malleability of a variety of copper-silver alloy compositions may suggest that these alloys approach superplastic behavior. Superplasticity has been demonstrated in the annealed equiaxed structure of the Cu-Ag eutectic composition (28.1 wt% Cu – 71.9 wt% Ag) (Cline and Lee 1970). Further investigations are required to reproduce this effect and to

determine under what conditions other compositions or microstructures may exhibit superplastic behavior.

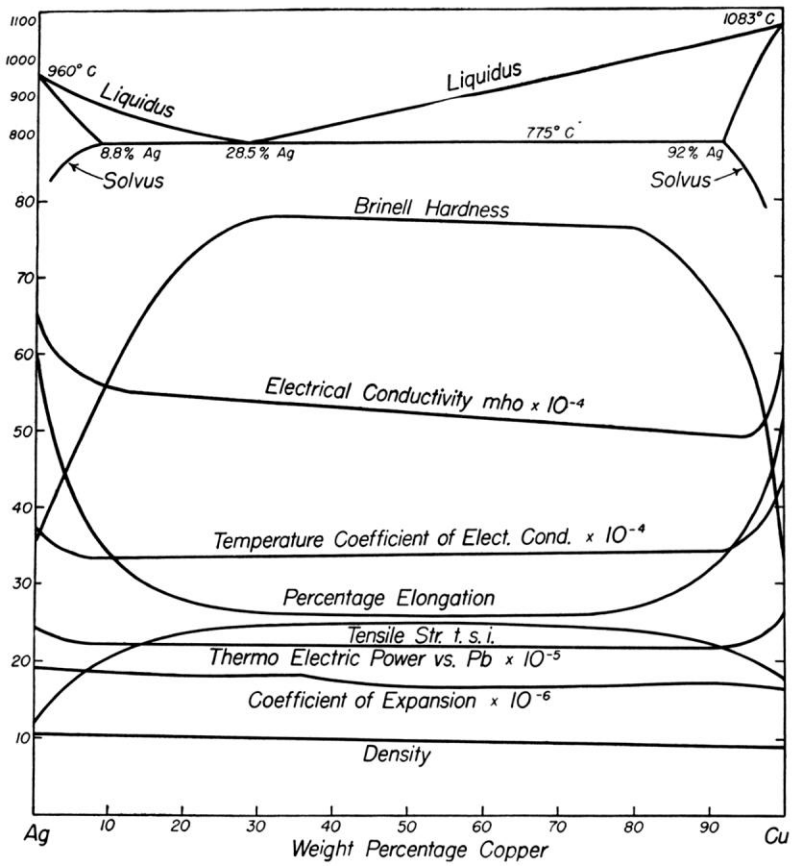

Figure 16. Properties of annealed silver-copper alloys at room temperature (after Rhines 1956: Figure 4-21)

5 Thesis Objectives

Knowledge of the mechanical and physical properties of copper-silver alloys is important in understanding why this binary alloy system became central to the metallurgies that developed among prehistoric societies of the Andean zone of South America and in Mesoamerica. This thesis determines the physical and mechanical properties of copper-silver alloys for five distinct alloys ranging from 95 wt% Cu – 5 wt% Ag to 30 wt% Cu – 70 wt% Ag and compares them to one another, with pure Cu as a standard.

The mechanical properties of copper-silver alloys that contributed to their central role in the ancient metallurgies of the Americas are their malleability and their toughness (the extent to which the alloys can be cold worked without fracture). This thesis investigates the extent to which copper-silver alloys can be cold worked and the hardening they develop during working as well as changes in microstructure that result from different processing methods.

The physical properties of copper-silver alloys that contributed to their central role in the ancient metallurgies of South America and Mesoamerica are closely related to the final color that develops at the surfaces of copper-silver alloy objects. This thesis investigates the recrystallization and annealing temperatures of the copper-silver alloy system, since these conditions are fundamental to the development of enriched silver surfaces – and thus the final color – of the finished artifacts.

6 Materials and Methods

6.1 Selection of Alloy Compositions

The following Cu-Ag alloy compositions were chosen for analysis: 95 wt% Cu – 5 wt% Ag, 80 wt% Cu – 20 wt% Ag, 70 wt% Cu – 30 wt% Ag, 60 wt% Cu – 40 wt% Ag, 30 wt% Cu – 70 wt% Ag. Pure Cu was used as a standard. In the archaeological record of the Andes and Mesoamerica, the compositions of artifacts made of copper-silver alloys include nearly every composition between pure Cu and Pure Ag (Gordon and Knopf 2007; Hörz and Kallfass 2001; Hosler 1994; Lechtman 1979, 1988, 2007; Root 1949). Engineering data for pure copper, pure silver and alloys with high silver contents such as sterling (92.5 wt% Ag – 7.5 wt% Cu) and coin silver (90 wt% Ag – 10 wt% Cu) are available in the literature. Very little data exist for copper-silver alloys with copper concentrations above 10 wt%. The Cu-Ag alloy compositions for this study were chosen deliberately to include the higher copper concentrations, and they correspond to compositions that have been determined commonly for ancient New World objects made from copper-silver alloys. Additionally, some compositions represent key regions of the Cu-Ag phase diagram, shown in Figure 9. For example the 30 wt% Cu – 70 wt% Ag alloy is very close to the eutectic composition (28.1 wt% Cu – 71.9 wt% Ag), and the 95 wt% Cu – 5 wt% Ag alloy is close to the solid solubility limit of silver in copper (92 wt% Cu – 8 wt% Ag).

6.2 Ingot Casting

Beginning in July 2010, six 325 ounce (9.21 kg) ingots of the compositions listed above were cast at Cookson Precious Metals (now part of LeachGarner) in Attleboro, MA using the continuous casting method. Professor Thomas Eagar provided the initial contact with metallurgists at Cookson Precious Metals who were interested in this project given the company's expertise in precious metal production. Cookson Precious Metals carries out almost all of its ingot production using continuous casting methods. One of the advantages of continuous casting is that it minimizes the formation of porosity in the ingots. One of the drawbacks of continuous casting is the large grain size that accompanies slow cooling of the melt.

For each alloy composition, the pure copper and pure silver stock were mixed by weight in the desired ratios in a graphite crucible and then heated until at least 65° C of superheat was achieved. The molten metal was then poured through a ½" x 4 5/16" x 8 ¾" (1.27 cm x 10.95 cm x 22.23 cm) graphite die with a 4" (10.16 cm) copper cooling jacket as shown in Figure 17.

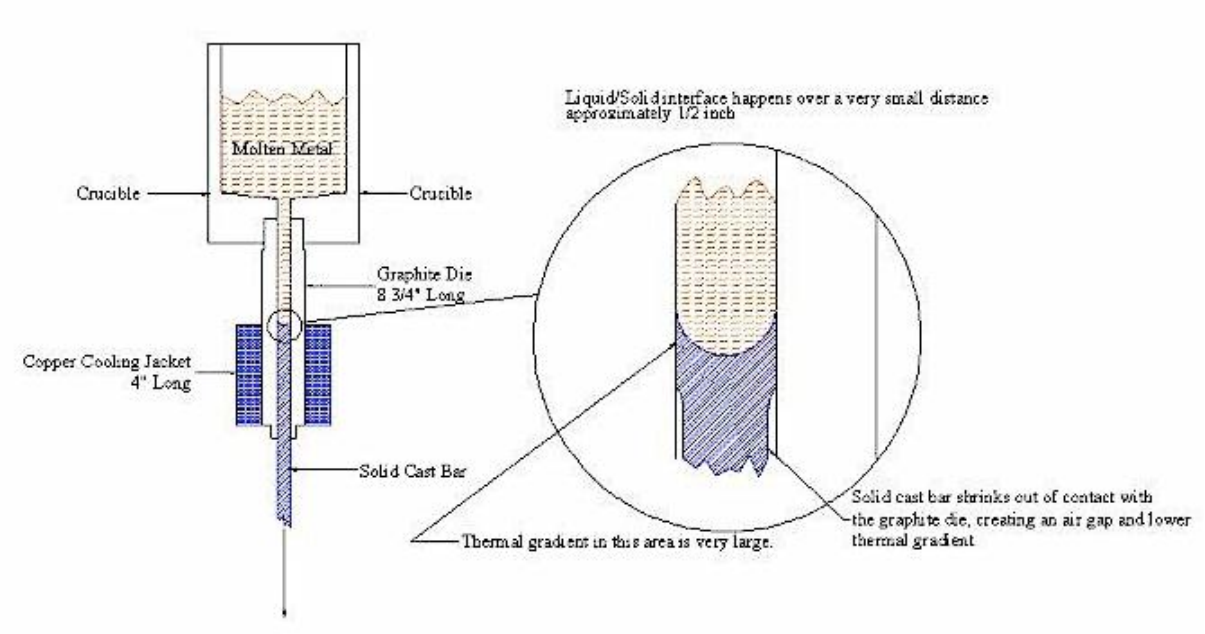

Figure 17. Schematic of Continuous Casting Assembly used at Cookson Co. The average cooling rate in the graphite die is about 281° C per minute. Solidification occurs in the ½" tall region near the top of the cooling jacket where the cooling rate is estimated to be about 1000° C per minute. There is a large thermal gradient near the top of the copper cooling jacket that causes the solid cast bar to shrink out of contact with the graphite die. This creates an air gap and lowers the thermal gradient. (courtesy of John Riskalla)

During melting graphite rods were inserted into the melt to prevent the molten metal from oxidizing and to minimize porosity in the cast ingots. Powdered charcoal was added continuously to the crucible, and a carbon monoxide gas jet cover was also used to cover the exposed surface of the melt during casting. Figure 18 shows a cast ingot before any samples were cut from it. Table 2 indicates the MIT sample identification numbers assigned to each of the ingots.

Figure 18. 30 wt% Cu – 70 wt% Ag alloy ingot (MIT 5476) prior to the removal of any samples for analysis or testing.

Table 2. Cu-Ag Ingot Compositions and Identification Numbers

MIT ID Number	**Cookson Bar No.**	**Composition (wt%)**	**Casting Date**
MIT 5489	10	pure Cu	September 2011
MIT 5484	9	95% Cu – 5% Ag	February 2011
MIT 5483	8	80% Cu – 20% Ag	February 2011
MIT 5482	7	70% Cu – 30% Ag	February 2011
MIT 5481	6	60% Cu – 40% Ag	February 2011
MIT 5476	1	30% Cu – 70% Ag	July 2010

During the first casting session in July 2010, the five alloy compositions were cast. As a result of a high porosity volume fraction in some of the ingots it was necessary to recast four of the alloy compositions (95 wt% Cu – 5 wt% Ag, 80 wt% Cu – 20 wt% Ag, 70 wt% Cu – 30 wt% Ag, 60 wt% Cu – 40 wt% Ag). Some modifications were made to the casting procedure in an effort to reduce the porosity volume fractions in the ingots. Finally, the pure copper ingot was cast in a third casting session in September 2011.

6.3 Compositional Analysis of Cast Ingots

Several different types of analysis were performed at Cookson Precious Metals to verify the copper and silver concentrations in the crucible melt and the chemical composition of the cast ingots. Computer Aided, Conductivity Based, End Point Titration (TIAG) was used to determine the concentrations of both Cu and Ag in the melt and in the ingots. Direct-Coupled Plasma Spectrometry (DCP) was used to determine the concentration of trace elements. The compositions of the molten alloy in the crucible and the solidified ingots from the first casting session can found in Appendix B.

6.4 Metallographic Analysis of Cast Ingots

Figure 19 shows the location and orientation of metallographic cross section samples removed from the cast ingots. The samples were mounted in Mark V Laboratory Fina-Met powder. These samples were then ground on a Beuhler Strip Grinder with silicon carbide grits 240, 320, 400, and 600. Then, the samples were polished on polishing wheels using 6 μm and 1

μm synthetic diamond paste followed by a 0.3 μm alumina suspension. Vickers microhardness tests were performed on as-polished samples. Potassium dichromate or a mixture of ammonium hydroxide and hydrogen peroxide were used to etch the samples to reveal microstructure. The chemical compositions of the etchants are presented in Table 3. Photomicrographs were taken using a Canon EOS 60D digital SLR camera mounted on a Leica DM LM metallurgical microscope.

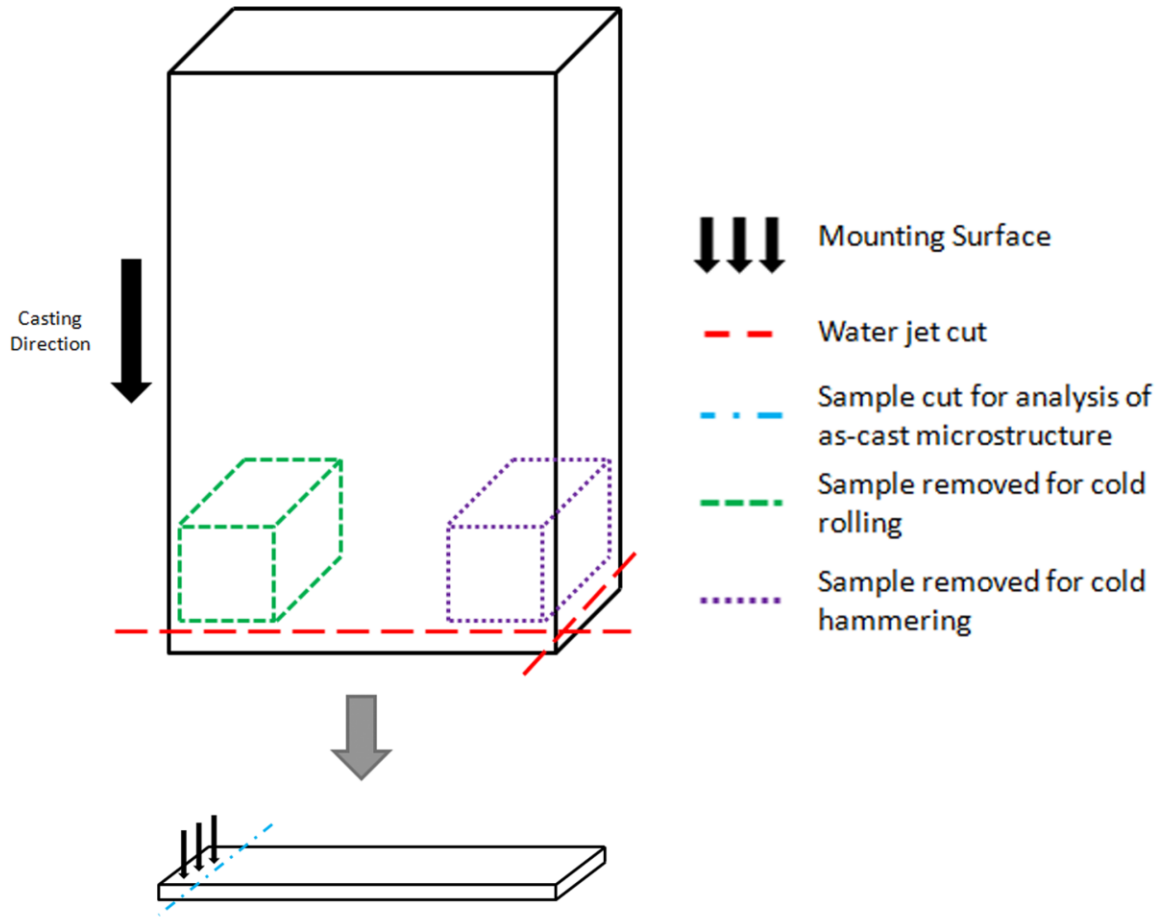

Figure 19. Locations of samples cut from cast ingots for microstructural analysis, cold rolling, and cold hammering. Note: Not to Scale

Table 3. Etchants Used for Microstructural Analysis of Cu-Ag Alloys

Etchant	Ingredients
potassium dichromate	2 g $K_2Cr_2O_7$ + 5 mL saturated NaCl solution + 8 mL H_2SO_4 (per 100 mL of distilled water)
1:9 dilute potassium dichromate	10 mL potassium dichromate + 90 mL distilled water
1:19 dilute potassium dichromate	5 mL potassium dichromate + 95 mL distilled water
ammonium hydroxide + hydrogen peroxide	$NH_3(aq) + H_2O_2$
chromium oxide	1 g CrO_3 + 1 mL H_2SO_4 + 250 mL H_2O

6.5 Porosity Volume Fraction of Cast Ingots

In order to minimize the possibility of pores compromising the mechanical performance of the ingot samples a low porosity volume fraction was necessary. The porosity volume fraction of each of the as-cast ingots was determined using Random Walk Point Counting at a magnification of 200 using a Leitz Periplan GF 10XM Eyepiece (as a substitute for a crosshair eyepiece) on polished metallurgical samples cut from the ingots, as indicated Figure 19. Vickers microhardness tests and microstructural analyses were also performed on these samples. Two porosity volume fractions, each based on a 200 point count, were determined for each sample and then averaged. Table 4 presents the porosity volume fractions for the cast ingots.

Table 4. Average Porosity Volume Fractions of Cast Cu-Ag Ingots

Ingot ID Number	Cast No.	Alloy Composition (wt%)	Average Porosity Volume Fraction (%)	Standard Deviation
MIT 5480	1	95% Cu – 5% Ag	4	0
MIT 5479	1	80% Cu – 20% Ag	5.5	0.71
MIT 5478	1	70% Cu – 30% Ag	12	0
MIT 5477	1	60% Cu – 40% Ag	6.5	2.12
MIT 5476	1	30% Cu – 70% Ag	0.25	0.35
MIT 5484	2	95% Cu – 5% Ag	3.25	0.35
MIT 5483	2	80% Cu – 20% Ag	2.5	0.71
MIT 5482	2	70% Cu – 30% Ag	9	0.71
MIT 5481	2	60% Cu – 40% Ag	9.5	0.71

The porosity volume fractions for the ingots cast in July 2010 (Cast No. 1) were higher than desired for all alloy compositions except for the 30 wt% Cu – 70 wt% Ag (MIT 5476). Thus, these compositions were recast using new pure materials in February 2011 (see Table 2). The porosity volume fractions of the ingots from the second casting session (Cast No. 2) were determined using the method described above. Overall the porosity volume fractions of the ingots from the second casting session were lower than those from the first casting session. In the case of the 60 wt% Cu – 40 wt% Ag alloy, however, the porosity of the second ingot was higher than that of the first ingot. Due to time constraints, the 60 wt% Cu – 40 wt% Ag alloy was not recast a third time.

6.6 Cold Rolling

One 1” x 1” x ½ (25.4 x 25.4 x 12.7 mm) square slab was cut from each of the six ingots as shown in Figure 20. This square slab was then cut in half longitudinally to produce two 1” x 1” x 0.24” (25.4 x 25.4 x 6.1 mm) square slabs (see Figure 20). The slab dimensions were chosen based on the safety requirements for the rolling mill and the thickness of the cast ingots. The square slabs were cut using an OMAX 2626 water jet. Figure 21 shows the cut square slabs prior to cold rolling.

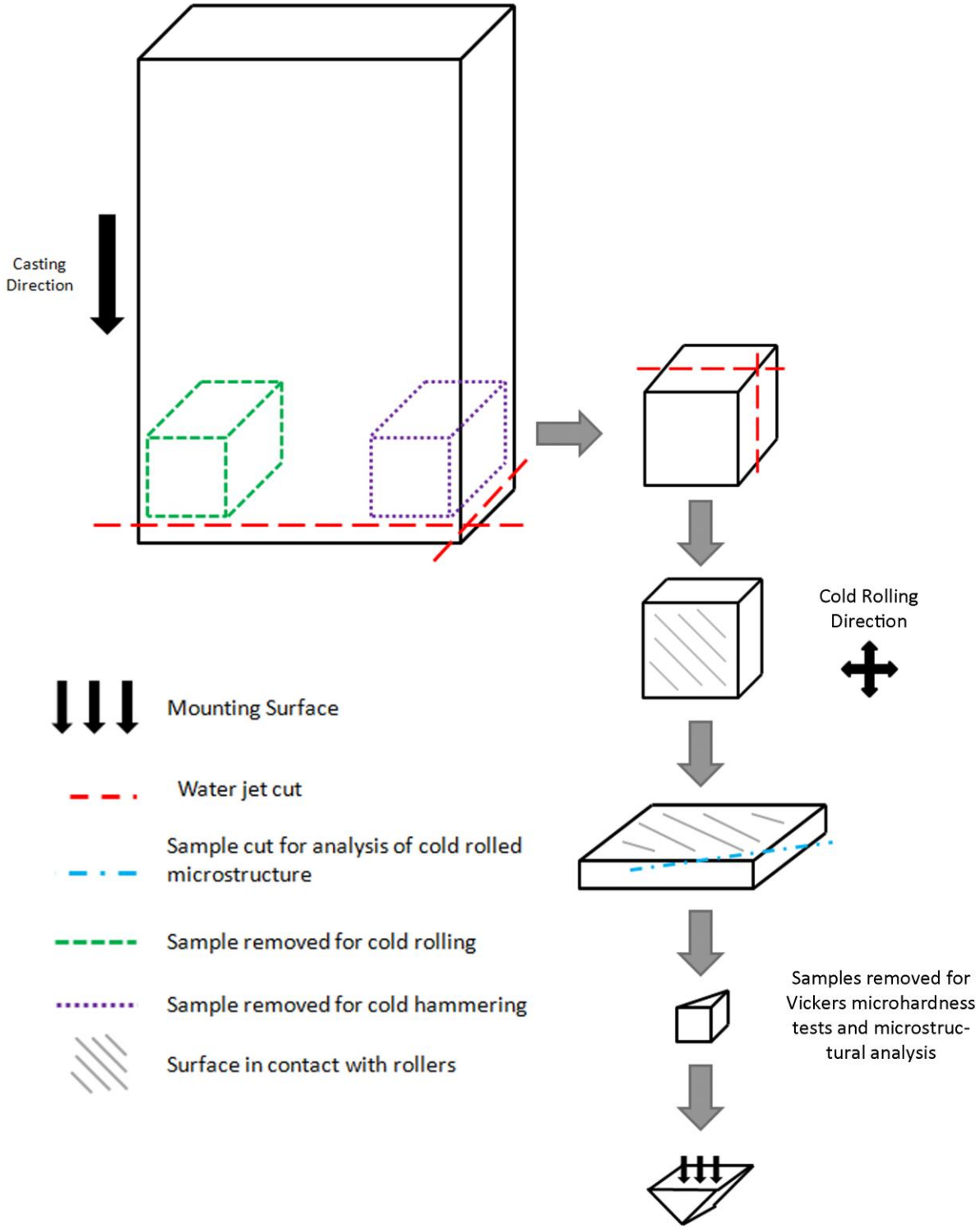

Figure 20. Location and orientation of cold rolled square slabs and samples removed for Vickers microhardness tests and microstructural analysis. NOTE: Not to scale.

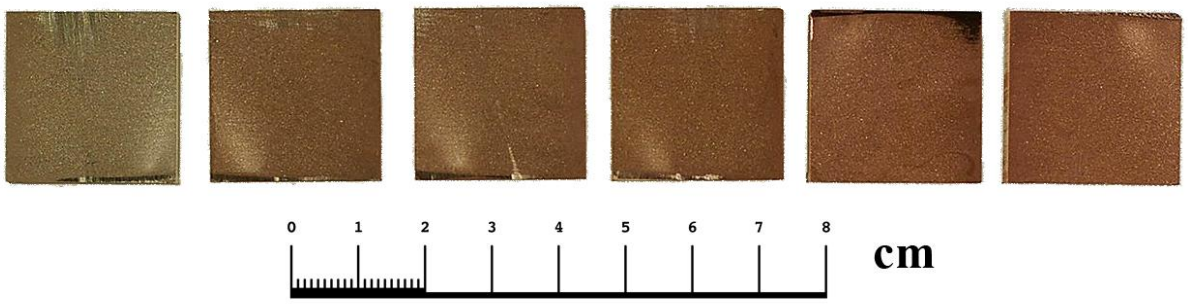

Figure 21. Square slabs cut from cast ingots prior to cold rolling. In order from left to right the alloy compositions are: 30 wt% Cu – 70 wt% Ag, 60 wt% Cu – 40 wt% Ag, 70 wt% Cu – 30 wt% Ag, 80 wt% Cu – 20 wt% Ag, 95 wt% Cu – 5 wt% Ag, pure Cu.

One of the final square slabs of each alloy composition was reduced by rolling in 15% increments from an initial thickness of 6.1 mm to the minimum possible thickness obtained with a non-lubricated International Rolling Mills Model No. 175 electric rolling mill. The sample thickness was reduced by cold rolling until the reduction interval final thickness was reached. Table 5 presents the thicknesses of each of the reduction intervals. The samples were rotated 90° between each revolution of the rolling mill, in order to maintain equiaxed grains and to avoid any preferential elongation in the direction of rolling. When edge cracks deeper than 1 mm developed, they were removed using the water jet.

Table 5. Sample Thickness for Reduction Intervals Used for Cold Rolled Cu-Ag Samples

Reduction in Thickness (%)	**Sample Thickness (mm) [+/- 0.1 mm]**
0	6.100
15	5.185
30	4.270
45	3.355
60	2.440
75	1.525
90	0.610

Once the desired thickness was reached, a portion of the sample was removed from a corner of the square for metallographic analysis and microhardness tests. These samples were cut using a Raytech Jem Saw 45 with a Raytech's Blazer yellow diamond blade. The metallographic samples were then mounted and polished. Figure 20 shows the orientation of the cut samples with respect to the rolling direction and the orientation of the cut samples in the mounts. The Vickers microhardness was measured on the polished samples for each reduction interval in order to determine the effects of cold working on the hardness of the Cu-Ag alloys. Photomicrographs were taken of etched samples at each reduction interval to document changes in microstructure as well as any edge cracking or the development of other flaws during rolling.

After a metallographic sample was removed, the test slab was cold rolled to the next reduction interval. A second square slab of each composition was cold rolled in the same manner as described above to the maximum possible reduction of which the rolling mill was capable;

however, no samples were cut from the corners. In this way, the maximum extent of reduction, a measure of malleability without annealing, could be determined for each alloy composition.

6.7 Hardness Testing of Cold Rolled Samples

Vickers microhardness determinations were measured on as-polished samples using a Tukon 2100B Microhardness Tester with a diamond indenter. A 100 g load was used for samples from alloy compositions containing more than 60 wt% Cu (MIT 5489, MIT 5484, MIT 5483, and MIT 5481) and a 1000 g load was used for samples from alloy compositions with less than or equal to 60 wt% Cu (MIT 5482 and MIT 5476). Five microhardness values were measured on each sample in the locations shown in Figure 22. If any of the first five values was rejected due to asymmetry of the indentation, additional measurements were taken until five valid microhardness values were obtained per sample. The average and standard deviation of the middle three microhardness values were calculated for a given sample.

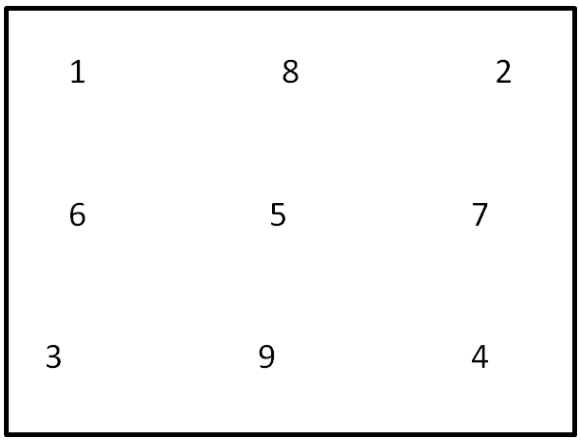

Figure 22. Location of Vickers microhardness tests in as-cast and cold rolled samples. NOTE: The geometry of each sample is rectangular but the dimensions are not necessarily the same as those reflected in this image.

6.8 Cold Hammering

The cold rolling experiments performed in this thesis demonstrate that greater than a 90% reduction in thickness can be achieved in all of the six compositions tested, but the ancient metalsmiths had access only to stone hammers. To demonstrate that similar reductions in thickness can be achieved without the use of a large rolling mill and without intermittent annealing, 1" x 1" x 0.24" (25.4 x 25.4 x 6.1 mm) square slabs of the alloy compositions with the highest and lowest silver contents (30 wt% Cu - 70 wt% Ag and 95 wt% Cu – 5 wt% Ag, respectively) were cold hammered by an experienced blacksmith[1] with a 5 pound sledge hammer and a 1000 g Peddinghaus hammer, both with polished face. The square slabs to be hammered were cut using the same procedure as the slabs that were cold rolled (see Figure 20). The sample thickness at which the samples began to crack along the edges was recorded, after which the cracks were removed using a file. The final thickness of each of the samples after hammering was also recorded.

6.9 Determination of Recrystallization Temperature

6.9.1 Annealing

To determine a more specific temperature range for the recrystallization temperature of cold rolled alloys for two alloy compositions (70 wt% Cu – 30 wt% Ag and 30 wt% Cu – 70 wt% Ag), six 1 cm x 1 cm x 0.61 mm samples were cut from each of the two 90% reduction samples using a Raytech Jem Saw 45 with a Raytech's Blazer yellow diamond blade. One

[1] Michael Tarkanian, a DMSE Lecturer and experienced blacksmith, performed these cold hammering experiments.

sample from each of the two Cu-Ag alloys was annealed for 30 minutes at six different temperatures (300°C, 400°C, 450°C, 500°C, 600°C, and 700°C). The samples were placed on an alumina tray, which was then placed in an Omegalux Benchtop muffle LMF-A550 furnace. The temperature was measured using an Omega DP460 thermocouple. Acceptable temperatures were deemed to be +/- 5°C of the desired temperatures. Table 6 presents the temperature of the furnace before placing the samples into the furnace and after 30 minutes of annealing, just before removing them from the furnace.

Table 6. Furnace Temperatures for Cu-Ag Recrystallization Temperature Experiments

Desired Temperature (°C)	**Initial Temperature (°C)**	**Final Temperature (°C)**
300	299.7	300.6
400	398.0	398.8
450	446.3	447.4
500	502.3	503.2
600	598.0	598.6
700	703.4	703.9

After 30 minutes of annealing, the samples were removed from the furnace and allowed to cool in air. Because the samples were very thin, they cooled quickly in air. There was no need or time to quench them.

6.9.2 Microhardness of Annealed Samples

The transverse sections of the annealed metallurgical samples were mounted in epoxy. These samples were then ground and polished. Vickers microhardness values were determined on the as-polished samples. By plotting hardness vs. annealing temperature, the recrystallization temperature of each of the alloys tested was determined. Photomicrographs were taken to document the grain recovery, recrystallization, and growth process.

7 Results

7.1 Microstructural Analysis of As-cast Ingots

Figure 23 shows the as-cast microstructure of four of the Cu-Ag alloy compositions and pure Cu. As a result of the continuous casting process and the associated long cooling times, the grains in the cast ingots are quite large (0.5 – 2.6 mm across). The grains in the 30 wt% Cu – 70 wt% Ag alloy, which is close to the eutectic composition, are much smaller (0.01 – 0.1 mm across) than those in the other ingots and can be recognized at high magnifications from the change in orientation of the lamellar structures (see Figure 24). In some samples grain boundaries are also visible as in Figure 25. Along the edges of the samples, where the ingots were in contact with the graphite die, the columnar grains are longer and thinner than the grains at the center of the ingots which are more equiaxed (see Figure 23b). In the 70 wt% Cu – 30 wt% Ag (Figure 23d) and the 60 wt% Cu – 40 wt% Ag (Figure 23e) alloys, a silver-enriched and silver-colored zone is present at the surface of the sample that was in contact with the graphite die. The grains are much smaller in this region which consists almost entirely of eutectic microconstituent as a result of inverse segregation during solidification (see Figure 26).

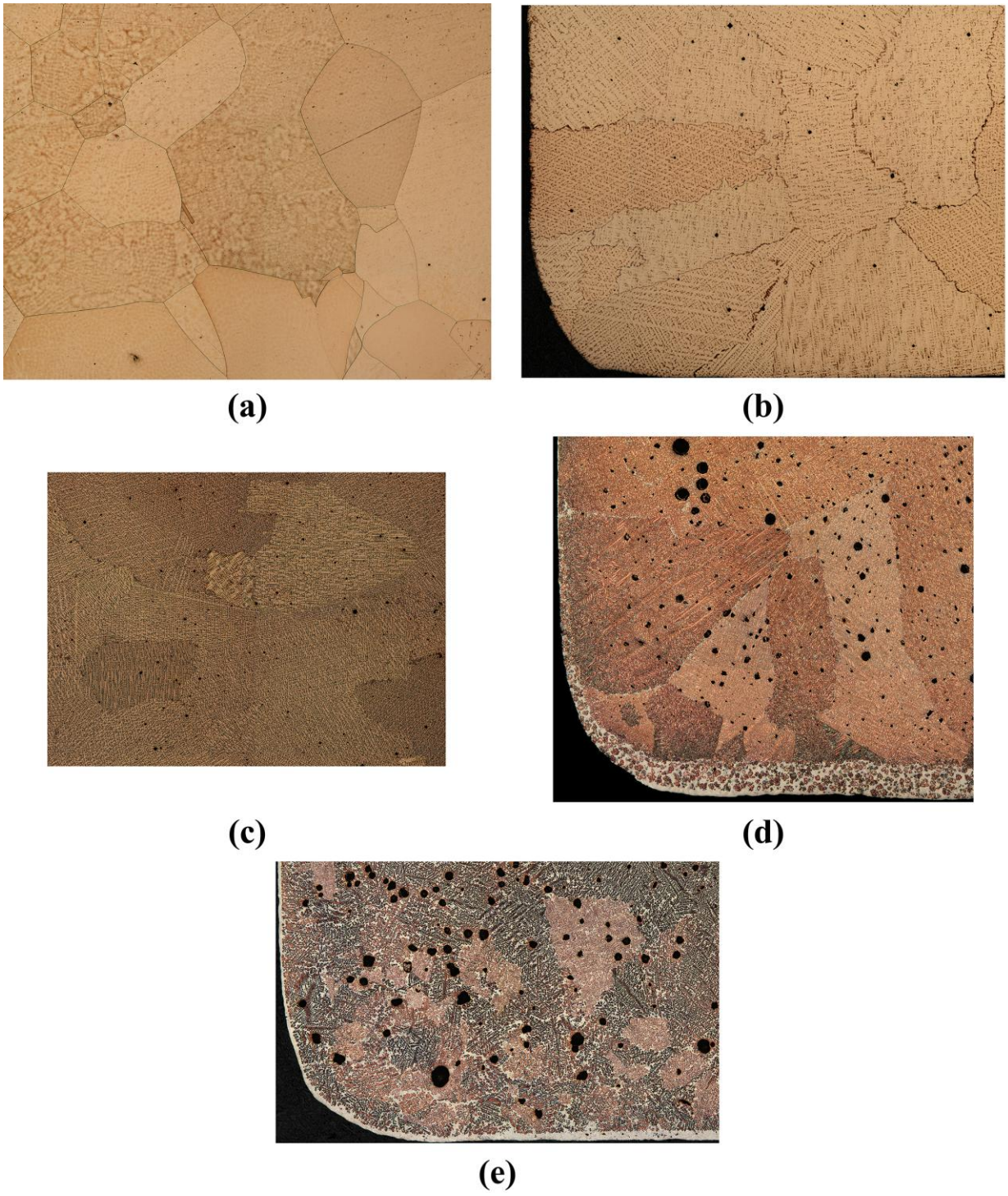

Figure 23. As-cast microstructures: (a) pure Cu, (b) 95 wt% Cu – 5 wt% Ag, (c) 80 wt% Cu – 20 wt% Ag, (d) 70 wt% Cu – 30 wt% Ag, (e) 60 wt% Cu – 40 wt% Ag. MAG: 18. Etchant: (a-d) 1:9 dilute potassium dichromate, (e) 1:19 dilute potassium dichromate

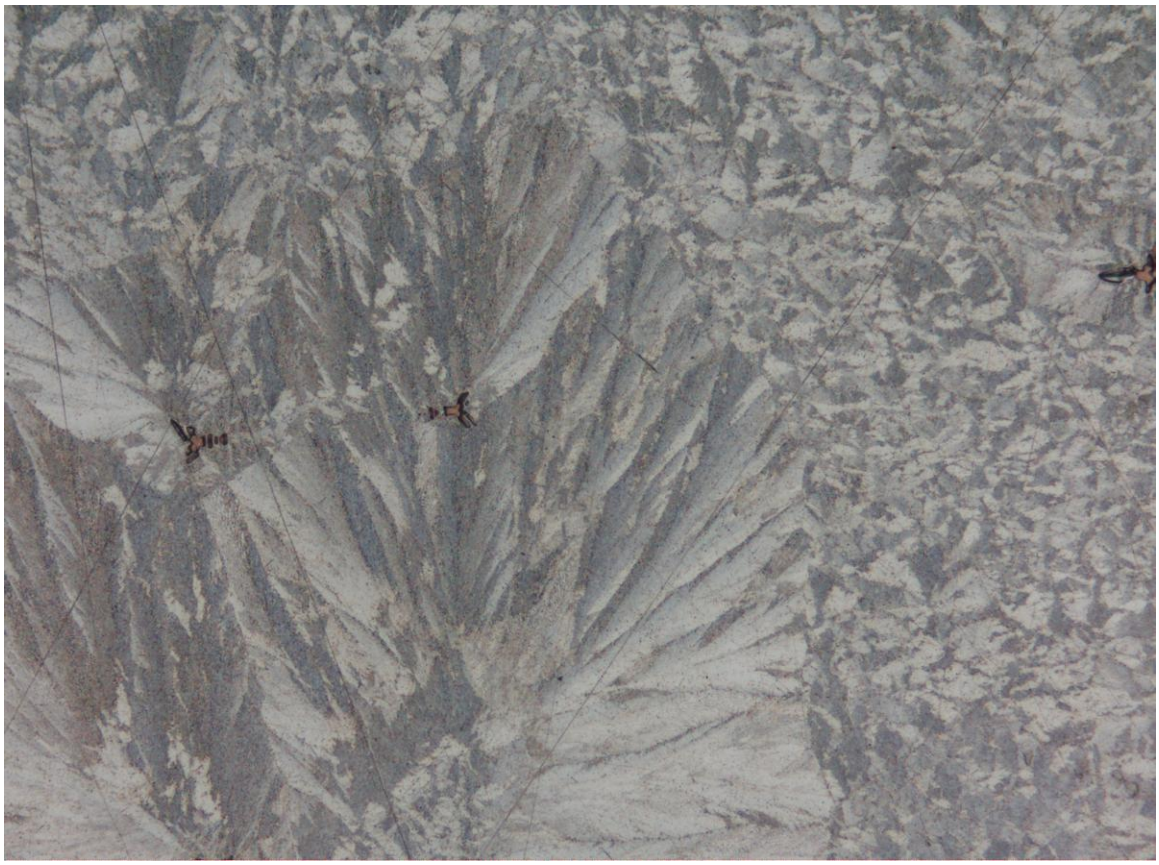

Figure 24. Microstructure of as-cast 30 wt% Cu – 70 wt% Ag alloy sample. The composition is very close to the eutectic composition (28.1 wt% Cu – 71.9 wt% Ag), and the microstructure consists of a few Cu-rich β-phase dendrites surrounded by the eutectic microconstituent of alternating lamellae. Grains can be discerned by the changes in direction of the lamellae. MAG: 300; Etchant: chromium oxide

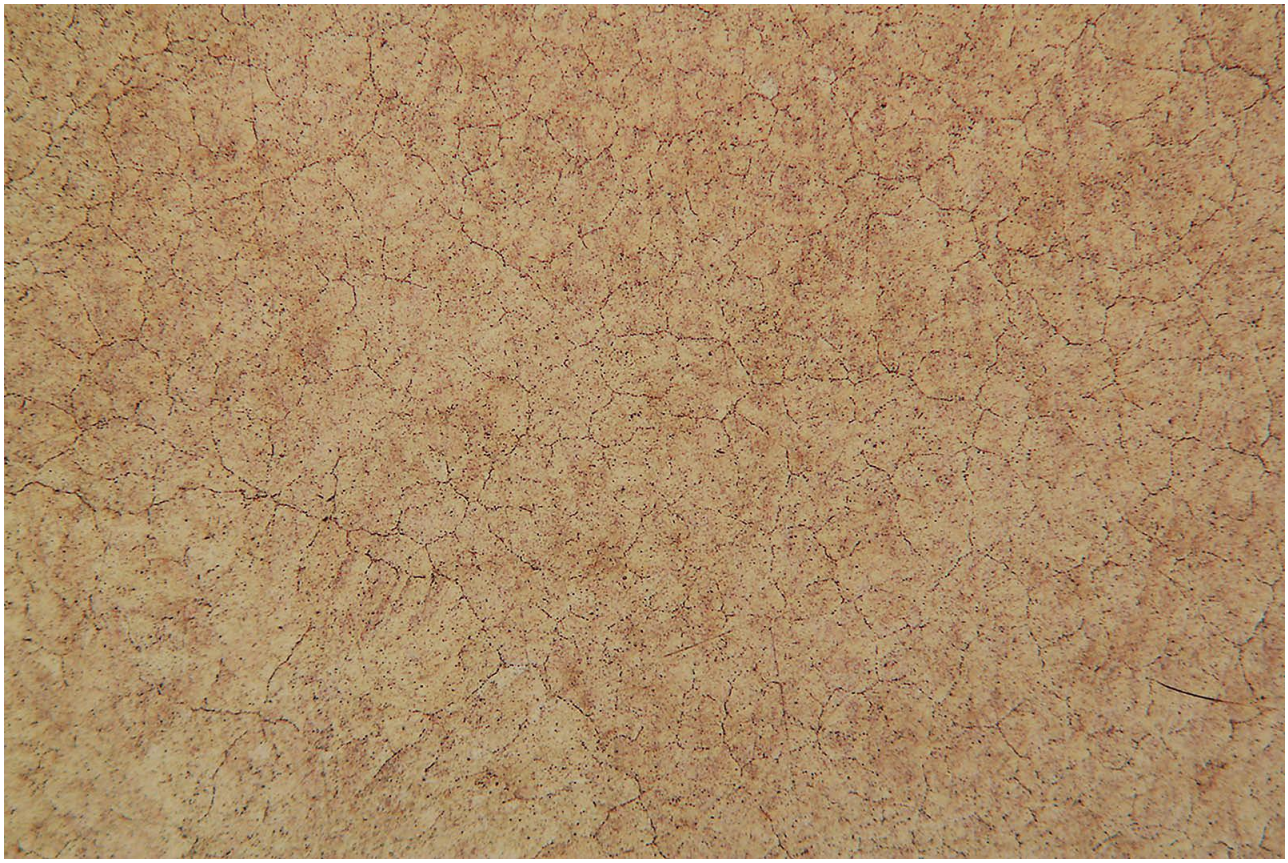

Figure 25. Grain boundaries in as-cast 30 wt% Cu – 70 wt% Ag alloy sample. The composition is very close to the eutectic composition (28.1 wt% Cu – 71.9 wt% Ag). MAG: 300; Etchant: chromium oxide

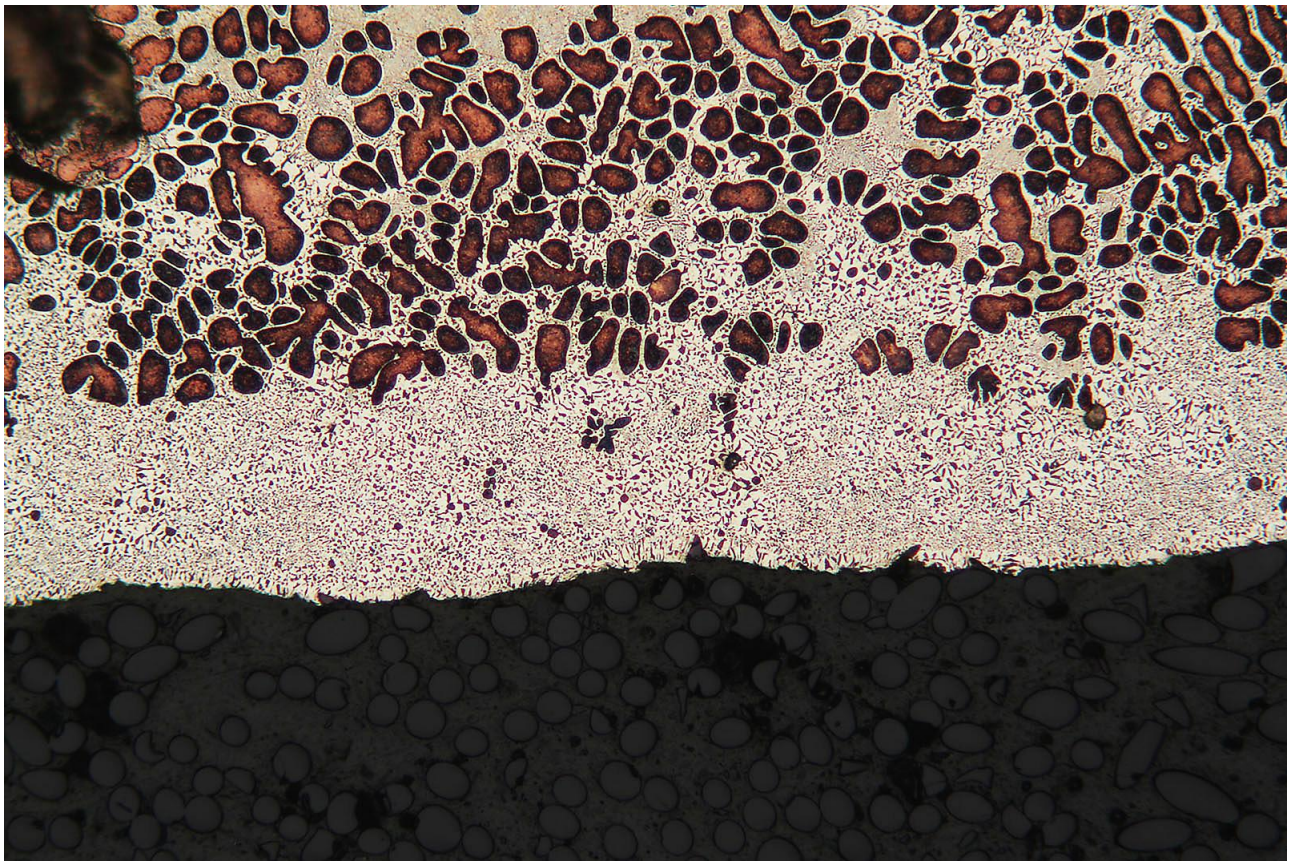

Figure 26. Inverse segregation at the surface of the as-cast microstructure of a 60 wt% Cu – 40 wt% Ag sample. At high pressures the last liquid to solidify is pushed through the interdendritic spaces toward the edges of the mold where it solidifies. Because this liquid is close to the eutectic composition (28.1 wt% Cu – 71.9 wt% Ag), the solid that forms is mostly lamellar with small Cu-rich β-phase regions. MAG: 750; Etchant: 1:19 dilute potassium dichromate

In the pure Cu (Figure 23a) and the 95 wt% Cu – 5 wt% Ag alloy (Figure 23b) samples, the grain boundaries are well defined at low magnifications. The grain boundaries in the pure Cu are smooth, whereas there are multiple types of grain boundary in the 95 wt% Cu – 5 wt% Ag alloy: 1) a fine, jagged line connecting high concentrations of Ag-rich α-phase; 2) a smooth boundary similar to those seen in pure Cu; and 3) boundaries exhibiting characteristics of 1 and 2. Figure 27 shows an intersection of three grains of the 95 wt% Cu – 5 wt% Ag alloy at which the three different grain boundary morphologies are present. Based on the phase diagram, the

95 wt% Cu – 5 wt% Ag alloy should be a solid solution; however, small interdendritic regions of Ag-rich α-phase material are present in the microstructure (see Figure 27) because of segregation of the alloy upon cooling from the melt.

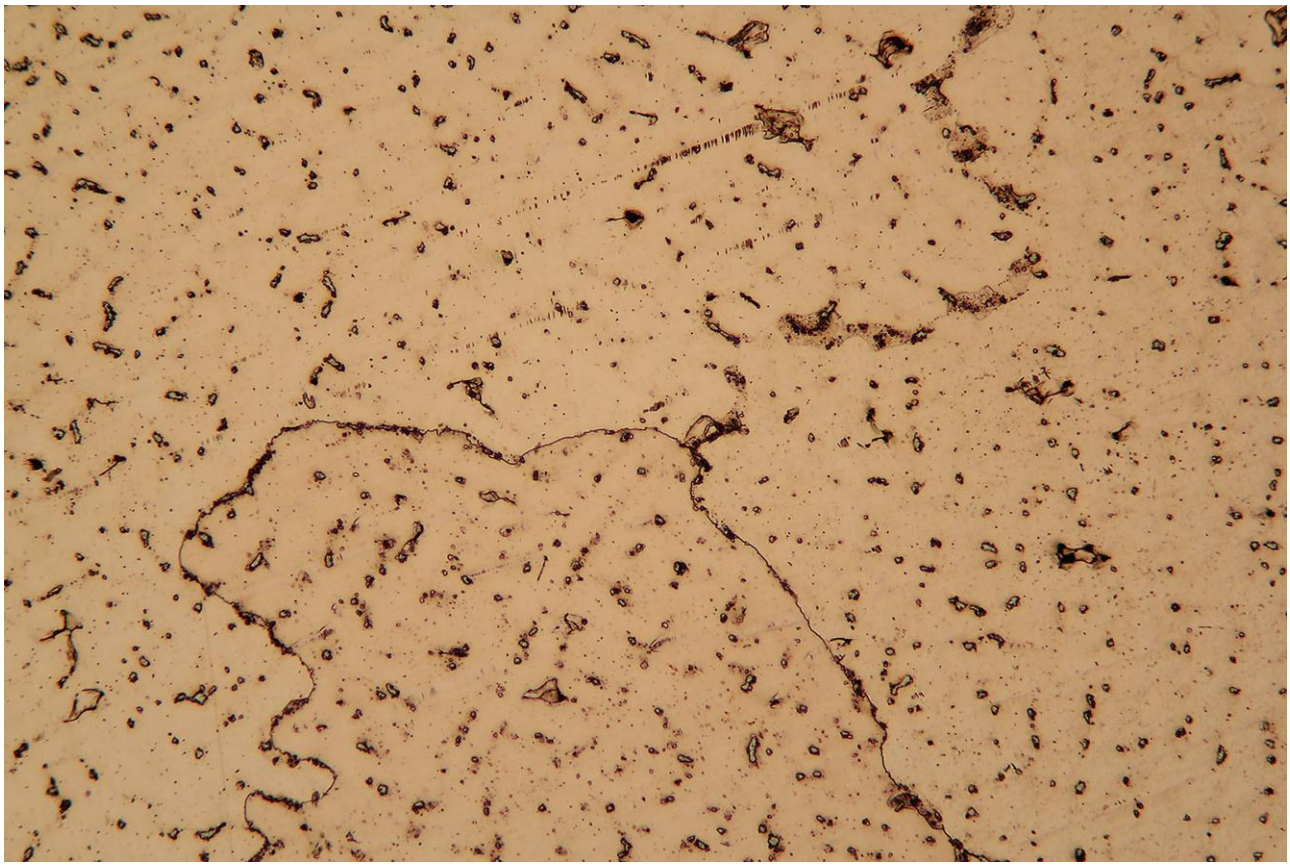

Figure 27. Intersection of three different types of grain boundary in a 95 wt% Cu – 5 wt% Ag sample that has been reduced in thickness by 15% via cold rolling. The uppermost grain boundary exemplifies boundaries that exhibit a very fine line connecting more heavily etched regions of higher Ag-rich α-phase concentration. The grain boundary on the right exhibits a smooth line similar to the grain boundaries in pure Cu. The grain boundary on the left exhibits characteristics of both types of grain boundary. MAG: 200; Etchant: 1:9 dilute potassium dichromate

In the samples with greater than 20 wt% Ag, the grain boundaries are not well defined at low magnifications. This occurs as the etchants used attack the alloy preferentially in response to

changes in segregated alloy composition rather than at the grain boundaries, thus grains can be differentiated most easily by the changes in orientation of the Cu-rich β-phase dendrites (see Figure 28).

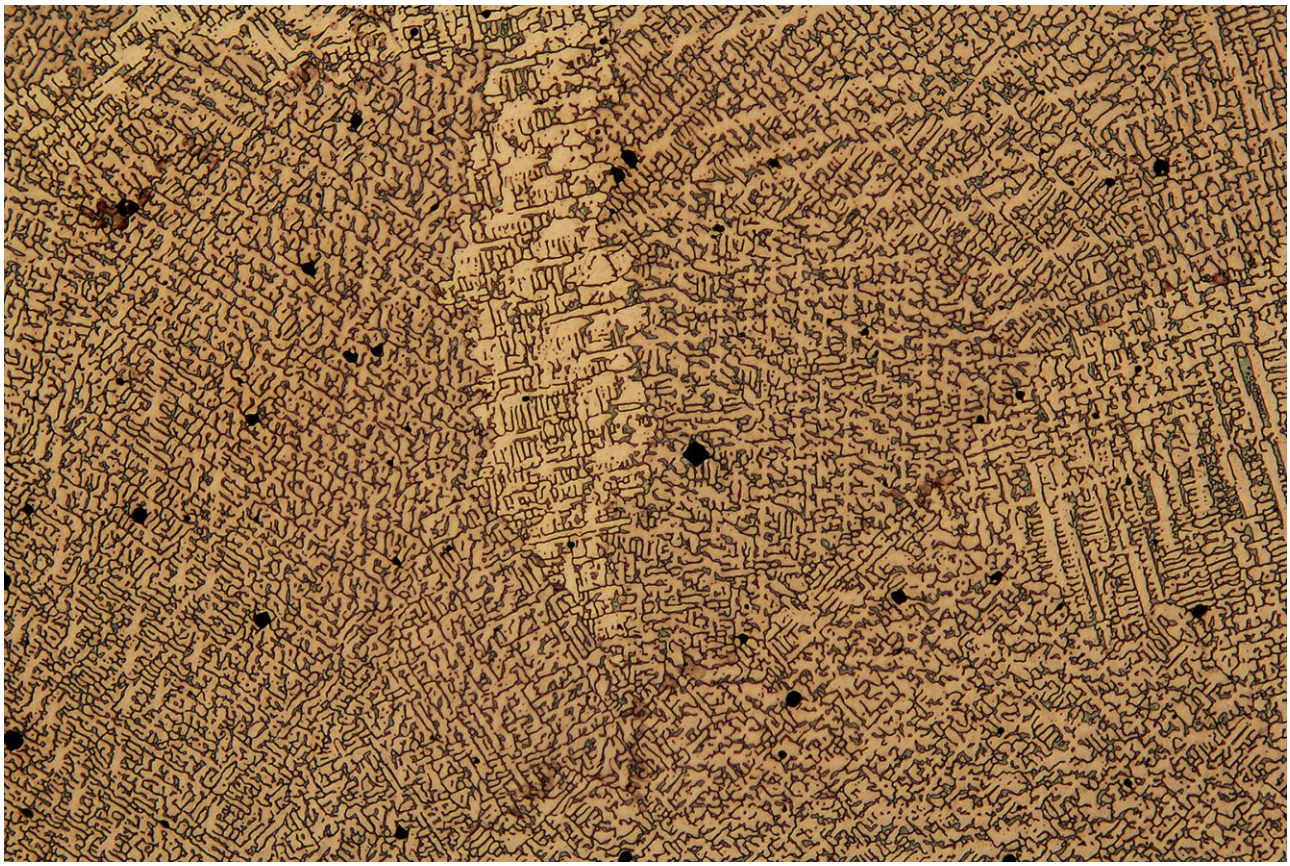

Figure 28. As-cast microstructure of 80 wt% Cu – 20 wt% Ag alloy. Grains can be discerned from the changes in orientation of the Cu-rich β-phase dendrites. MAG: 75; Etchant: 1:9 dilute potassium dichromate

In some samples, partial grain boundaries are visible at higher magnifications as shown in Figure 29.

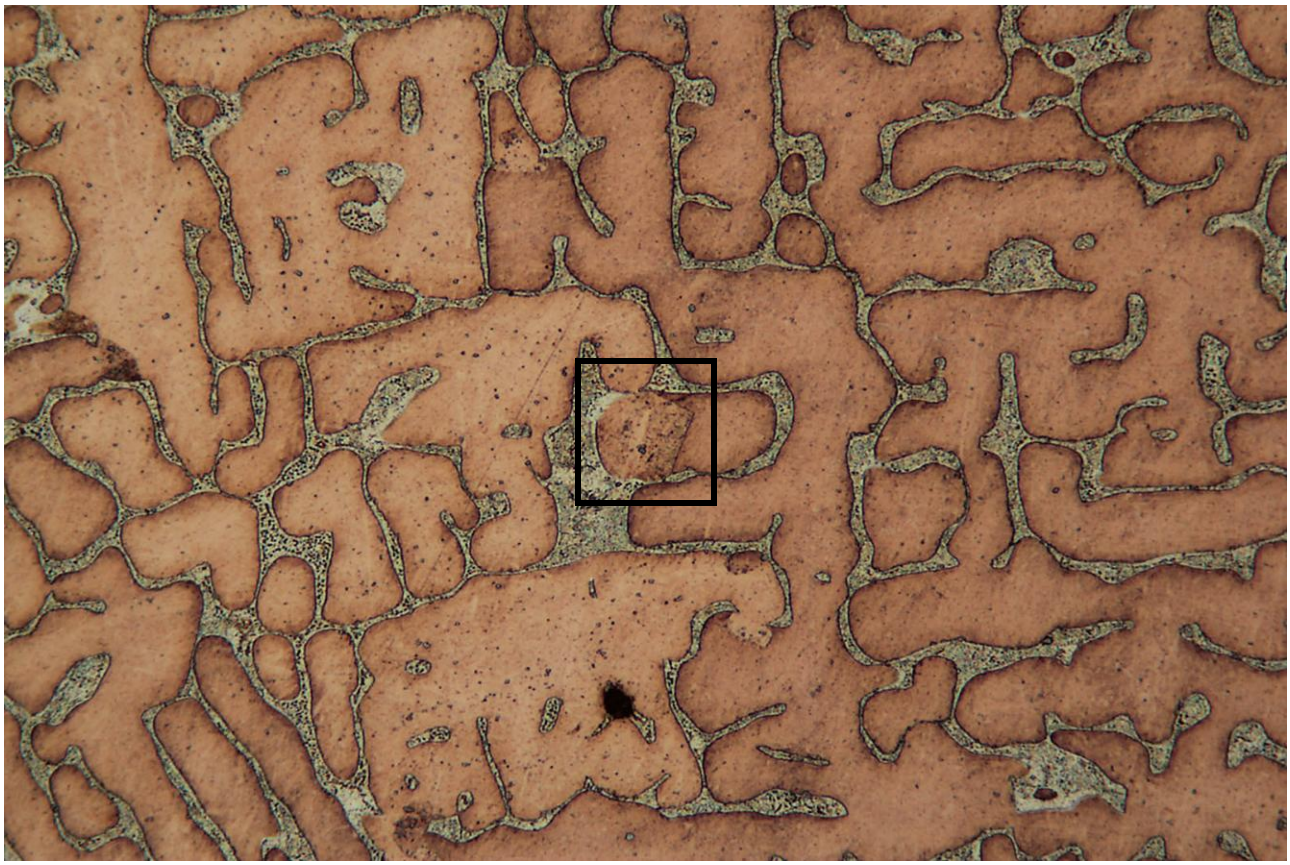

Figure 29. Grain boundary in as-cast sample of 80 wt% Cu – 20 wt% Ag alloy. At lower magnifications the grains can be distinguished by differences in shading, but at higher magnifications some possible partial grain boundaries are visible within the Cu-rich β-phase dendrites. MAG: 750; Etchant: 1:9 dilute potassium dichromate

In the 30 wt% Cu – 70 wt% Ag alloy, grain boundaries are visible from changes in orientation of the eutectic lamellae as seen in Figure 30.

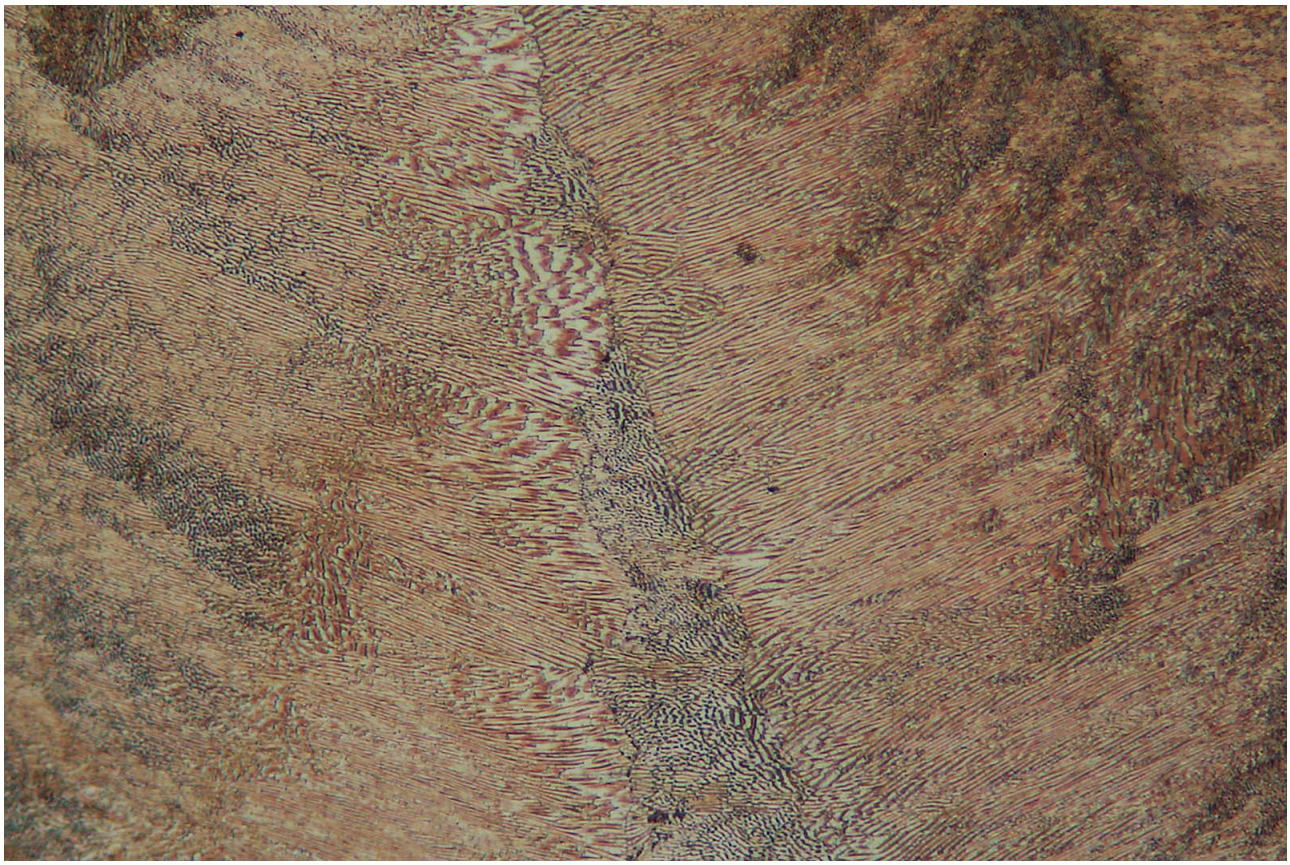

Figure 30. Grain boundary in a sample of a 30 wt% Cu – 70 wt% Ag alloy reduced in thickness 30% via cold rolling. A lamellar structure is present because this composition is close to the eutectic composition (28.1 wt% Cu – 71.9 wt% Ag). MAG: 750; Etchant: ammonium hydroxide + hydrogen peroxide

7.2 Cold Rolling

7.2.1 Vickers Microhardness

Figure 31 presents a graph of the Vickers Hardness Number (VHN) plotted against the percent reduction achieved through cold rolling of the five Cu-Ag alloys and the pure Cu standard. As the amount of cold work increases, the microhardness also increases. For the five

alloy compositions, the microhardness increases at approximately the same rate, especially beyond a 15% reduction in thickness.

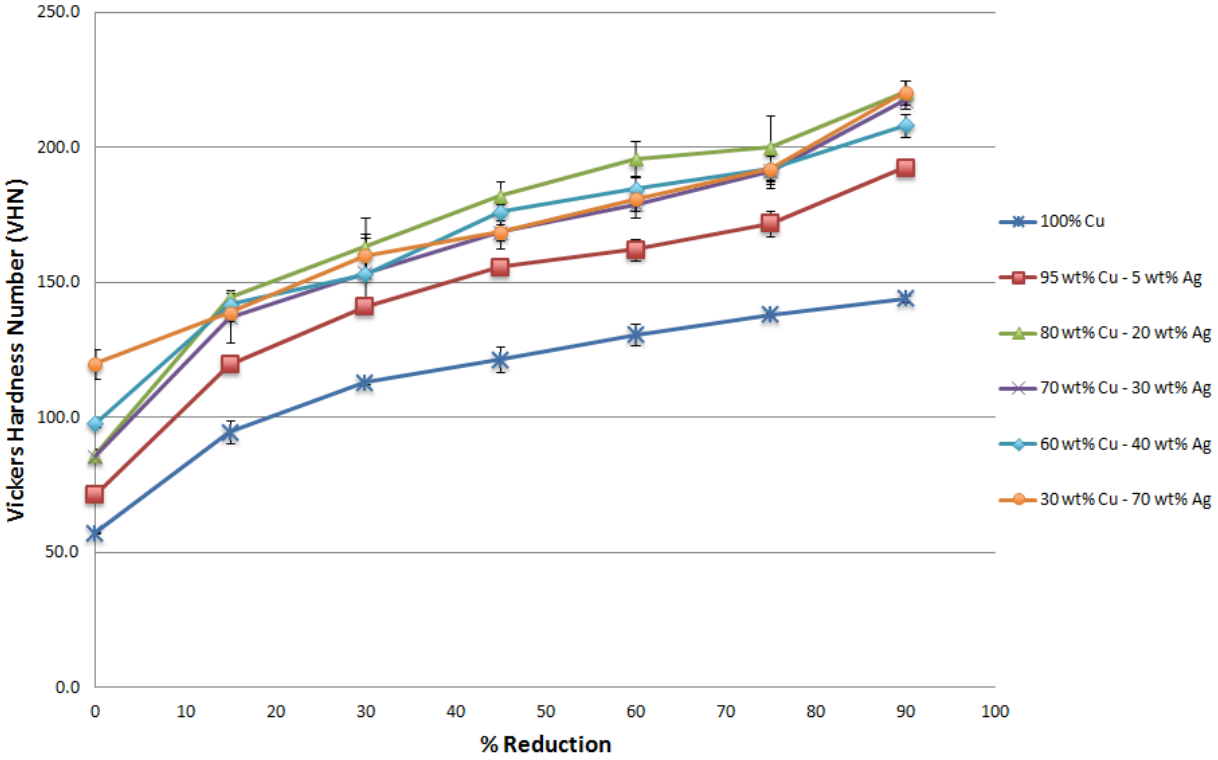

Figure 31. Vickers microhardness vs. % reduction for cold rolled Cu-Ag alloys

Moreover, for alloy compositions ranging between 30 and 80 wt% Cu there is little difference between the VHN values of the worked samples for each reduction interval (see Figure 32). This is in agreement with the data collected for Cu-Ag alloys by Broniewski and Koslacz (1932, 1938). On the other hand, the VHN value for the as-cast 30 wt% Cu – 70 wt% Ag alloy, which is very close to the eutectic composition for Cu-Ag alloys (28.1 wt% Cu – 71.9 wt% Ag), is approximately twice the value for pure Cu and is higher than the as-cast microhardness values for any of the five alloys tested (see Figure 31). The VHN values for the 80 wt% Cu –

20 wt% Ag alloy are consistently higher between 15 and 75% reduction in thickness than the VHN values for any of the other alloys (see Figure 32). At 90% reduction, the 30 wt% Cu – 70 wt% Ag alloy (near eutectic) reaches the same microhardness value as the 80 wt% Cu – 20 wt% Ag alloy.

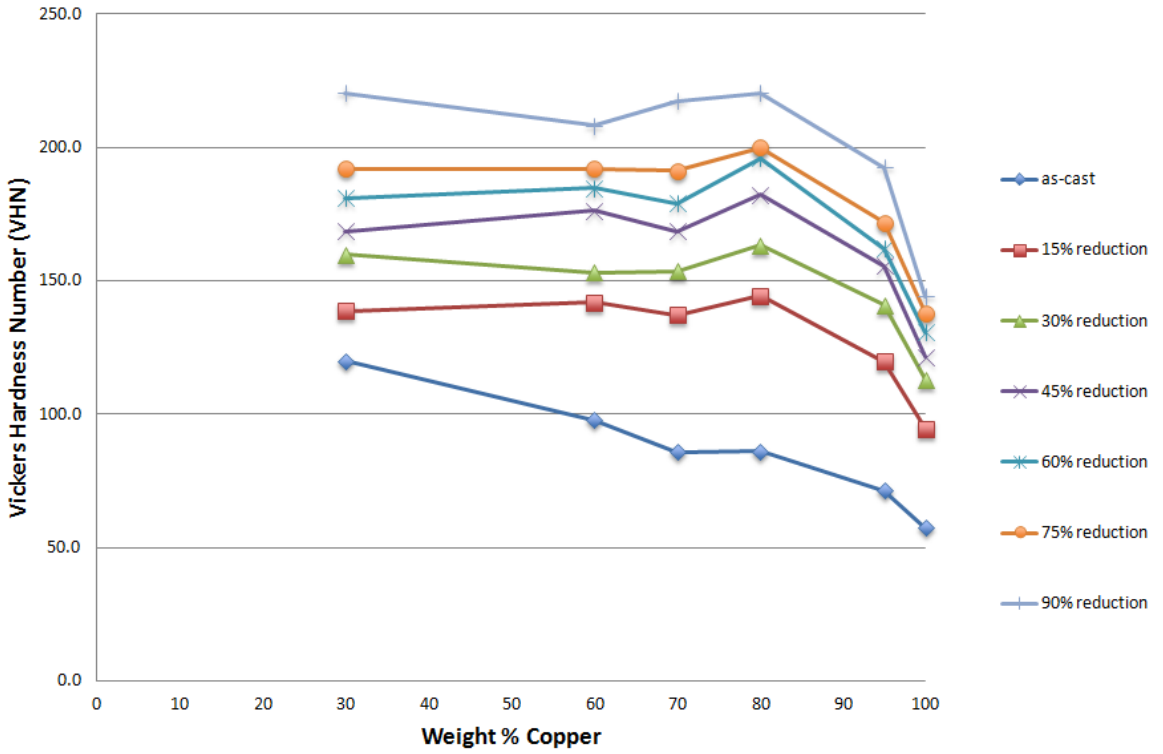

Figure 32. Vickers microhardness vs. composition for cold rolled Cu-Ag alloys. For a given reduction interval, the values of the microhardness do not change significantly as a function of alloy composition for alloy compositions containing between 30 and 80 wt% Cu, although for reductions intervals greater than 15% reduction, the VHN values for the 80 wt% Cu – 20 wt% Ag alloy sample are consistently higher than the VHN values for the other alloy compositions.

7.2.2 Maximum Percent Reduction in Thickness Achieved by Cold Rolling

Results of the cold rolling experiments indicate that over the Cu-Ag alloy compositional range studied, the alloys can be cold worked without annealing to over 90% reduction in

thickness (see Table 7). The percent reductions in thickness achieved in these Cu-Ag samples correspond to the minimum separation distance achievable between the rollers of the rolling mill. Therefore, higher percentages of reduction may be achieved using a mill with smaller rollers, which would exert greater pressure on the material when the rollers are at the minimum separation distance. Some variations in the maximum reduction in thickness can be attributed to the small variations in the initial thicknesses of the cold rolled samples.

Table 7. Maximum Reduction in Thickness of Cu-Ag Alloys by Cold Rolling

Sample ID	**Composition (wt%)**	**Maximum Reduction in Thickness (%)**	**Reduction at Onset of Edge Cracking (%)**	***Δ* (%)**
MIT 5489.I.R2	100% Cu	95.1	82.0	14
MIT 5484.I.R2	95% Cu – 5% Ag	93.0	88.5	5
MIT 5483.I.R2	80% Cu – 20% Ag	92.6	82.8	11
MIT 5482.I.R2	70% Cu – 30% Ag	91.7	81.7	11
MIT 5481.I.R2	60% Cu – 40% Ag	92.1	74.6	19
MIT 5476.I.R2	30% Cu – 70% Ag	90.7	67.0	26

Although the maximum reductions in thickness obtained in each of the alloy compositions and in the pure Cu standard were similar, the percent reductions at which edge cracks developed differed according to the concentration of silver in the alloy. By calculating *Δ*, the percent difference between the maximum reduction in thickness and the reduction in thickness at the onset of edge cracking, it becomes clear that, for these Cu-Ag alloy compositions, as the concentration of Ag increases, *Δ* also increases. This means that for Cu-Ag

alloy compositions with high Ag contents, edge cracking begins with a lesser degree of deformation than for alloys with lower Ag contents. High Δ values indicate a lower malleability with respect to edge crack formation. The malleability of the 30 wt% Cu – 70 wt% Ag alloy is the lowest in this regard. This makes sense because the composition is very close to that of the eutectic alloy, which is very tough due to its lamellar structure. One would expect the pure Cu sample to exhibit the lowest Δ; however, it has the third highest value of Δ.

7.2.3 Microstructural Analysis of Cold Rolled Samples

Figures 33 – 41 show the microstructures of the cold rolled samples at each of 15% reduction intervals up to a reduction of 90% in thickness. These images demonstrate the thinning and elongation of the grains as a result of the cold rolling (reduction in thickness). As the amount of cold working increases, the grains become thinner and more elongated. In the case of the 30 wt% Cu – 70 wt% Ag alloy, which is close to the eutectic composition, the elongation is primarily visible in the Cu-rich β-phase dendrites and in the lamellar eutectic microconstituent (Figures 38 – 41). For comparison, the as-cast microstructure of the 30 wt% Cu – 70 wt% Ag alloy sample is shown in Figure 24. Additionally, for those alloy compositions with higher porosity volume fractions, the pores also become increasingly compressed and more elongated as the amount of cold working increases, often appearing as thin fissures in the metal. This is especially evident in the 60 wt% Cu – 40 wt% Ag alloy (see Figure 37). For alloy compositions which exhibit primary dendrites and eutectic microconstituent, elongation occurs not only in the Cu-rich β-phase dendrites but is also marked in the eutectic microconstituent. Figures 43 – 49

show photomicrographs of the cold-rolled alloy microstructures at magnifications between 100 and 500.

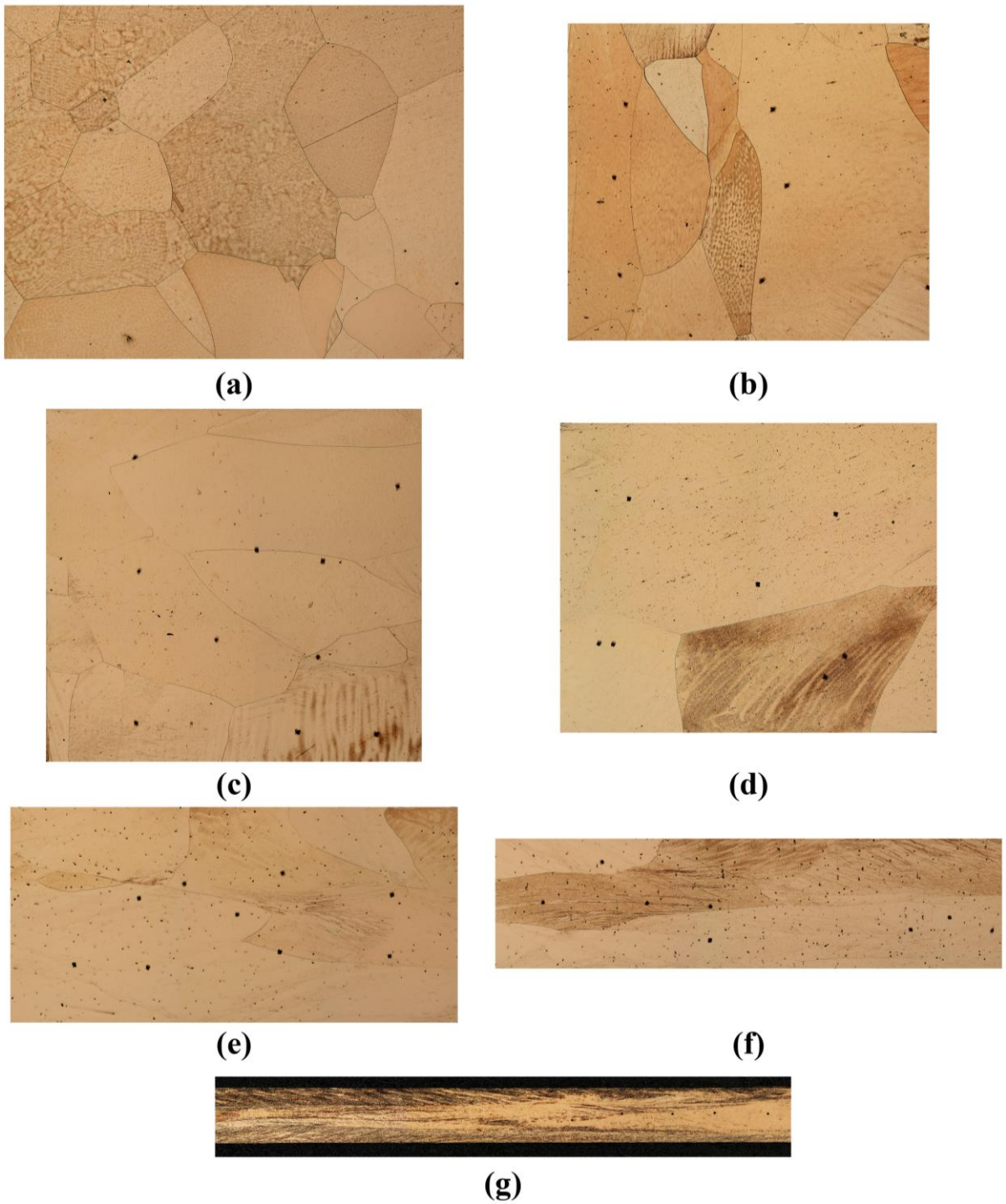

Figure 33. Etched Cold Rolled Microstructures for Pure Cu: (a) as-cast microstructure, (b) 15% reduction, (c) 30% reduction, (d) 45% reduction, (e) 60% reduction, (f) 75% reduction, (g) 90% reduction. MAG: 18; Etchant: 1:9 dilute potassium dichromate

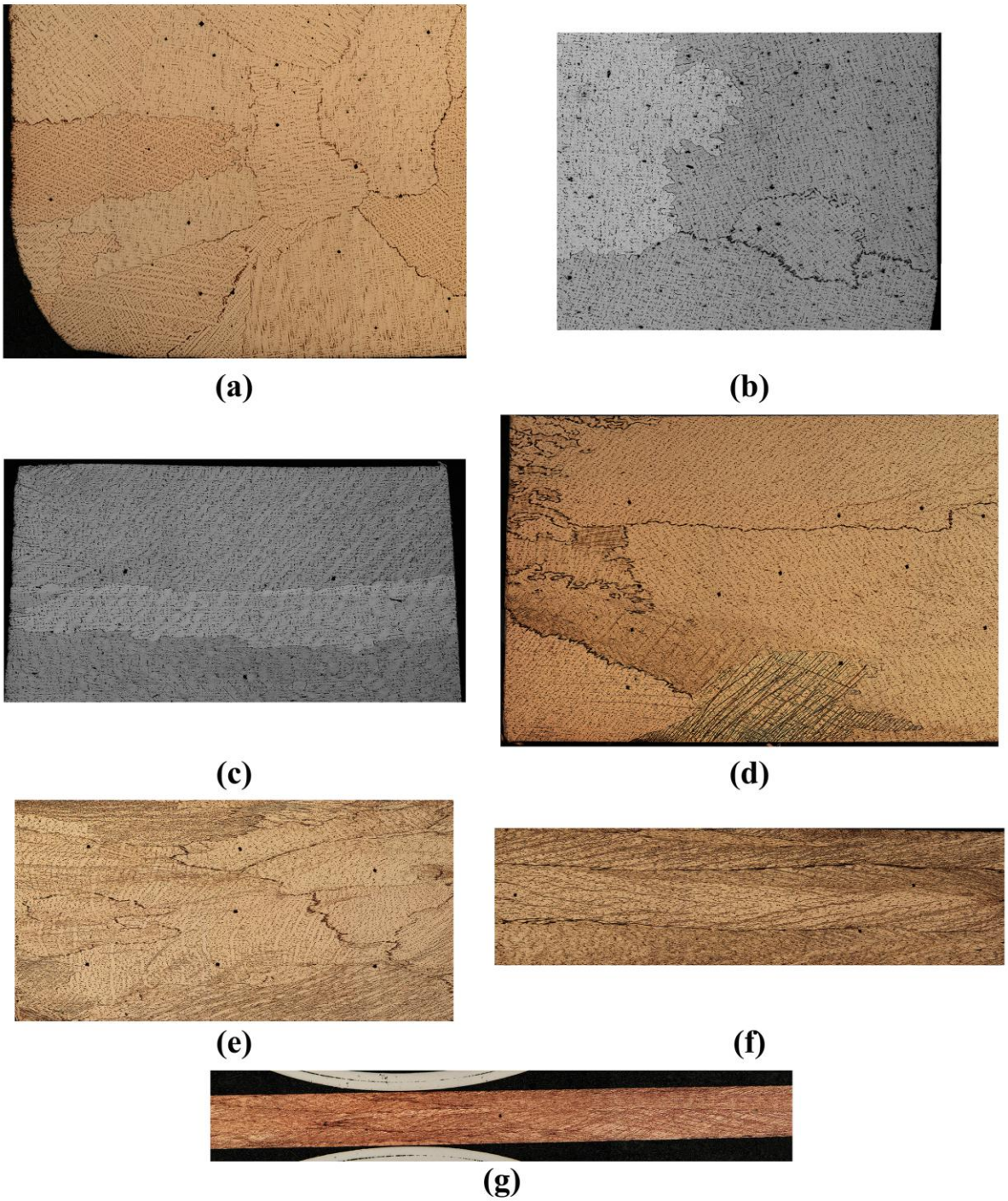

Figure 34. Etched Cold Rolled Microstructures for 95 wt% Cu – 5 wt% Ag: (a) as-cast microstructure, (b) 15% reduction, (c) 30% reduction, (d) 45% reduction, (e) 60% reduction, (f) 75% reduction, (g) 90% reduction. MAG: 18; Etchant: 1:9 dilute potassium dichromate

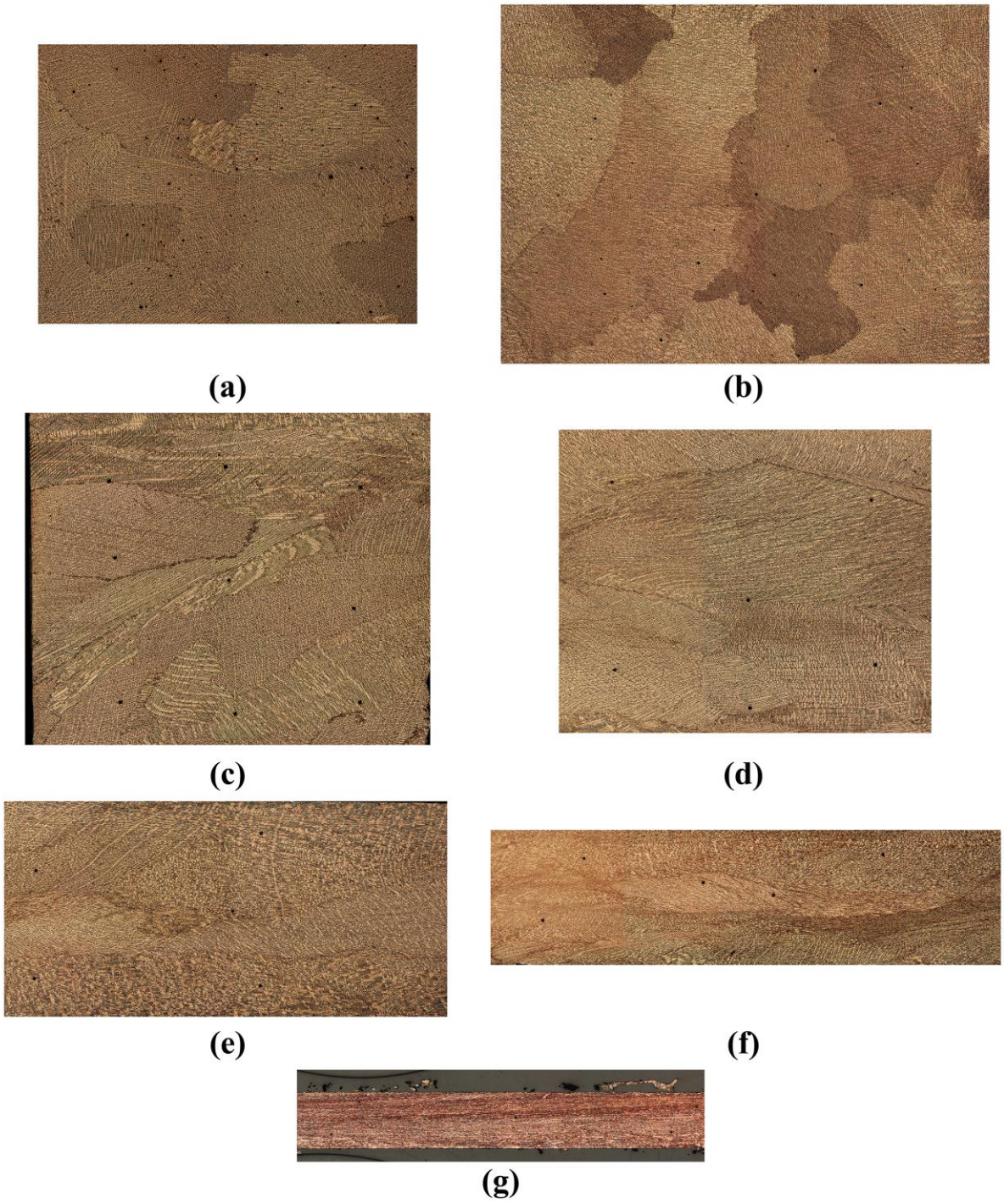

Figure 35. Etched Cold Rolled Microstructures for 80 wt% Cu – 20 wt% Ag: (a) as-cast microstructure, (b) 15% reduction, (c) 30% reduction, (d) 45% reduction, (e) 60% reduction, (f) 75% reduction, (g) 90% reduction. MAG: 18; Etchant: 1:9 dilute potassium dichromate

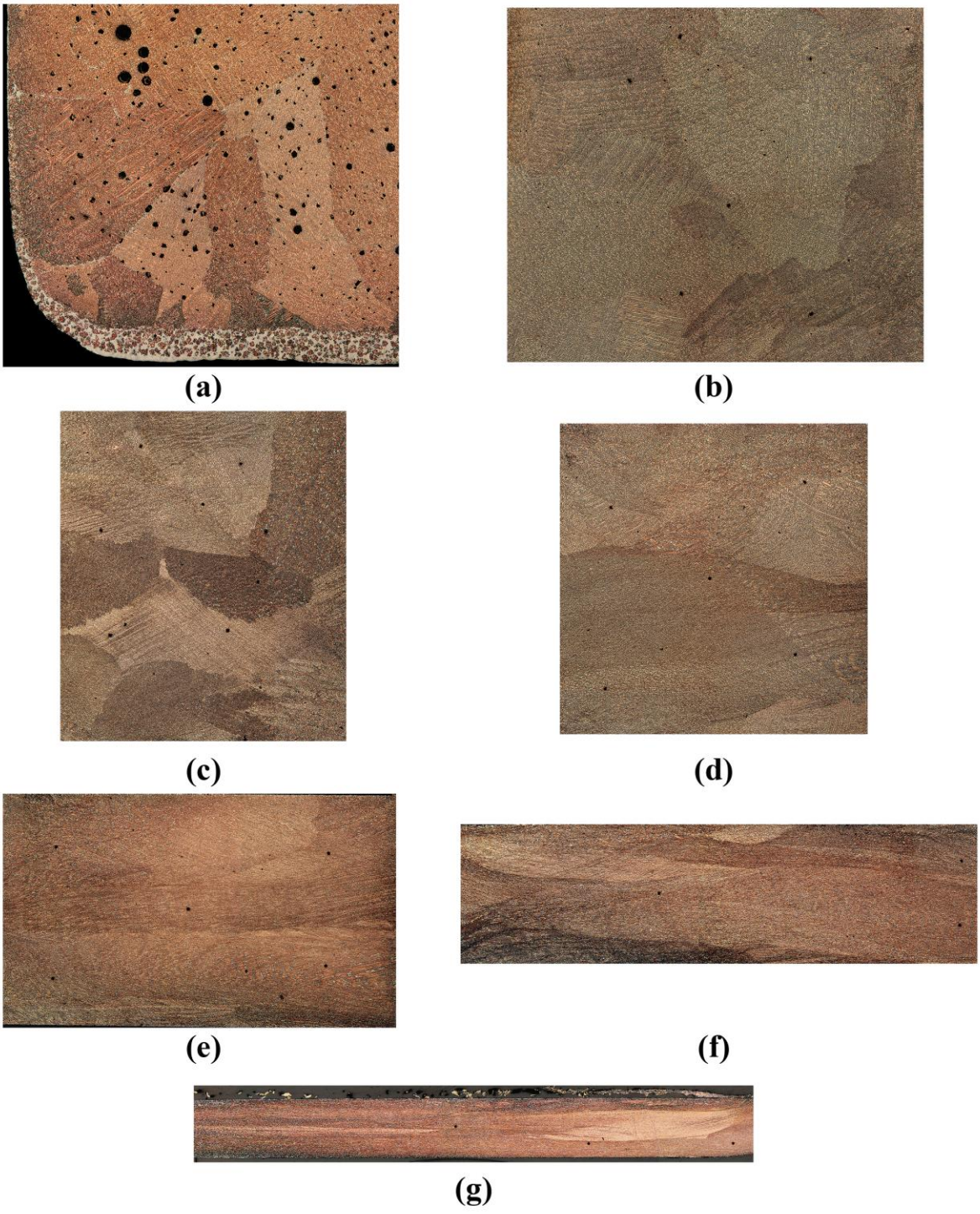

Figure 36. Etched Cold Rolled Microstructures for 70 wt% Cu – 30 wt% Ag: (a) as-cast microstructure, (b) 15% reduction, (c) 30% reduction, (d) 45% reduction, (e) 60% reduction, (f) 75% reduction, (g) 90% reduction. MAG: 18; Etchant: 1:9 dilute potassium dichromate

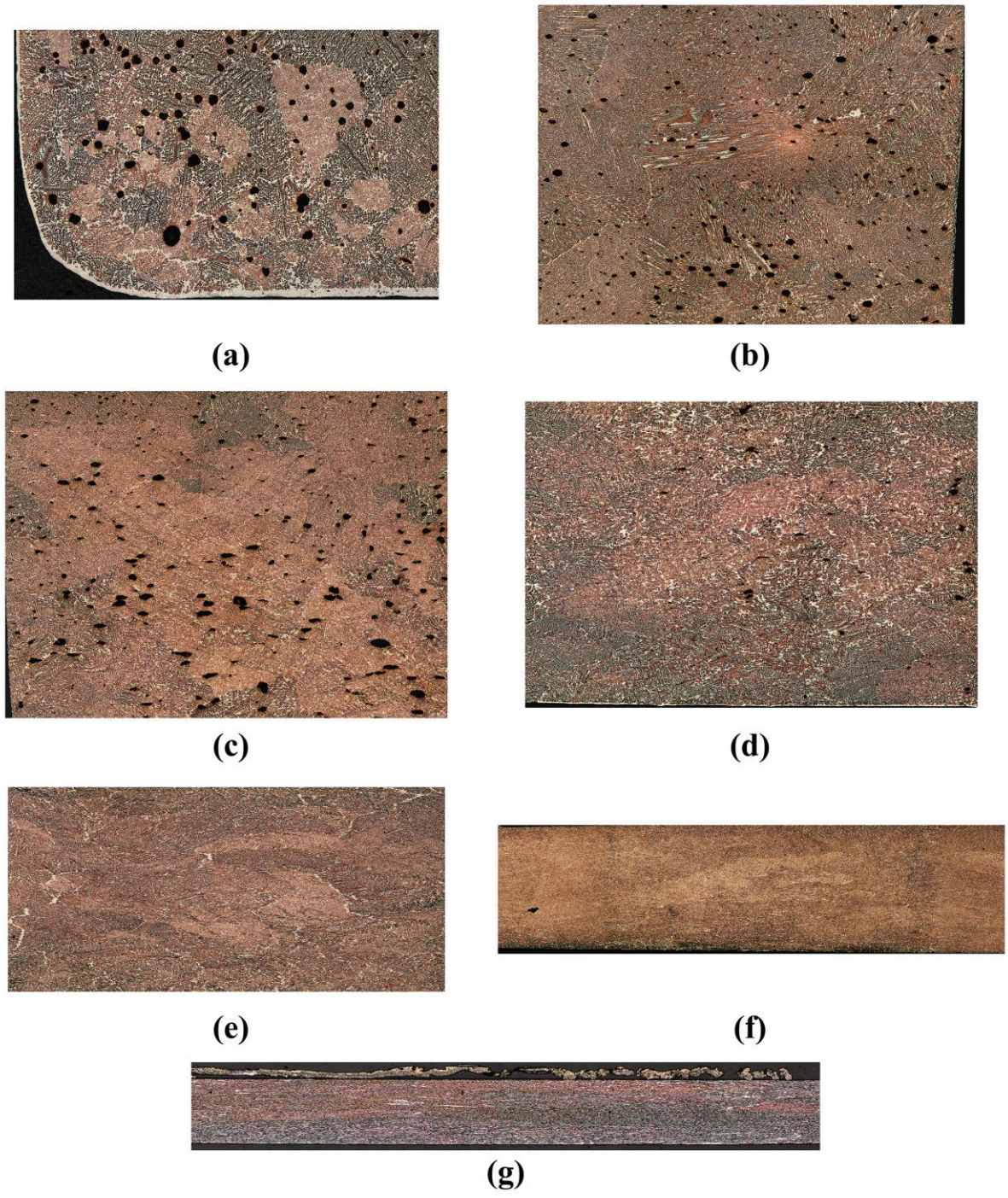

Figure 37. Etched Cold Rolled Microstructures for 60 wt% Cu – 40 wt% Ag: (a) as-cast microstructure, (b) 15% reduction, (c) 30% reduction, (d) 45% reduction, (e) 60% reduction, (f) 75% reduction, (g) 90% reduction. MAG: 18; Etchant: 1:19 dilute potassium dichromate

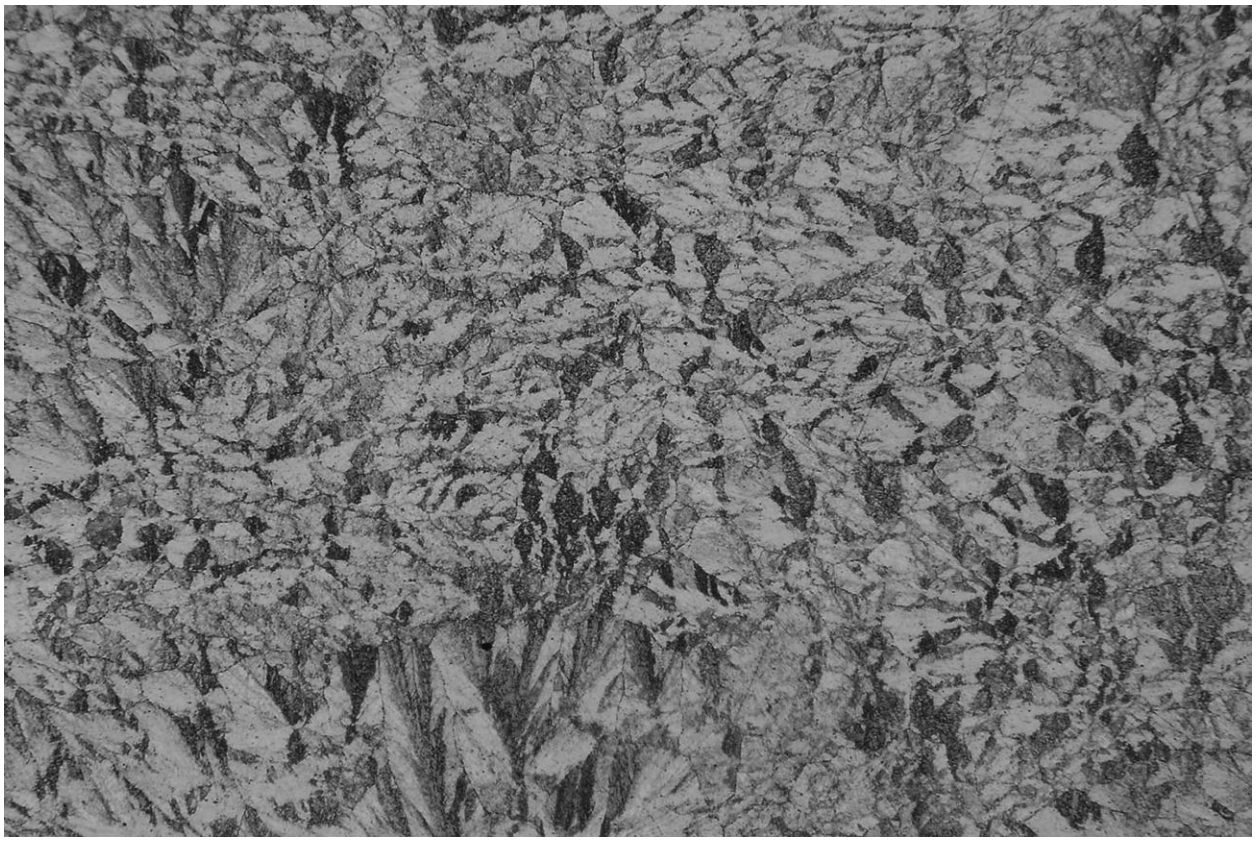

Figure 38. Etched cold rolled microstructure for a 30 wt% Cu – 70 wt% Ag alloy sample reduced by 15% in thickness. The dark regions are the Ag-rich α-phase lamellae and the lighter regions are the Cu-rich β-phase lamellae. MAG: 300; Etchant: ammonium hydroxide + hydrogen peroxide

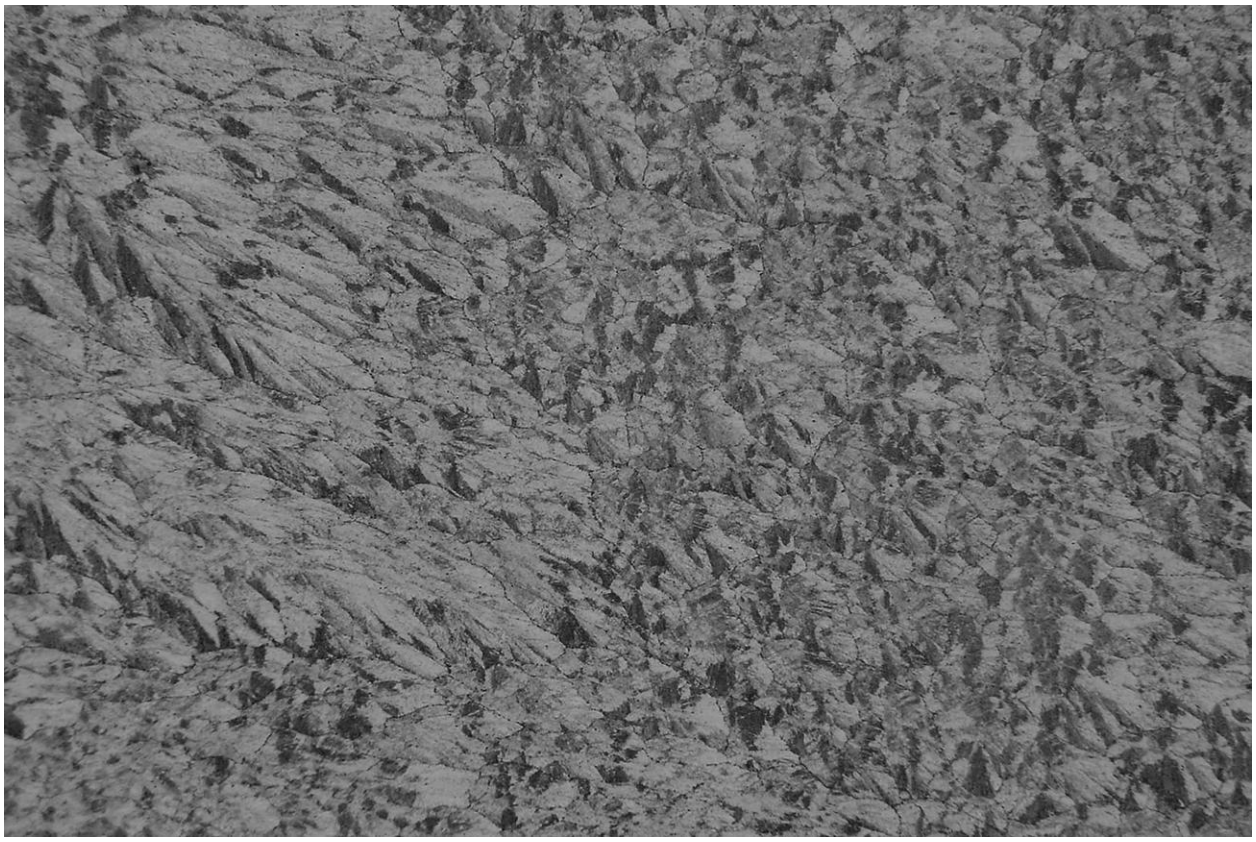

Figure 39. Etched cold rolled microstructure for a 30 wt% Cu – 70 wt% Ag alloy sample reduced by 30% in thickness. The dark regions are the Ag-rich α-phase lamellae and the lighter regions are the Cu-rich β-phase lamellae. MAG: 300; Etchant: ammonium hydroxide + hydrogen peroxide

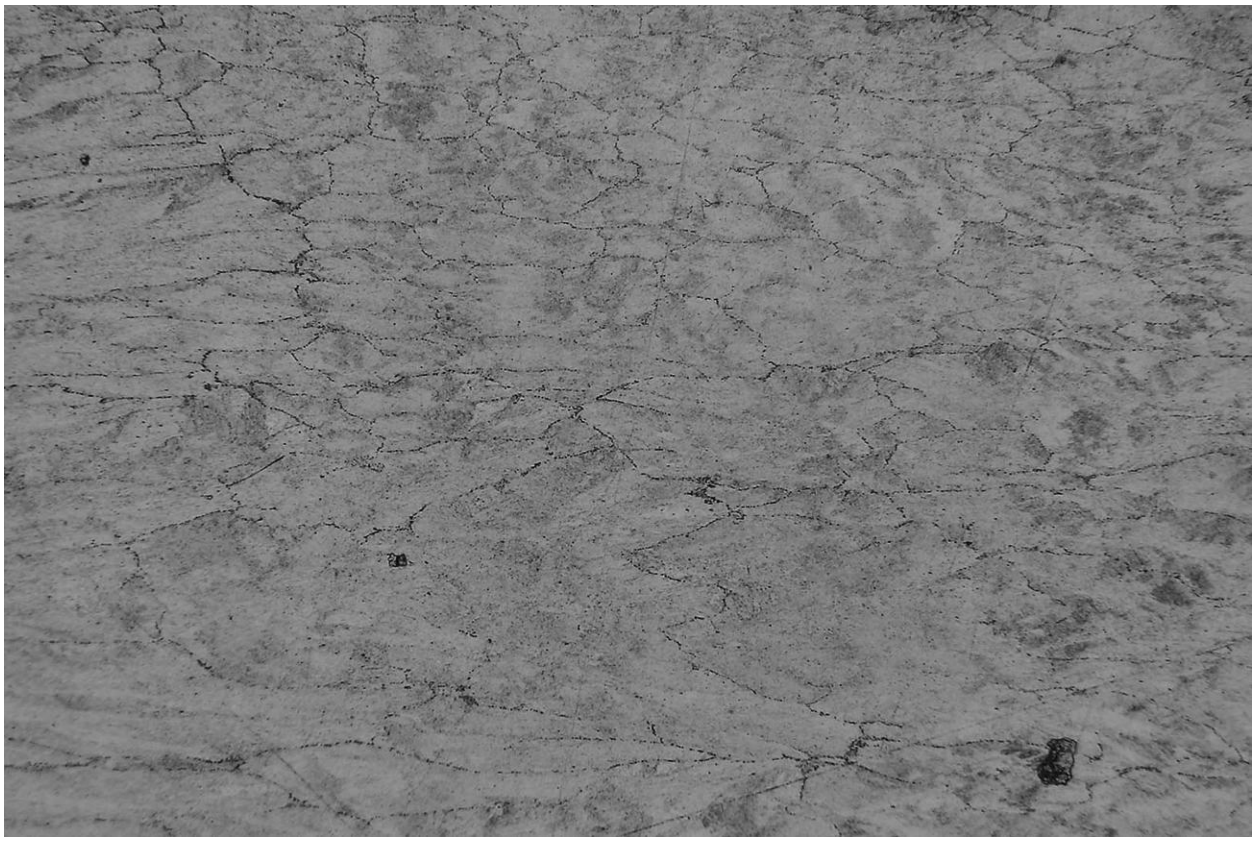

Figure 40. Etched cold rolled microstructure for a 30 wt% Cu – 70 wt% Ag alloy sample reduced by 60% in thickness. The dark regions are the Ag-rich α-phase lamellae and the lighter regions are the Cu-rich β-phase lamellae. In this sample small grains are visible from both the changes in orientation of the lamellae and the etched grain boundaries. The grains have been compressed and elongated compared to the grains seen in Figure 25. MAG: 300; Etchant: ammonium hydroxide + hydrogen peroxide

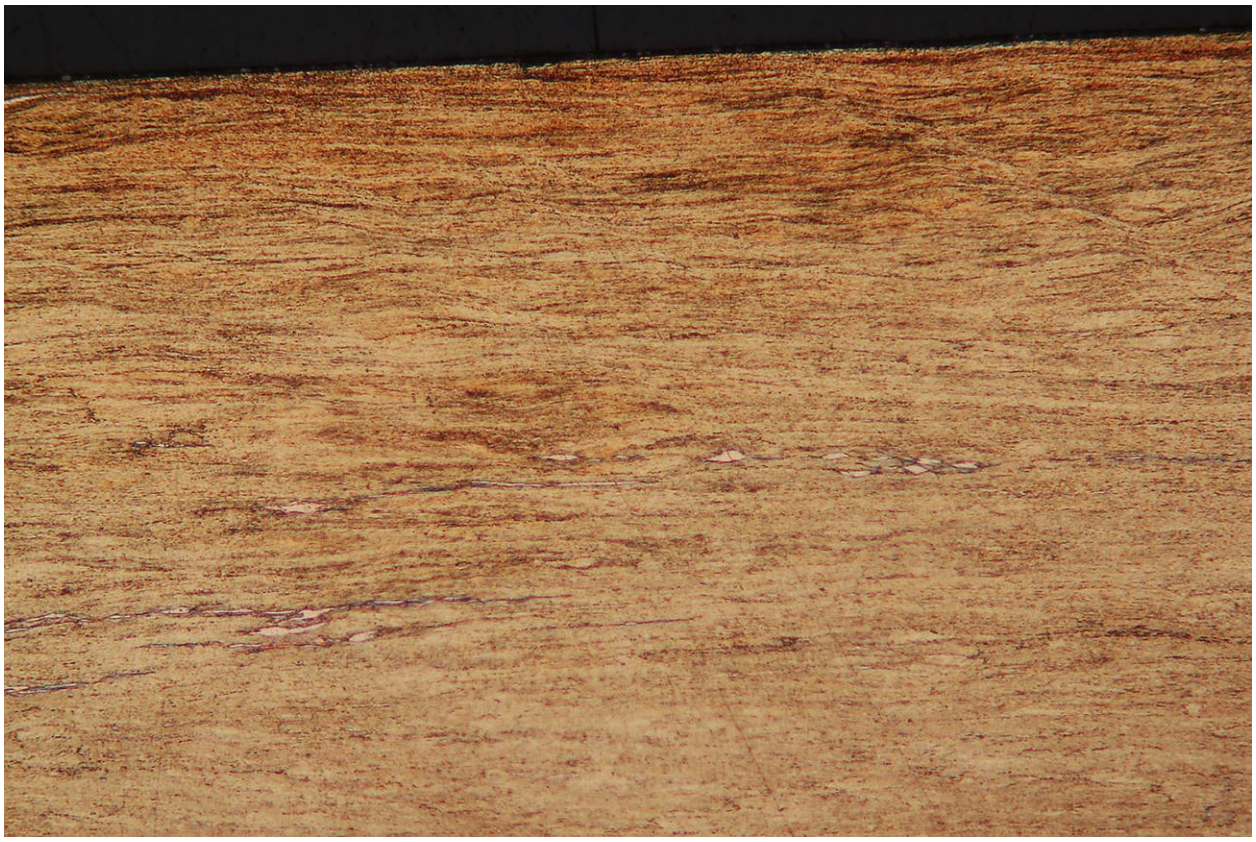

Figure 41. Etched cold rolled microstructure for a 30 wt% Cu – 70 wt% Ag alloy sample reduced by 90% in thickness. The dark regions are the Ag-rich α-phase lamellae and the lighter regions are the Cu-rich β-phase lamellae. Grains are no longer visible. MAG: 300; Etchant: ammonium hydroxide + hydrogen peroxide

The as-cast microstructures show equiaxed grains of varying sizes. At 30% reduction in thickness, the elongation of the grains becomes evident and deformation lines are visible in most samples. In the pure Cu sample, at 30% reduction in thickness, the grain boundaries begin to deform, becoming somewhat jagged, instead of smooth, as shown in Figure 42.

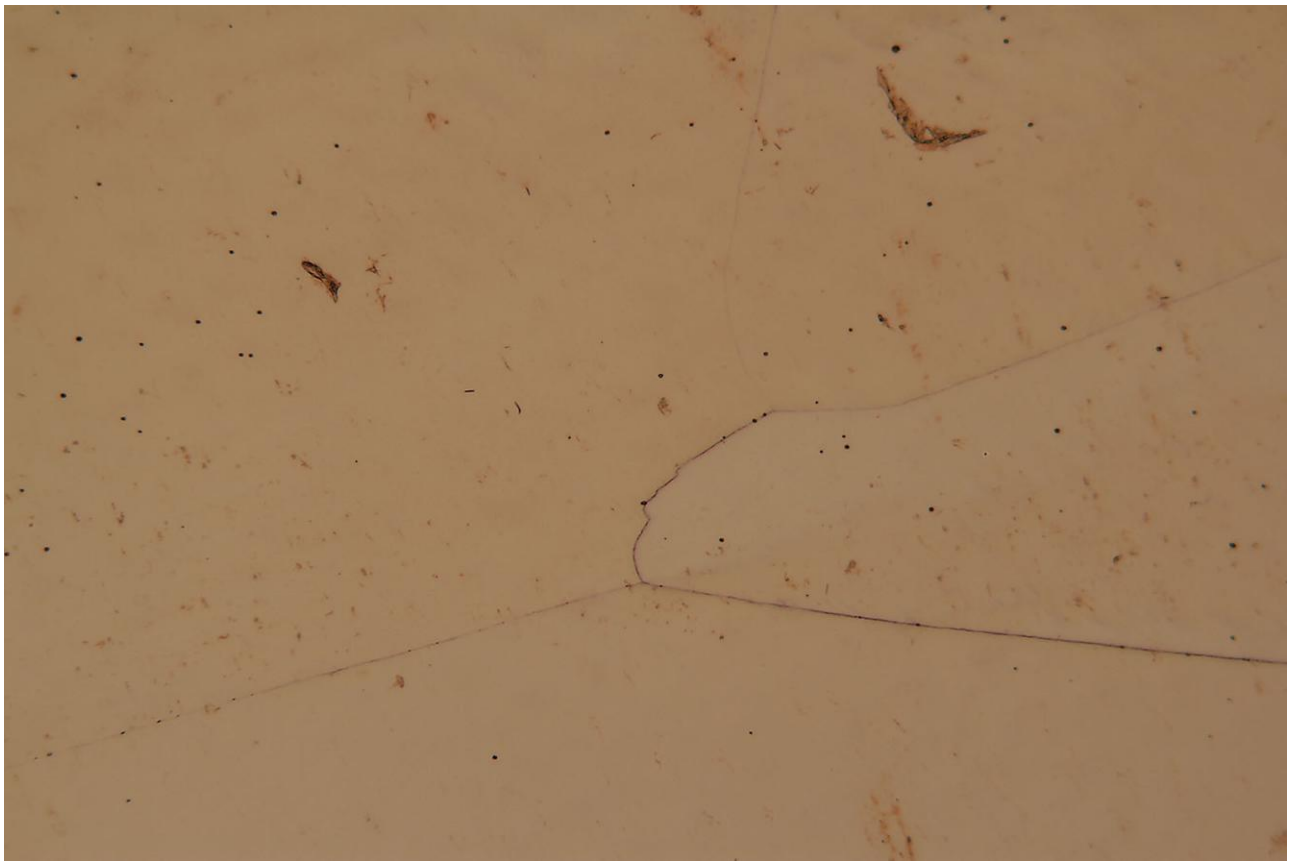

Figure 42. Grain boundary deformation in cold worked pure Cu (30% reduction in thickness). The center grain boundary is beginning to deform and become jagged, while the other grain boundaries remain undeformed and smooth at this degree of cold working. MAG: 300: Etchant: 1:9 dilute potassium dichromate

Figures 43 – 50 show the elongation of primary dendrites and of pools of eutectic microconstituent in the samples that have been reduced by 90% in thickness. Elongation of the Cu-rich dendrites is visible in all samples and the elongation of the eutectic microconstituent is clearly present in the 80 wt% Cu – 20 wt% Ag alloy (Figure 45). As the volume fraction of eutectic microconstituent increases in the alloy, the effect of the plastic deformation is to produce thinner and thinner lamellae of Cu-rich (β) and Ag-rich (α) phases, elongated, and strung out in the direction of rolling. At these extremes of plastic deformation of the as-cast microstructure, all evidence of grain boundaries has been lost, even at magnifications of 500 or more. In the

30 wt% Cu – 70 wt% Ag sample, which is composed primarily of eutectic microconstituent, individual lamellae are also very difficult to distinguish (see Figure 50). The elongation is more visible in the few Cu-rich β-phase dendrites shown in Figure 50.

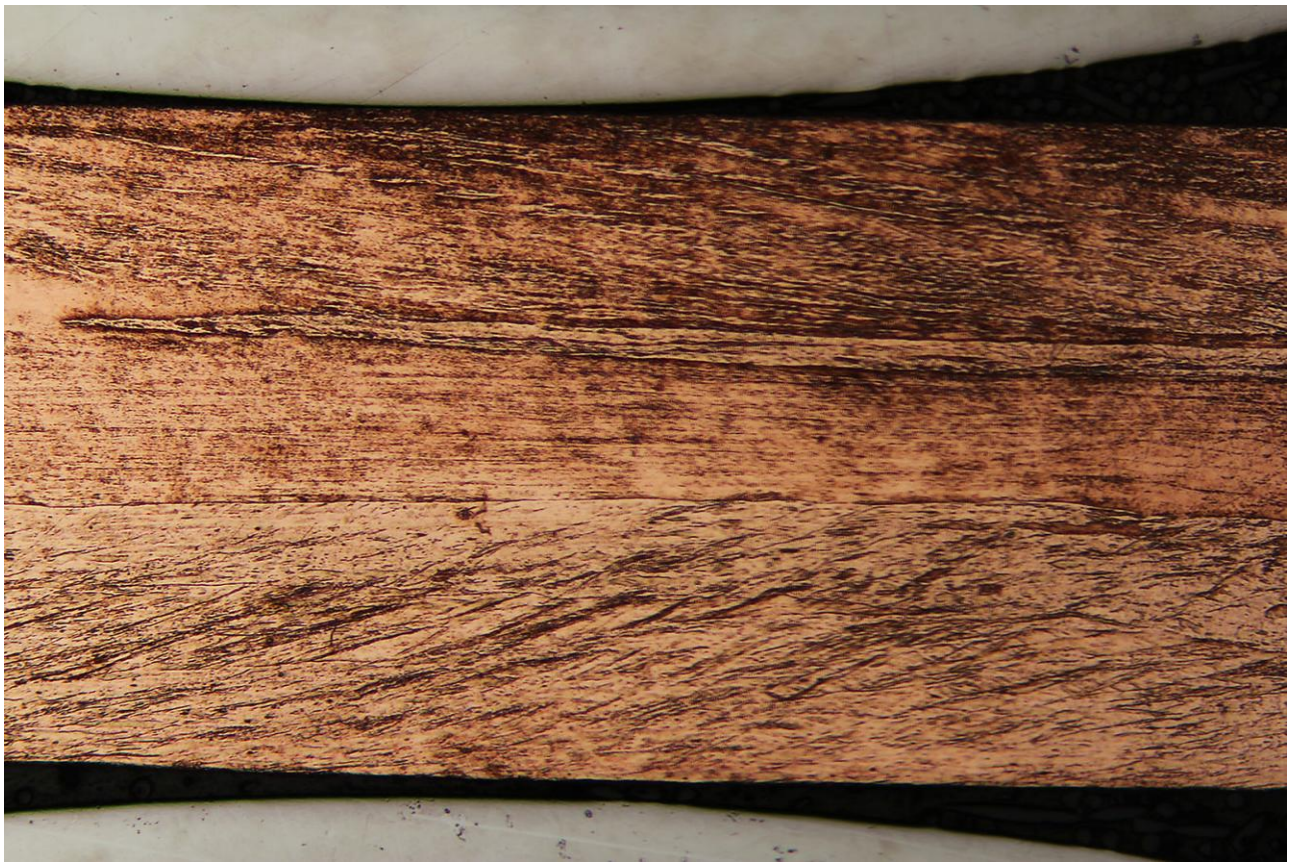

Figure 43. Pure Cu sample reduced 90% in thickness by cold rolling. The diagonal lines across the top and bottom grains are the deformation lines from the cold rolling. MAG: 200; Etchant: potassium dichromate.

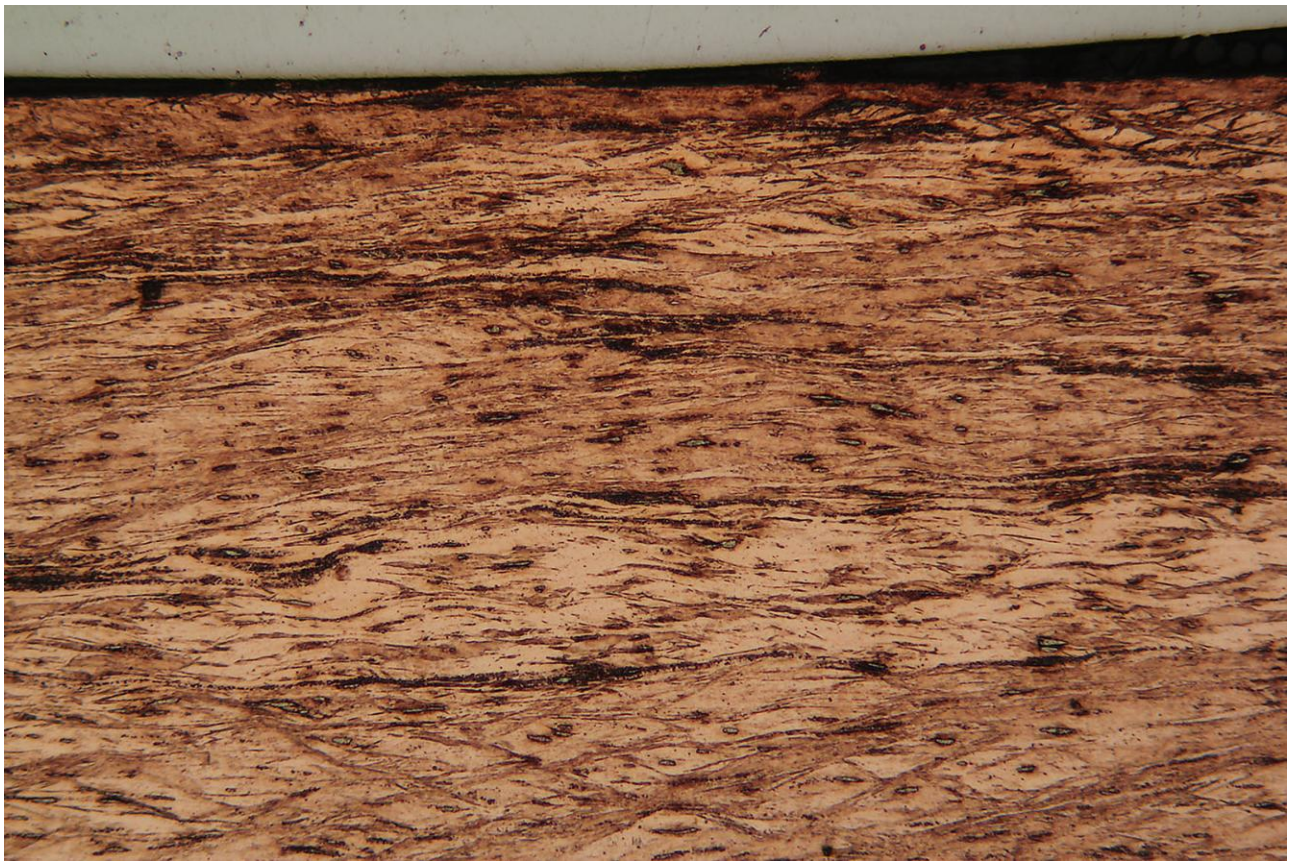

Figure 44. 95 wt% Cu – 5 wt% Ag sample reduced 90% in thickness by cold rolling. Both the grains and the Ag-rich α-phase are elongated in the direction of cold rolling. Deformation lines are present throughout the sample but are more prevalent near the top and bottom edges (the surfaces in contact with the rolling mill). The grains in the center of the sample show less compression than the grains near the edges of the sample. MAG: 300; Etchant: 1:9 dilute potassium dichromate

Figure 45. 80 wt% Cu – 20 wt% Ag sample reduced 90% in thickness by cold rolling. This photomicrograph shows the thinning, elongation, and orientation in the direction of rolling of both the primary Cu-rich dendrites and the eutectic microconstituent. MAG: 300; Etchant: 1:9 dilute potassium dichromate

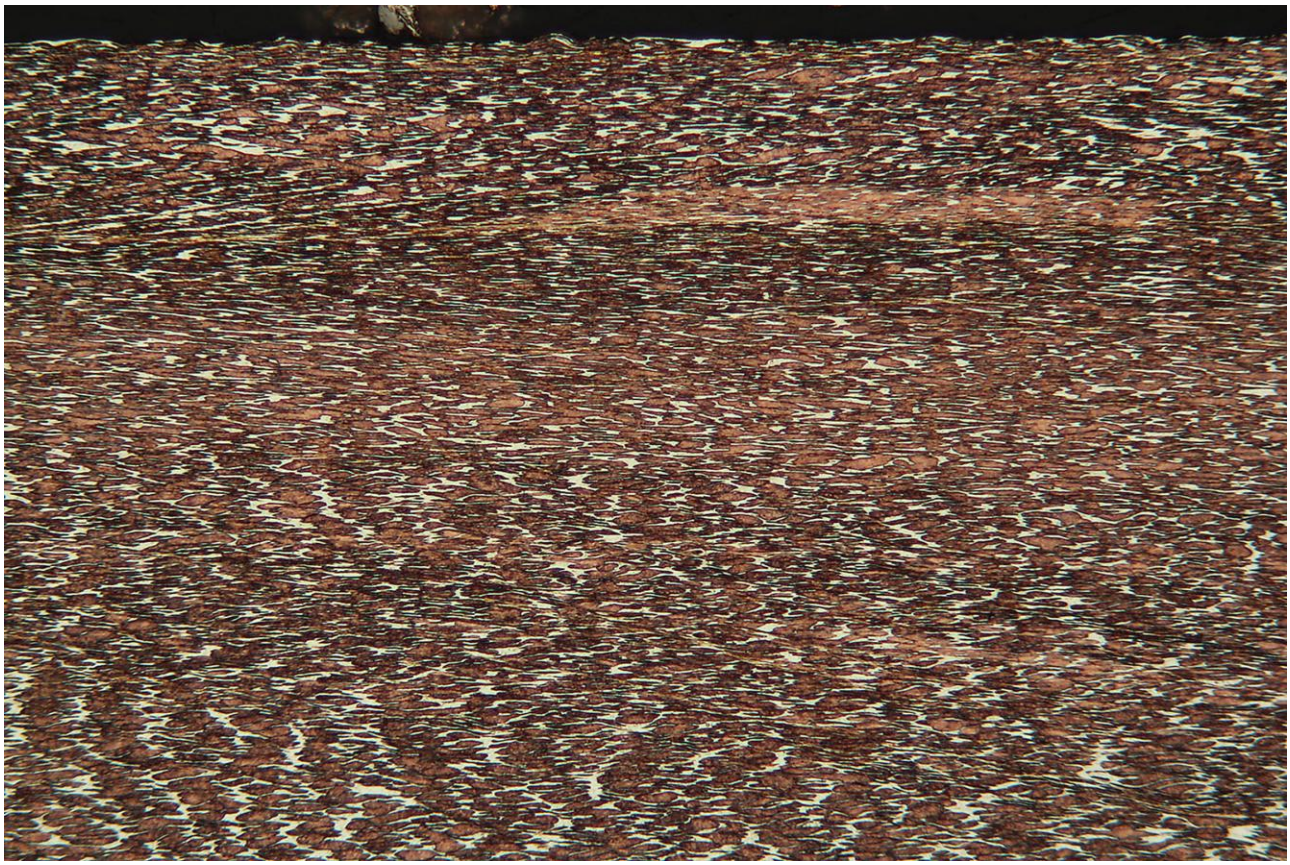

Figure 46. 70 wt% Cu – 30 wt% Ag sample reduced 90% in thickness by cold rolling. This photomicrograph shows the thinning, elongation, and orientation in the direction of rolling of both the primary Cu-rich dendrites and the eutectic microconstituent. The dendrites and pools of eutectic microconstituent at the top of the sample show more elongation and thinning than those closer to the center. From the differential shading of the Cu-rich dendrites the elongation of the grains is also visible. MAG: 300; Etchant: 1:9 dilute potassium dichromate

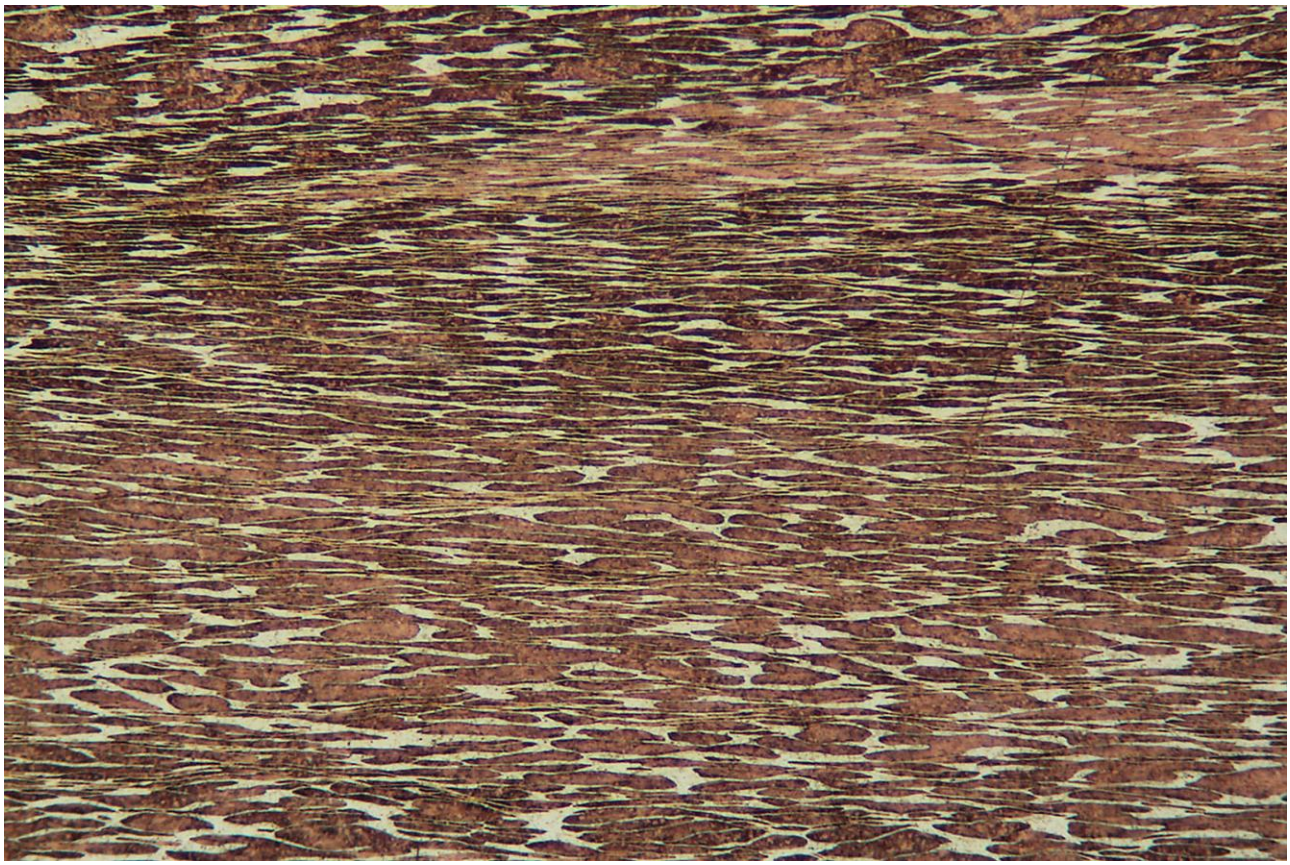

Figure 47. 70 wt% Cu – 30 wt% Ag sample reduced 90% in thickness by cold rolling. The Cu-rich dendrites and the eutectic microconstituent at the top of the sample show more elongation and thinning than those closer to the center. The formation of distinct lamellae of the Cu-rich β-phase and the Ag-rich α-phase is also present. MAG: 750; Etchant: 1:9 dilute potassium dichromate

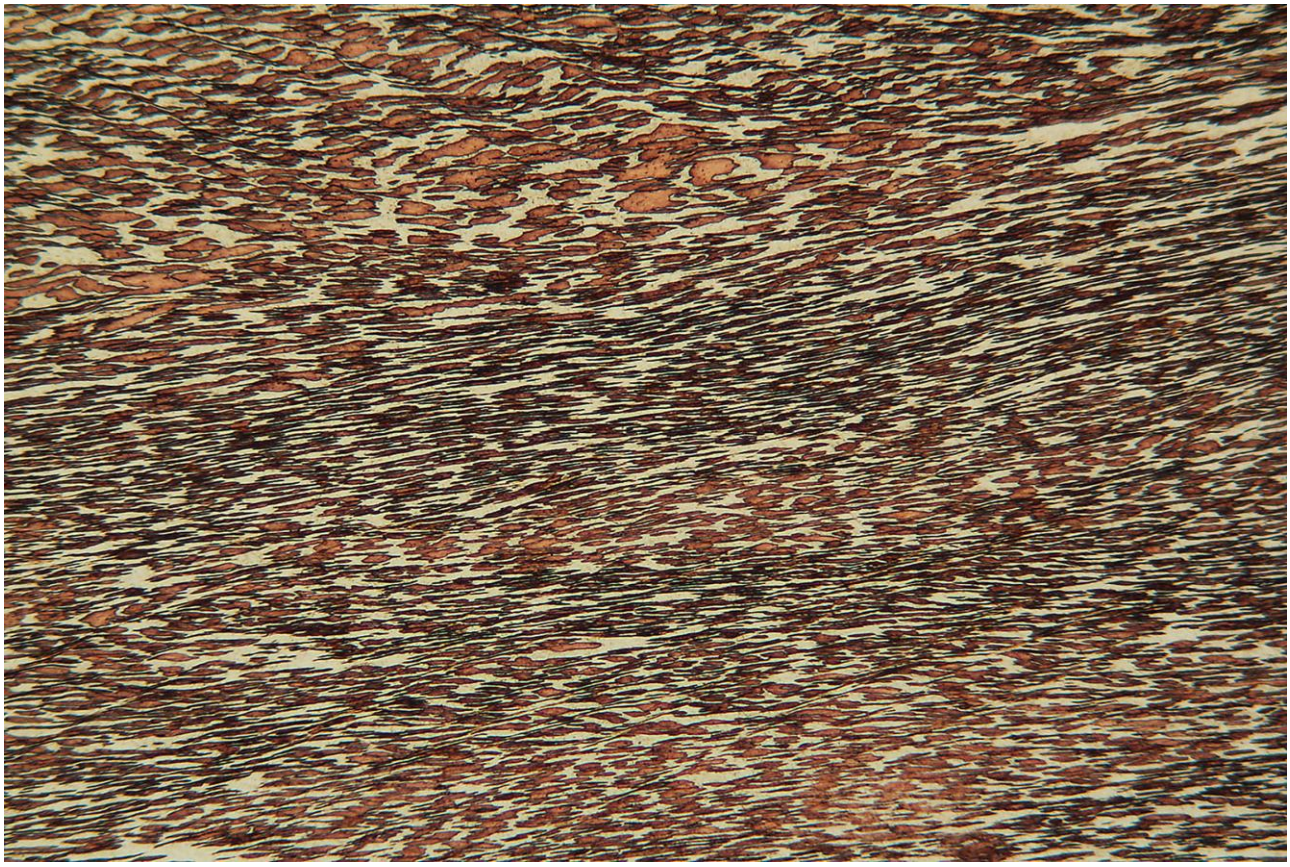

Figure 48. 60 wt% Cu – 40 wt% Ag sample reduced 90% in thickness by cold rolling. The Cu-rich dendrites and eutectic microconstituent are elongated and the dendrites near the center of the sample show more elongation and thinning than those at the top of the sample. From the differential shading of the Cu-rich dendrites the elongation of the grains is also visible. MAG: 300; Etchant: 1:19 dilute potassium dichromate

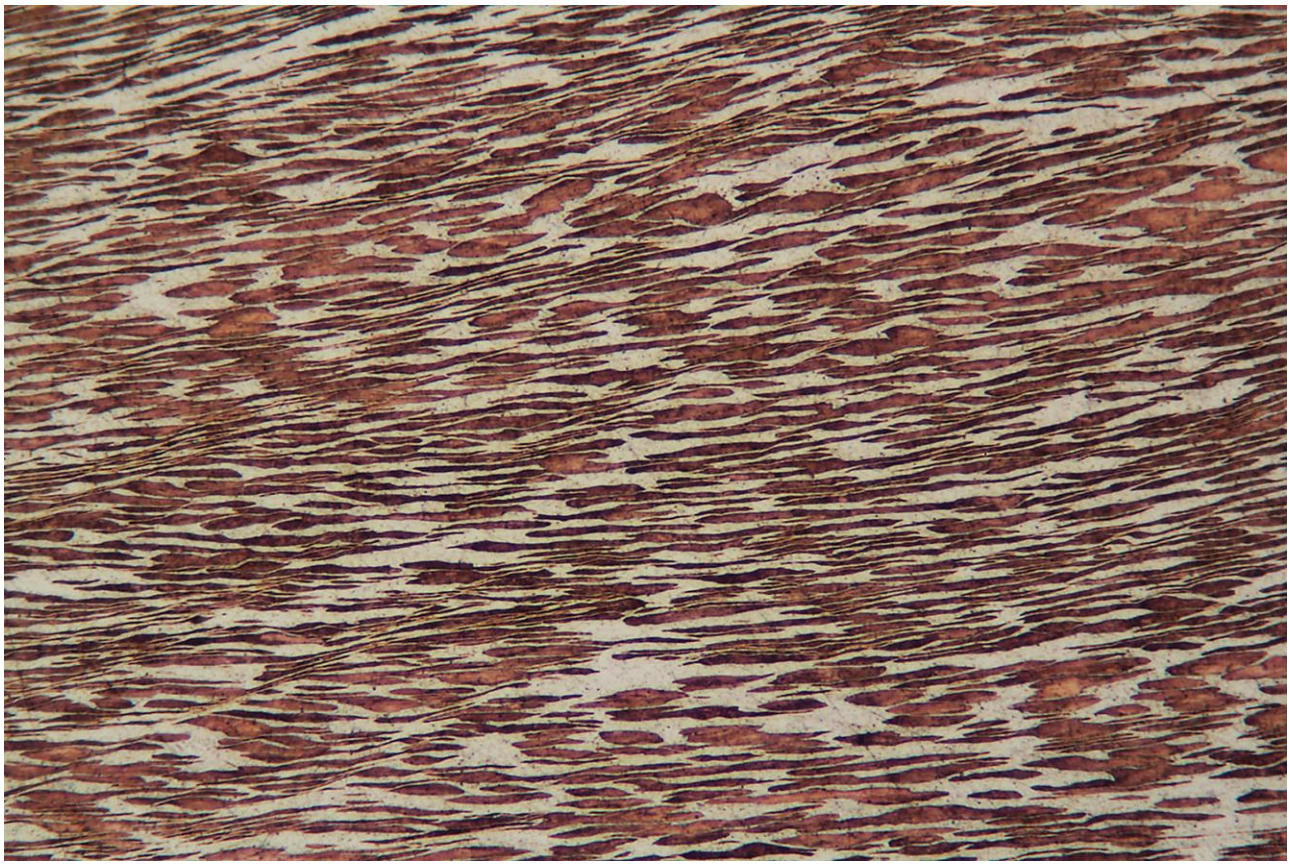

Figure 49. 60 wt% Cu – 40 wt% Ag sample reduced 90% in thickness by cold rolling. Elongation of both the eutectic microconstituent and the Cu-rich dendrites is visible at higher magnifications and distinct lamellae of the Cu-rich β-phase and the Ag-rich α-phase have formed. MAG: 750; Etchant: 1:19 dilute potassium dichromate

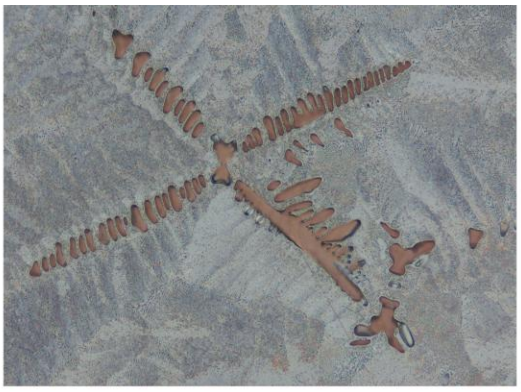

(a)

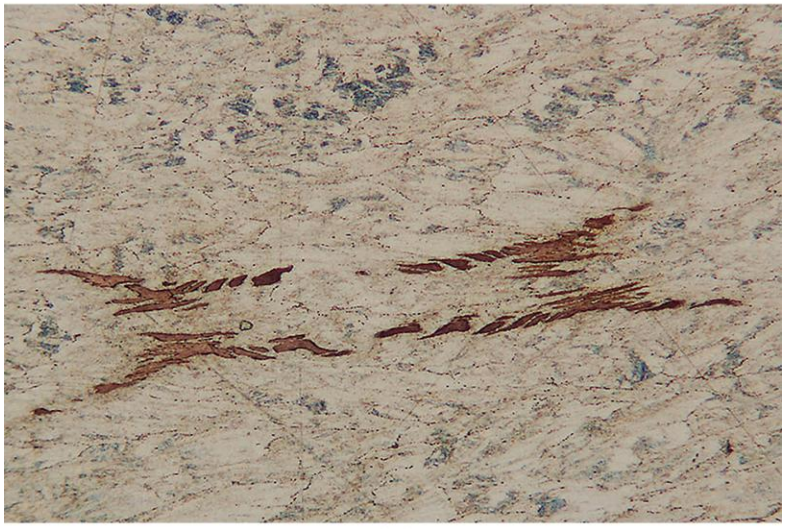

(b)

(c)

Figure 50. Cu-rich β-phase dendrites in 30 wt% Cu – 70 wt% Ag sample: (a) as-cast, (b) 60% reduction, (c) 90% reduction. Dendrites in the as-cast microstructure are equiaxed and undeformed. As the degree of deformation increases, the dendrites become thinner and more elongated, until they are barely discernible from the alternating lamellae of the eutectic microconstituent. MAG: 300; Etchant: (a) chromium oxide, (b-c) ammonium hydroxide + hydrogen peroxide

7.3 Cold Hammering

7.3.1 Maximum Reduction in Thickness Achieved by Cold Hammering

Approximately a 90% reduction in thickness was achieved in both the 95 wt% Cu – 5 wt% Ag and the 30 wt% Cu – 70 wt% Ag samples during cold hammering (see Table 8). Further reductions in thickness could have been achieved had more time been available to work the samples. According to Michael Tarkanian, who carried out the cold hammering, neither alloy composition was significantly more difficult to work than the other. Edge cracking began at 77.1% reduction in the 95 wt% Cu – 5 wt% Ag sample and at a 42.5% reduction in the 30 wt% Cu – 70 wt% Ag sample.

Table 8. Maximum Reduction in Thickness of Cu-Ag Alloys by Cold Hammering

Sample ID	Composition (wt%)	Maximum Reduction in Thickness (%)	Reduction at Onset of Edge Cracking (%)	Δ (%)
MIT 5484.I.H-1	95% Cu – 5% Ag	90.7	77.1	15
MIT 5476.I.H-1	30% Cu – 70% Ag	88.8	42.5	52

Edge cracking began at lower reductions in thickness for the cold hammered samples than for the cold rolled samples. Cold hammering is a much more severe deformation process than cold rolling (Professor Thomas Eagar, personal communication). In cold rolling the same pressure is exerted over the entire sample, whereas in cold hammering, there is much more variation in the applied force, the area over which the force is applied, and the direction in which the force is applied. The earlier onset of edge cracking in the cold hammered samples can be

attributed to these differences in control over the worked area. Both the 95 wt% Cu – 5 wt% Ag and the 30 wt% Cu – 70 wt% Ag alloy are less malleable (higher Δ values) when cold hammered than when cold rolled. Nevertheless, similar percent reductions in thickness were achieved with both cold working processes.

7.3.2 Microstructural Analysis of Cold Hammered Samples

Figure 51 and 52 show the microstructures of the 95 wt% Cu – 5 wt% Ag and the 30 wt% Cu – 70 wt% Ag cold hammered samples.

Figure 51. 95 wt% Cu – 5 wt% Ag alloy sample reduced to 90.7% of the original thickness by cold hammering. Both the Cu-rich β-phase and the Ag-rich α-phase are thin and elongated. Deformation lines, present at the surfaces of the sample where there is more extensive deformation, are not present in the center of the sample. The deformation lines in this sample are more pronounced than the deformation lines in the 95 wt% Cu – 5 wt% Ag alloy sample reduced to the same thickness by cold rolling (see Figure 44). MAG: 300X; Etchant: 1:9 dilute potassium dichromate

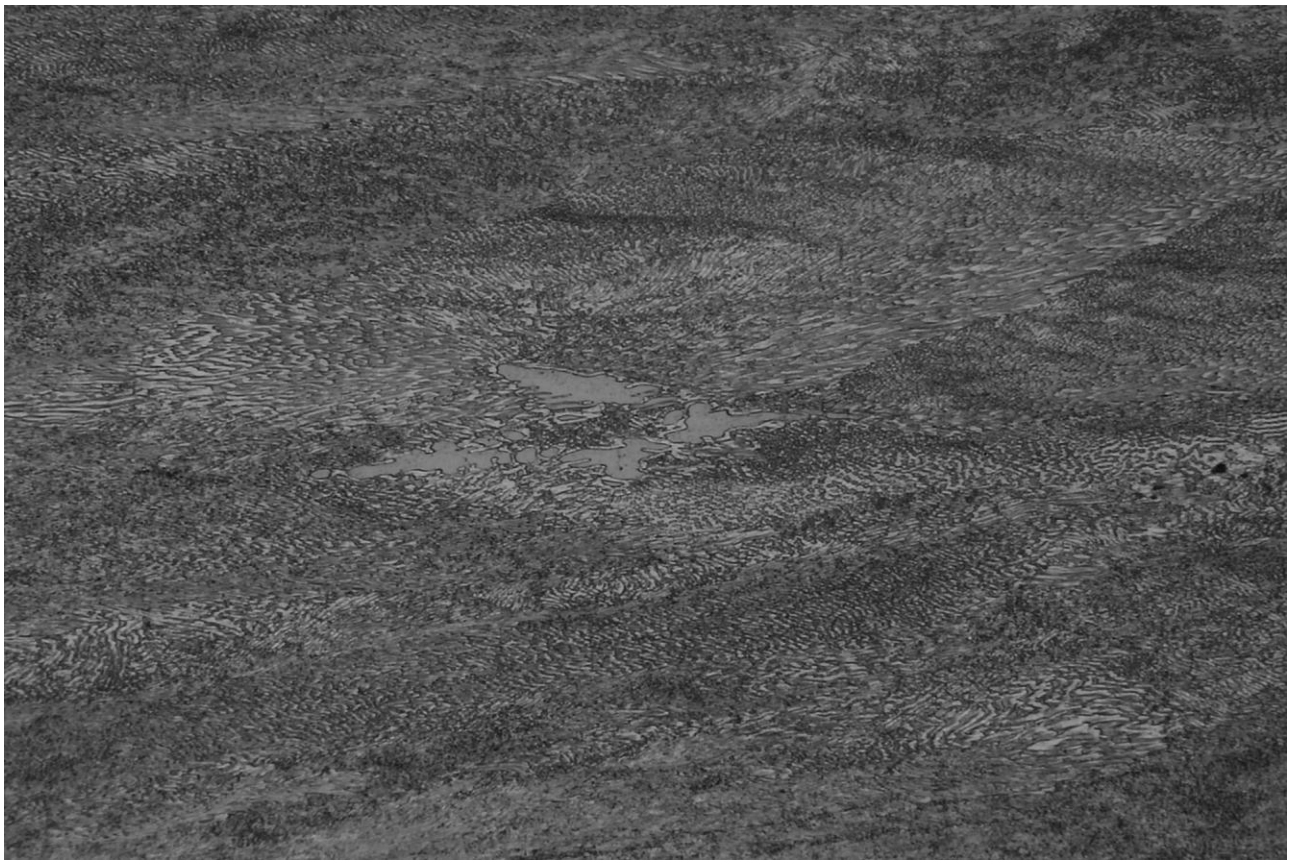

Figure 52. 30 wt% Cu – 70 wt% Ag alloy sample reduced to 88.8% of the original thickness by cold hammering. The Cu-rich β-phase dendrites and the eutectic microconstituent are thin and elongated. Grain boundaries are not visible but remnants of some grain structure can be seen from slight changes in the orientation of the lamellae in the eutectic microconstituent.
MAG: 750; Etchant: ammonium hydroxide + hydrogen peroxide

7.4 Recrystallization Temperature

Analysis of the alloy microstructures at various annealing temperatures along with the relative values of the Vickers microhardness at these temperatures allows the identification of temperature ranges for the recovery, recrystallization, and grain growth phases for the alloys. Figure 53 presents a plot of Vickers microhardness vs. annealing temperature for two Cu-Ag

alloy compositions tested (95 wt% Cu – 5 wt% Ag and 30 wt% Cu – 70 wt% Ag). The Vickers microhardness values at 25º C are those of the cold rolled samples before annealing.

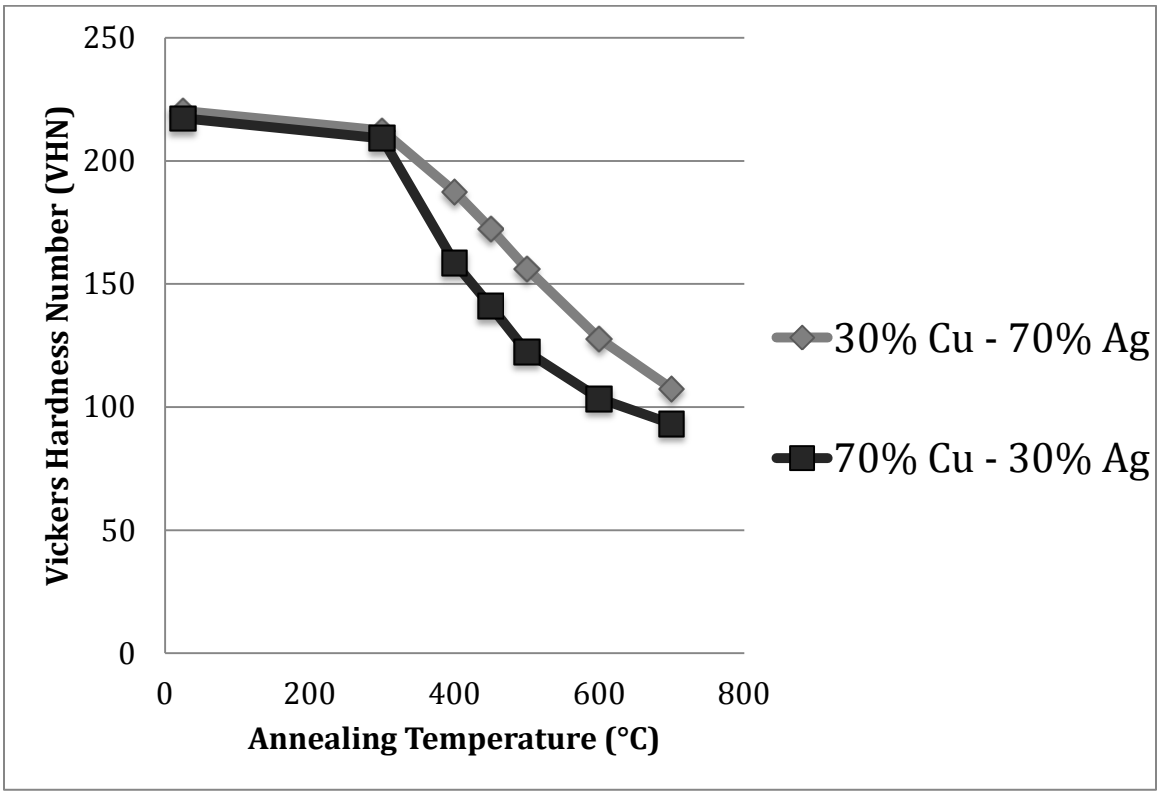

Figure 53. Vickers microhardness vs. annealing temperature for two Cu-Ag alloy compositions. Samples were annealed for 30 minutes at each of the indicated temperatures between 300º C and 700º C. The Vickers microhardness values at 25º C are those of the cold rolled samples before annealing.

The shape of the Vickers microhardness vs. annealing temperature curve is similar to the shape of the curve for tensile strength vs. annealing temperature shown in Figure 15. For temperatures between 0° C and 300° C, the grains are in the recovery phase. For temperatures between 300° C and 700° C (300° C, 400° C, 450° C , 500° C, 600° C, and 700° C), the grains are in the recrystallization phase during which new, strain-free grains nucleate at the grain

boundaries. For temperatures above 700° C, the grains are in the growth phase when they increase in size. Figure 54 shows the partial recrystallization of the grains in the 70 wt% Cu – 30 wt% Ag sample annealed at 500ºC.

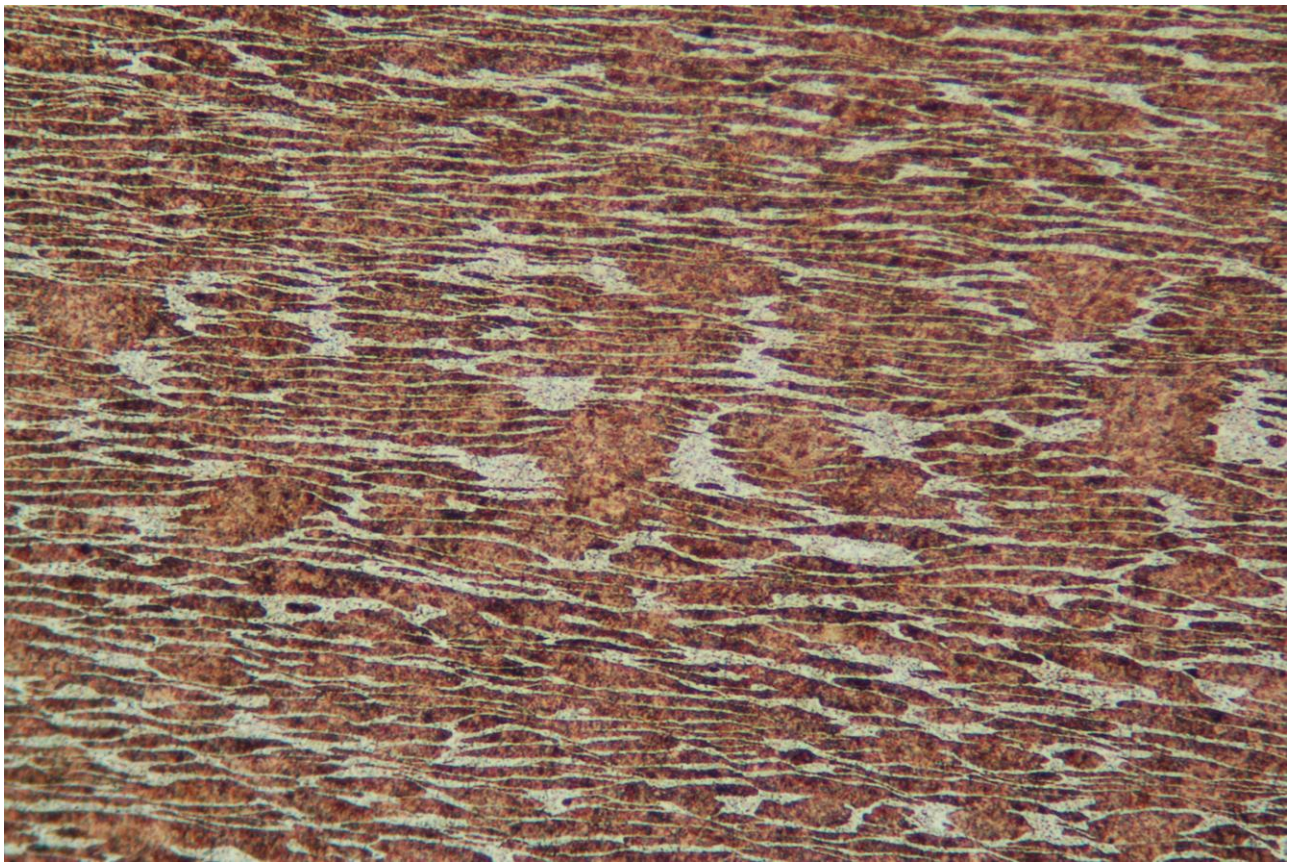

Figure 54. 70 wt% Cu – 30 wt% Ag cold rolled sample (90% reduction) annealed for 30 minutes at 500ºC. Partially recrystallized grains are visible within the Cu-rich dendrites. In some regions of the eutectic microconstituent recrystallized grains are also visible. Magnification: 750; Etchant: 1:9 dilute potassium dichromate

Given the temperature span over which recrystallization occurs (here, 300 – 700° C), the recrystallization temperature – the temperature at which 50% of the grains have recrystallized after 30 minutes of annealing – can be calculated. Assuming that at 300° C the grains are at the end of the recovery phase (no recrystallization) and that at 700° C the grains are entering the

grain growth phase, and assuming also that the hardness vs. temperature curves are approximately linear and follow the same slope for both samples within this temperature range, the recrystallization temperature can be calculated as the average of the temperatures at the beginning and end of the recrystallization phase (300° C and 700° C). Thus for a 90% reduction in thickness of both the 95 wt% Cu – 5 wt% Ag and 30 wt% Cu – 70 wt% Ag alloys the recrystallization temperature is about 500° C given a 30 minute annealing time. Determination of the recrystallization temperature of these two Cu-Ag alloy compositions is important for understanding the development of the silver-enriched surfaces of finished Cu-Ag artifacts.

8 Significance of the Results within an Archaeological Context

Results of the cold working experiments indicate that over the broad copper-silver alloy compositional range studied, no annealing is required during cold hammering or cold rolling to achieve over 90% reductions in metal thickness. The results also indicate that the rate of work hardening and the VHN values are similar for alloy compositions containing between 30 and 80 wt% Cu. The fact that copper-silver alloys exhibit similar malleability and toughness over a broad range of compositions may explain the wide variety of copper-silver alloy compositions found in archaeological artifacts. Since no single composition exhibits significantly improved properties over others, metalsmiths produced objects in a variety of compositions. A particular composition could have been determined, for example, on the basis of the relative abundances and availabilities of copper and silver stocks in each region. One of the factors that must have favored use of copper-silver alloys in object fabrication is that two requirements of the final metal produced could be achieved with relatively low concentrations of silver: namely, high malleability and toughness on one hand and development of enriched, silver-colored surfaces on the other.

In Gordon and Knopf's (2007) study of Cu-Ag alloys, they achieved reductions in thickness similar to those reported here in the alloys they tested by cold rolling the metals, with no intermediate anneals: 68.3 wt% Cu – 29.2 wt% Ag – 2.2 wt% Sn, 74.7 wt% Cu – 24.5 wt% Ag – 0.5 wt% Sn – 0.2 wt% As – 0.1 wt% Pb, 28 wt% Cu – 72 wt% Ag, 34 wt% Cu – 76 wt % Ag. They report having hand hammered a 4 mm thick 68.3 wt% Cu – 29.2 wt% Ag –

2.2 wt% Sn alloy sample (Alloy M)[2] to a reduction in thickness of 55% without any annealing (see Table 9). The same sample was hammered to a 91% reduction in thickness with three intermediate anneals of 500ºC each.

In the experimental research reported here, Michael Tarkanian, an experienced blacksmith, hand-hammered each of two samples measuring 6.1 x 25.4 x 25.4 mm with no intermediate anneals. He achieved a reduction in thickness of 90.7% with the 95 wt% Cu – 5 wt% Ag alloy sample and a reduction of 88.8% with the 30 wt% Cu – 70 wt% Ag alloy sample. Michael Tarkanian also hand-hammered a 75 wt% Cu – 25 wt% Ag cylindrical pouring sprue with a 0.625" (11.55 mm) diameter to a 93.6% reduction in thickness with no intermediate anneals until he observed some edge cracks. The casting method and conditions for this pouring sprue differed from the conditions for the ingots used in this study. The sprue alloy was melted in the forge at MIT using pure Cu and Ag beads. The beads were melted in a ceramic crucible to a temperature of approximately 1000ºC. The molten alloy was poured through the sprue into a two-piece sand mold for small ingots, where it cooled and solidified. Michael Tarkanian hammered the cast sprue cylinder perpendicular to its long axis using first a five pound sledge hammer followed by a 2000 g Peddinghaus hammer, both with polished faces.

Table 9 presents a comparison of cold hammering Cu-Ag alloys as reported in this study with those published by Gordon and Knopf (2007).

[2] The composition of Alloy M was chosen to replicate the composition of a bar of copper-silver alloy stock from Machu Picchu. The composition of Alloy M is very similar to the composition of the pouring sprue (65.7 wt% Cu – 29.8 wt% Ag – 4.5 wt% Sn) from Pambamarca, Ecuador shown in Figure 10.

Table 9. Comparison of Results of Cold Hammering Experiments Reported in this Study and by Gordon and Knopf (2007)

Sample ID	**Composition (wt %)**	**Maximum Reduction in Thickness by Cold Hammering without Annealing (%)**	**Reduction at Onset of Edge Cracking (%)**	***Δ* (%)**
MIT 5484.I.H	95% Cu – 5% Ag	90.7	77.1	15
MIT 5476.I.H	30% Cu – 70% Ag	88.8	42.5	52
MIT 5490	75% Cu – 25% Ag	93.6	93.6	0
Gordon and Knopf (2007) Alloy M	68.3% Cu – 29.2% Ag – 2.2% Sn	55*	50-55	n/a

*The authors report achieving a 91% reduction in thickness of this sample using three intermediate anneals at 500ºC.

These thesis results indicate that the ancient metalsmiths were able to deform plastically their Cu-Ag alloys by hammering them into metal sheets as thin as those reported here. No intermediate annealing was required. Laboratory studies of such artifacts demonstrate that the thicknesses of Andean Cu-Ag alloy sheet metal are of the same order as the thicknesses achieved in this study by hammering. This suggests that the annealing exhibited in the microstructures of copper-silver alloy artifacts was for a different purpose. The ancient metalsmiths were annealing the copper-silver alloy objects intentionally to produce the desired silver surface color. A recrystallization temperature of 500ºC given a 30 minute anneal time was determined for the 30 wt% Cu – 70 wt% Ag and the 70 wt% Cu – 30 wt% Ag alloys tested. This information will be helpful for an understanding of the development of the silver-enriched surfaces present on finished Cu-Ag artifacts from the ancient Americas.

The silver surface color of a finished object was as important if not more important than the mechanical properties of the material of which the object was made in both Mesoamerican and Andean cultures. It conveyed political, economic, and cultural status and was associated with the powerful moon deity (Hosler 1988, 1994, 1995; Lechtman 1979b, 1984a, 1988, 2007). In Andean societies, silver was also associated with the left side or female aspect of the body, in juxtaposition to gold, which was associated with the right side or male aspect (Lechtman 2007). Copper was also often associated with elite and powerful women (Lechtman 2007). An alloy of copper and silver combines the two metals associated with females. Objects made of copper-silver alloys conveyed the symbolism and status of the two individual metals through both the internal composition of the copper-silver alloy objects and through the color of their outer surfaces (Lechtman 1988). This, along with their extraordinary malleability and toughness over a broad compositional range, made copper-silver the alloys of choice throughout the Andean metalworking zone and in Mesoamerica.

9 Conclusions

The primary objective of this thesis was to determine the mechanical and physical properties of copper-silver alloys that were important to understanding why this binary alloy system became central to the metallurgies that developed among prehistoric societies of the Andean zone of South America and Mesoamerica. The development of silver-enriched surfaces during annealing, extraordinary malleability, and toughness of copper-silver alloys made them an alloy of choice throughout the Andean zone and Mesoamerica. Results of the cold rolling and cold hammering experiments reported here indicate that over the copper-silver alloy compositional range studied, the alloys can be cold rolled without annealing to over 90% reduction in thickness. The same is true for the two alloys (95 wt% Cu – 5 wt% Ag and 30 wt% Cu – 70 wt% Ag) that were cold hammered. The results also indicate that the rate of work hardening and the Vickers Hardness Number are similar for alloy compositions containing between 30 and 80 wt% Cu. This suggests that ancient metalsmiths likely annealed the copper-silver alloy artifacts intentionally to produce the desired silver surface color rather than for any improvement in malleability. The recrystallization temperature for the copper-silver alloys tested (70 wt% Cu – 30 wt% Ag and 30 wt% Cu – 70 wt% Ag) is determined to be 500ºC given a 30 minute anneal time.

10 Acknowledgements

I would first like to thank my thesis advisor, Professor Heather Lechtman, for her invaluable guidance and support during my time here at CMRAE. I would also like to thank engineers Anthony Staniovski and Mr. John Riskalla for overseeing the ingot casting process and foundrymen Orlando Ortiz, Paul Fleming, and Fernando Guerrero for their expertise in carrying out the castings.

At MIT I would like to thank Dr. Sidney Carter (CMRAE) for help and patience in teaching me metallography, Michael Tarkanian (DMSE) for his invaluable help and guidance in designing my lab research and in machining, rolling, and hammering my samples; Dr. Michael Short (NSE) for assistance in cold rolling my samples; Professor Thomas Eagar for his advice throughout this project. Janine Recio provided the photograph and photomicrograph of the Cu-Ag Ecuadorian pouring sprue.

I would also like to thank the MIT UROP Office for funding my research for this thesis from Fall 2010 through Summer 2012.

Finally, I would like to thank Professor Dorothy Hosler for introducing me to the application of materials science to archaeology.

11 References

Abbaschian, Reza, Lara Abbaschian, and Robert E. Reed-Hill
2009 *Physical Metallurgy Principles*, 4th edition. Stamford, CT: Cengage Learning.

ASM International
2002a Consil 901. *Alloy Digest.* Upper Montclair, NJ: Engineering Alloys Digest, Inc.

2002b Sterling Silver. *Alloy Digest.* Orange, NJ: Alloy Digest, Inc.

Broniewski, M.W.
1938 Sur les propriétés mécaniques de quelques alliages du cuivre à la température ordinaire. *Revue de Métallurgie 35(8): 333-348.*

Broniewski, M.W. and S. Koslacz
1932 Sur les alliages argent-cuivre. *Comptes rendus* 194: 973-975.

Butts, Alison (ed.)
1975 *Silver: Economics, Metallurgy, Use.* New York: Rober E. Krieger Publishing Co.

Callister, William D.
2003 *Materials Science and Engineering: An Introduction,* 6th edition. New York: John Wiley & Sons, Inc.

Cline, H.E. and D. Lee
1970 Stengthening of Lamellar vs. Equiaxed Ag-Cu Eutectic. *Acta Metallurgica* 18: 315-323.

D'Altroy, Terence N.
1992 *Provincial Power in the Inka Empire.* Washington D.C.: Smithsonian Institution.

Davis, Joseph R.
2001 *Copper and Copper Alloys.* Materials Park, OH: ASM International.

Dewan, Leslie and Dorothy Hosler
2008 Ancient Maritime Trade on Balsa Rafts: An Engineering Analysis. *Journal of Anthropological Research* 64(1): 19-40.

Gordon, Robert and Robert Knopf
2007 Late horizon silver, copper, and tin from Machu Picchu, Peru. *Journal of Archaeological Science* 34: 38-47.

Hansen, M. and K. Anderko
1958 *Constitution of Binary Alloys*. New York: McGraw-Hill Book Co., Inc.

Hosler, Dorothy
1988 The Metallurgy of Ancient West Mexico. In *The Beginning of the Use of Metals and Alloys,* R. Maddin (Ed.), 328-343. Cambridge: MIT Press.

1994 *The Sounds and Colors of Power: The Sacred Metallurgical Technology of Ancient West Mexico.* Cambridge, MA: MIT Press.

1995 Sound, Color and Meaning in the Metallurgy of Ancient West Mexico. *World Archaeology* 27(1): 100-115.

Hörz, G. and M. Kallfass
2000 The treasure of gold and silver artifacts from the Royal Tombs of Sipán, Peru – a study on the Moche metalworking techniques. *Materials Characterization* 45: 391-420.

Lechtman, Heather N.
1971 Ancient methods of gilding silver: Examples from the Old and New Worlds. In *Science and Archaeology,* R.H. Brill (Ed.), 2-30. Cambridge: Massachusetts Institute of Technology

1979a A Pre-Columbian Technique for Electrochemical Replacement Plating of Gold and Silver on Copper Objects. In *Journal of Metals* 31:154-60.

1979b Issues in Andean metallurgy. In *Pre-Columbian Metallurgy of South America,*ed. E.P. Benson, 1-40. Washington, D.C.: Dumbarton Oaks.

1980 The Central Andes: Metallurgy Without Iron. In *The Coming of the Age of Iron,* T.A. Wertime and J.D. Muhley (Eds.), 269-334. New Haven, Connecticut: Yale University Press.

1982 New perspectives on Moche metallurgy: Techniques of gilding copper at Loma Negra, Northern Peru. *American Antiquity* 47(1):3-30.

1984a Andean value systems and the development of prehistoric metallurgy. *Technology and Culture* 25(1):1-36.

1984b Pre-Columbian surface metallurgy. *Scientific American* 250(6):56-63.

1988 Traditions and styles in Central Andean metalworking. In *The Beginning of the Use of Metals and Alloys,* R. Maddin (Ed.), 344-78. Cambridge: MIT Press.

2007 The Inka and Andean Metallurgical Tradition. In *Variations in the Expression of Inka Power,* eds. R. Matos, R. Burger, and C. Morris 323-365. Washington, D.C.: Dumbarton Oaks.

in press Andean Metallurgy in Prehistory. In *A Global Perspective in Metallurgy,* Ben W. Roberts and Christopher P. Thornton, (Eds.). New York: Springer Publications.

Lechtman, Heather N., Lee A. Parsons, and William J. Young
1975 Seven Matched Hollow Gold Jaguars from Peru's Early Horizon. *Studies in Pre-Columbian Art and Archaeology* 16: 1-46.

Lothrop, Samuel K., William F. Foshag, and Joy Mahler
1959 *Pre-Columbian Art.* New York: Phaidon Publishers Inc.

Menzel, Dorothy
1976 *Pottery Style and Society in Ancient Peru: Art as a Mirror of History in the Ica Valley, 1350 - 1570.* Berkeley, CA: University of California Press

Rhines, Frederick N.
1956 *Phase Diagrams in Metallurgy.* New York: McGraw-Hill Book Co. 52-55.

Root, William C.
1949 The Metallurgy of the Southern Coast of Peru. *American Antiquity* 15(1): 10-37.

Silverman, Helaine
1993 *Cahuachi in the Ancient Nasca World.* Iowa City, IA: University of Iowa Press.

12 Appendix A

The tables on the following pages present published data for the chemical compositions of copper-silver alloy artifacts found throughout the Andean zone of South America and western Mexico. The artifact compositions encompass the entire range of compositions in the Cu-Ag alloy system. For the artifacts from William Root's 1949 study, the letter codes listed in the "Provenance" column refer to the specific sites from which the artifacts were excavated. All the sites are located along the southern coast of Peru. The dates corresponding to the time periods (i.e. Middle Ica II, Late Chincha I) listed in this same column can be found in the chronologies by Dorothy Menzel (1976) and Helaine Silverman (1993). The Ica culture occupied the Ica Valley on the southern coast of Peru from about A.D. 900 to 1476 (Silverman 1993). The Chincha culture also occupied the southern coast of Peru, but was farther north than the Ica, from about A.D. 1150 to 1476 (Menzel 1976).

Key

MAG = Museo Antropológico, Guayaquil, Ecuador

RMG = Regional Museum, Guadalajara, Mexico

Artifact ID	Description	Provenance	Reference	Wt. % Cu	Wt. % Ag	Wt. % Au	Wt. % Sn	Wt. % Pb	Wt. % As	Wt. % Fe	Wt. % Si	Wt. % Mg	Wt. % Bi	Wt. % Zn	Wt. % Ni	Wt. % Sb	Composition Analysis Method
18400	Disc	Machu Picchu, Peru	Gordon and Knopf 2007	3.7	93.1	0	3.1	0	0								JEOL JKA-8600 microprobe
17821	shawl pin	Machu Picchu, Peru	Gordon and Knopf 2007	19	81	0	0	0	0								JEOL JKA-8600 microprobe
18449	alloy bar	Machu Picchu, Peru	Gordon and Knopf 2007	68.6	29.4	0	2.2	0.2	0.06								JEOL JKA-8600 microprobe
17872	head band	Machu Picchu, Peru	Gordon and Knopf 2007	74.7	24.5	0	0.49	0.09	0.24								JEOL JKA-8600 microprobe
	silver ingot	Royal Tombs of Sipán, Peru	Hörz and Kallfass 2000	66.9	28.8	1.3	0	0									ICP-OES
	human-head bead	Royal Tombs of Sipán, Peru	Hörz and Kallfass 2000	79	20	1	0	0									structural analysis based on distribution of Cu-rich and Ag-rich phases
	peanut bead	Royal Tombs of Sipán, Peru	Hörz and Kallfass 2000	15	85	0	0	0									structural analysis based on distribution of Cu-rich and Ag-rich phases
	ceremonial knife (tumi)	Royal Tombs of Sipán, Peru	Hörz and Kallfass 2000	50	50	0	0	0									structural analysis based on distribution of Cu-rich and Ag-rich phases
816	bell	RMG	Hosler 1994	3.08	96.92	0	0	0	0	0		0	0	0	0	0	atomic absoprtion spectrometry
19	sheet	RMG	Hosler 1994	3.67	96.3	0	0	0	0	0		0	0	0	0	0	atomic absoprtion spectrometry
2586	sheet	RMG	Hosler 1994	4.78	95.22	0	0	0	0	0		0	0	0	0	0	atomic absoprtion spectrometry
Fx2a	sheet	RMG	Hosler 1994	5.5	94.4	0.011	0.08	0	0	0		0	0	0	0	0	atomic absoprtion spectrometry
874	open ring	RMG	Hosler 1994	6.28	93.43	0.29	0	0	0	0		0	0	0	0	0	atomic absoprtion spectrometry
Fx1	sheet	RMG	Hosler 1994	6.43	93.3	0.28	0	0	0	0		0	0	0	0	0	atomic absoprtion spectrometry
Fx	sheet	RMG	Hosler 1994	6.67	93.33	0.034	0	0	0	0		0	0	0	0	0	atomic absoprtion spectrometry
Fx4	pendant	Michoacan, Mexico	Hosler 1994	11.1	88.84	0.059	0	0	0	0		0	0	0	0	0	atomic absoprtion spectrometry
21	sheet	RMG	Hosler 1994	14.7	85.22	0.072	0	0	0	0		0	0	0	0	0	atomic absoprtion spectrometry
F885	wire	Colima, Mexico	Hosler 1994	29.5	70.5	0	0	0	0	0		0	0	0	0	0	atomic absoprtion spectrometry
2518	tweezer	RMG	Hosler 1994	44.1	55.9	0	0	0	0	0		0	0	0	0	0	atomic absoprtion spectrometry
3655	open ring	Salango, Ecuador	Hosler 1994	53.57	45.5	0.39	0	0.41	0	0			0.11	0.02	0	0	atomic absoprtion spectrometry
3681	nose ring	MAG	Hosler 1994	56.34	42.9	0.35	0	0.14	0.12	0			0.14	0.01	0	0	atomic absoprtion spectrometry
3740	open ring	MAG	Hosler 1994	59.682	40.18	0	0	0.02	0.06	0.008			0	0	0.02	0.03	atomic absoprtion spectrometry
3772	axe	MAG	Hosler 1994	65.205	33.34	0	0.02	0.13	1.25	0.03			0	0	0.02	0.005	atomic absoprtion spectrometry
3686	open ring	MAG	Hosler 1994	65.385	33.64	0.38	0.01	0.02	0.43	0.005			0.1	0	0.02	0.01	atomic absoprtion spectrometry

Artifact ID	Description	Provenance	Reference	Wt. % Cu	Wt. % Ag	Wt. % Au	Wt. % Sn	Wt. % Pb	Wt. % As	Wt. % Fe	Wt. % Si	Wt. % Mg	Wt. % Bi	Wt. % Zn	Wt. % Ni	Wt. % Sb	Composition Analysis Method
234		RMG	Hosler 1994	66.1	33.9	0	0	0	0	0		0	0	0	0	0	atomic absoprtion spectrometry
3631	bowl	MAG	Hosler 1994	67.983	30.86	0.14	0.001	0.36	0.57	0.005			0.07	0.001	0	0.01	atomic absoprtion spectrometry
3633	bowl	MAG	Hosler 1994	68.01	30.04	0.14	0	0.76	0.75	0.02			0.24	0	0.02	0.02	atomic absoprtion spectrometry
3632	bowl	MAG	Hosler 1994	70.431	28.2	0.37	0.002	0.06	0.85	0.02			0.05	0	0.007	0.01	atomic absoprtion spectrometry
3674	nose ring	MAG	Hosler 1994	70.79	28.3	0.55	0	0.02	0.12	0			0.15	0	0.02	0.05	atomic absoprtion spectrometry
3741	open ring	MAG	Hosler 1994	72.51	27.37	0	0	0.01	0.06	0.02			0	0	0.01	0.02	atomic absoprtion spectrometry
3742	open ring	MAG	Hosler 1994	73.409	25.82	0	0.004	0.05	0.7	0.007			0	0	0	0.01	atomic absoprtion spectrometry
F23	sheet	RMG	Hosler 1994	73.88	26.1	0.024	0	0	0	0		0	0	0	0	0	atomic absoprtion spectrometry
23b	sheet	RMG	Hosler 1994	73.88	26.1	0.024	0	0	0	0		0	0	0	0	0	atomic absoprtion spectrometry
3719	axe-money	MAG	Hosler 1994	75.366	24.58	0	0	0.01	0.03	0.004			0	0	0	0.01	atomic absoprtion spectrometry
3746	open ring	MAG	Hosler 1994	75.57	24.09	0	0.03	0.1	0.15	0.01			0	0.02	0	0.03	atomic absoprtion spectrometry
939/76	tweezer	RMG	Hosler 1994	75.69	24.3	0.009	0	0	0	0		0	0	0	0	0	atomic absoprtion spectrometry
3727	axe-money	MAG	Hosler 1994	77.434	21.36	0	0	0.13	1.02	0.006			0	0	0.02	0.03	atomic absoprtion spectrometry
3689	nose ring	MAG	Hosler 1994	77.692	21.5	0.37	0	0.06	0.33	0			0.04	0.008	0	0	atomic absoprtion spectrometry
3734	open ring	MAG	Hosler 1994	81.18	17.73	0	0.01	0.01	1.02	0.03			0	0	0.01	0.01	atomic absoprtion spectrometry
3747	open ring	MAG	Hosler 1994	81.972	17.76	0	0.01	0.06	0.17	0.008			0	0.01	0	0.01	atomic absoprtion spectrometry
F229	loop or earring	Michoacan, Mexico	Hosler 1994	85.7554	14.2	0.015	0	0.0296	0	0		0	0	0	0	0	atomic absoprtion spectrometry
3683	open ring	MAG	Hosler 1994	91.627	7.94	0.1	0	0.01	0.23	0.003			0.05	0	0.01	0.03	atomic absoprtion spectrometry
3739	open ring	MAG	Hosler 1994	91.86	7.33	0	0	0.02	0.75	0			0	0	0.02	0.02	atomic absoprtion spectrometry
3620	axe	MAG	Hosler 1994	95.958	3.64	0.08	0	0.11	0.16	0			0.02	0.002	0.03	0	atomic absoprtion spectrometry
MIT 137	bead	Malpaso, Lurín Valley, Peru	Lechtman 1979	41	45.3	0	0	<0.1	0	0.1	0.1-10	trace					
	pallion of solder from gold sheet jaguar figurine	Pampa Grande, Lambayque Valley, Peru	Lechtman 1988	48	52	0	0	0	0	0	0	0					quantitative metallurgy
	sandal bulk metal	Sipan	Lechtman 2007	45	50	2.5	0	2.55									
	ingot	Sipan tomb	Lechtman 2007	47	50	2.5	0	0									
	cylindrical bead		Lechtman 2007	80	18	1	0	0									

Artifact ID	Description	Provenance	Reference	Wt. % Cu	Wt. % Ag	Wt. % Au	Wt. % Sn	Wt. % Pb	Wt. % As	Wt. % Fe	Wt. % Si	Wt. % Mg	Wt. % Bi	Wt. % Zn	Wt. % Ni	Wt. % Sb	Composition Analysis Method
4446C	silver colored plate fragment	M, Middle Ica II	Root 1949	1	94	5	0	0									Bowdoin College chemical laboratory
4919	silver colored pendants (10)	T-a, Late Ica II	Root 1949	3	97	0	0	0									Bowdoin College chemical laboratory
5263	silver colored dish	T-h, 1, Late Ica I	Root 1949	3	95	2	0	0									Bowdoin College chemical laboratory
5275	silver colored earplug stems (2)	T-h, 1, Late Ica I	Root 1949	3	96	1	0	0.01-1									Bowdoin College chemical laboratory
5261	silver colored dish	T-h, 1, Late Ica I	Root 1949	3	97	0	0	0									Bowdoin College chemical laboratory
3710D	silver colored disc	B-8, Late Chincha I	Root 1949	4	96	0	0	0.1-1									Bowdoin College chemical laboratory
4931	silver colored bird ornament	T-a, Late Ica II	Root 1949	4	92	4	0	0.01-1									Bowdoin College chemical laboratory
4939	silver colored paddle, bird	T-a, Late Ica II	Root 1949	4	92	4	0	0									Bowdoin College chemical laboratory
5013	silver colored paddle, tacks	T-d, 8, Inca (Ica)	Root 1949	4	93	3	0	0									Bowdoin College chemical laboratory
3750	silver colored ornament fragment	C-5, Late Chincha II	Root 1949	5	92	3	0	0.01-1									Bowdoin College chemical laboratory
5272B	silver colored beaker	T-h, 1, Late Ica I	Root 1949	6	94	0	0	0									Bowdoin College chemical laboratory
5265	silver colored dish	T-h, 1, Late Ica I	Root 1949	7	93	0	0	0									Bowdoin College chemical laboratory
4910	silver colored effigy cup fragment	T-a, Late Ica II	Root 1949	8	92	0	0	0.01-1									Bowdoin College chemical laboratory
4917	silver colored beaker fragment	T-a, Late Ica II	Root 1949	8	92	0	0	0.01-1									Bowdoin College chemical laboratory
4917C	silver colored dish fragment	T-a, Late Ica II	Root 1949	8	92	0	0	0.01-1									Bowdoin College chemical laboratory
5262	silver colored dish	T-h, 1, Late Ica I	Root 1949	8	92	0	0	0									Bowdoin College chemical laboratory
5271A	silver colored beaker	T-h, 1, Late Ica I	Root 1949	8	92	0	0	0									Bowdoin College chemical laboratory
5271C	silver colored effigy cup fragment	T-h, 1, Late Ica I	Root 1949	8	92	0	0	0									Bowdoin College chemical laboratory
3984C	silver colored sheet fragment	E-13, 2, Inca (Chincha)	Root 1949	9	91	0	0	0									Bowdoin College chemical laboratory
3687	silver colored dish	B-5, Late Chincha I	Root 1949	10	89	1	0	0.01-1									Bowdoin College chemical laboratory
3930B	silver colored effigy cup	E-3, Late Chincha I	Root 1949	10	87	3	0	0.1-1									Bowdoin College chemical laboratory
4905A	silver colored effigy cup fragment	T-a, Late Ica II	Root 1949	10	87	3	0	0.01-1									Bowdoin College chemical laboratory
4915	silver colored dish fragment	T-a, Late Ica II	Root 1949	10	90	0	0	0.01-1									Bowdoin College chemical laboratory
5268	silver colored dish	T-h, 1, Late Ica I	Root 1949	10	88	2	0	0									Bowdoin College chemical laboratory
4916	silver colored dish	T-a, Late Ica II	Root 1949	11	89	0	0	0									Bowdoin College chemical laboratory

Artifact ID	Description	Provenance	Reference	Wt. % Cu	Wt. % Ag	Wt. % Au	Wt. % Sn	Wt. % Pb	Wt. % As	Wt. % Fe	Wt. % Si	Wt. % Mg	Wt. % Bi	Wt. % Zn	Wt. % Ni	Wt. % Sb	Composition Analysis Method
5356	silver colored plume holder	T-i, 5, Inca (Ica)	Root 1949	11	89	0	0	0									Bowdoin College chemical laboratory
5357A	silver colored pendant	T-i, 5, Inca (Ica)	Root 1949	11	89	0	0	0.01-1									Bowdoin College chemical laboratory
3627	silver colored armlet (?)	A, Late Chincha II (?)	Root 1949	12	88	0	0	0									Bowdoin College chemical laboratory
3781	silver colored links	C-9, Late Chincha I	Root 1949	12	88	0	0	0									Bowdoin College chemical laboratory
5267	silver colored dish	T-h, 1, Late Ica I	Root 1949	12	87	1	0	0									Bowdoin College chemical laboratory
5412	silver colored discs (2)	T-k, Inca (Ica)	Root 1949	12	88	0	0	0									Bowdoin College chemical laboratory
5112	silver colored disc	T-f, Late Ica I	Root 1949	13	87	0	0	0									Bowdoin College chemical laboratory
4911A	silver colored effigy cup fragment	T-a, Late Ica II	Root 1949	17	83	0	0	0.01-1									Bowdoin College chemical laboratory
3749B	cilver colored tweezer fragment	C-5, Late Chincha II	Root 1949	18	82	0	0	0.01-1									Bowdoin College chemical laboratory
5060A	silver colored pendant fragment	T-d, 8, Inca (Ica)	Root 1949	18	82	0	0	0.01-1									Bowdoin College chemical laboratory
3636	silver colored disc	A, Late Chincha II (?)	Root 1949	20	80	0	0	<10									Bowdoin College chemical laboratory
3920	silver colored earplug	E-3, Late Chincha I	Root 1949	25	75	0	0	0									Bowdoin College chemical laboratory
4092A	silver colored earplug, face	F-4, Late Chincha II	Root 1949	27	73	0	0	0									Bowdoin College chemical laboratory
5272C	silver colored beaker	T-h, 1, Late Ica I	Root 1949	28	72	0	0	0									Bowdoin College chemical laboratory
4852	silver colored cuff	Z-4, Middle Ica II	Root 1949	33	64	3	0	0									Bowdoin College chemical laboratory
4077	silver colored ornament fragment	F-1, Late Chincha II	Root 1949	34	66	0	0	0.01-1									Bowdoin College chemical laboratory
4125	silver colored headband	F-6, Late Chincha II	Root 1949	36	64	0	0.01-1	0.01-1									Bowdoin College chemical laboratory
4089B	silver colored headbands (3)	F-4, Late Chincha II	Root 1949	40	60	0	0	0									Bowdoin College chemical laboratory
3710E	silver colored embossed plate fragment	B-8, Late Chincha I	Root 1949	54	44	2	0	0.1-1									Bowdoin College chemical laboratory
36703A	silver colored plate fragment	B-5, Late Chincha I	Root 1949	56	44	0	0.1-1	0									Bowdoin College chemical laboratory
12233	silver colored sheet with embossed fishes	U.S. National Museum collection	Root 1949	60	40	0	0	0									Bowdoin College chemical laboratory
3689	silver colored tweezers	B-5, Late Chincha I	Root 1949	70	30	0	0	0.01-1									Bowdoin College chemical laboratory
4402C	silver colored disc fragment	M, Middle Ica II	Root 1949	75	25	2	0	0									Bowdoin College chemical laboratory
3776M	copper colored foil fragment	C-7, Late Chincha I	Root 1949	85	15	0	0	0.1-1									Bowdoin College chemical laboratory

Artifact ID	Description	Provenance	Reference	Wt. % Cu	Wt. % Ag	Wt. % Au	Wt. % Sn	Wt. % Pb	Wt. % As	Wt. % Fe	Wt. % Si	Wt. % Mg	Wt. % Bi	Wt. % Zn	Wt. % Ni	Wt. % Sb	Composition Analysis Method
4083A	silver colored earplug	F-3, Late Chincha II	Root 1949	<10	>90	0	0	0									Bowdoin College chemical laboratory
4104	silver colored headband	F-5, Late Chincha II	Root 1949	<10	>80	0	0	<10									Bowdoin College chemical laboratory
4444B	copper colored club head sheathing	M, Middle Ica II	Root 1949	<10	>20	>20	0	0									Bowdoin College chemical laboratory
4930	silver colored plume holder	T-a, Late Ica II	Root 1949	<10	>79	<10	0	0.01-1									Bowdoin College chemical laboratory
4933	silver colored rings (70-80)	T-a, Late Ica II	Root 1949	<10	>79	<10	0	0.01-1									Bowdoin College chemical laboratory
4938	silver colored paddle, sheathing	T-a, Late Ica II	Root 1949	<10	>79	<10	0	0.01-1									Bowdoin College chemical laboratory
4940D	silver colored club head sheathing	T-a, Late Ica II	Root 1949	<10	>88	0.01-1	0	0.01-1									Bowdoin College chemical laboratory
4947	silver colored plume holders (4)	T-a, Late Ica II	Root 1949	<10	>88	0.1-1	0	0.01-1									Bowdoin College chemical laboratory
4952	silver colored tweezers (7)	T-a, Late Ica II	Root 1949	<10	>88	0.01-1	0	0.01-1									Bowdoin College chemical laboratory
4953	silver colored tweezers (2)	T-a, Late Ica II	Root 1949	<10	>88	0.01-1	0	0.01-1									Bowdoin College chemical laboratory
4905	silver colored effigy cup fragment	T-a, Late Ica II	Root 1949	<10	>89	0	0	0.01-1									Bowdoin College chemical laboratory
4913	silver colored dish	T-a, Late Ica II	Root 1949	<10	>89	0	0	0.01-1									Bowdoin College chemical laboratory
4918A	silver colored armlet, fragment (?)	T-a, Late Ica II	Root 1949	<10	>89	0	0	0.01-1									Bowdoin College chemical laboratory
4926	silver colored earplug	T-a, Late Ica II	Root 1949	<10	>89	0	0	0.01-1									Bowdoin College chemical laboratory
4949A	silver colored head band (3)	T-a, Late Ica II	Root 1949	<10	>90	0	0	0									Bowdoin College chemical laboratory
5067	silver colored earplug fragment	T-d, 8, Inca (Ica)	Root 1949	<10	>89	0	0	0.01-1									Bowdoin College chemical laboratory
5112	silver colored tweezers	T-f, Late Ica I	Root 1949	<10	>88	0.01-1	0	0.01-1									Bowdoin College chemical laboratory
5318	silver colored dish	T-g, Late Ica I (?)	Root 1949	<10	>89	0	0	0.01-1									Bowdoin College chemical laboratory
5276	silver colored pendants (39)	T-h, 1, Late Ica I	Root 1949	<10	>89	0	0	0.01-1									Bowdoin College chemical laboratory
5271D	silver colored effigy cup rim	T-h, 1, Late Ica I	Root 1949	<10	>90	0	0	0									Bowdoin College chemical laboratory
4918	silver colored crescent	T-a, Late Ica II	Root 1949	>10	>88	0.01-1	0	0.01-1									Bowdoin College chemical laboratory
3690	silver colored plate fragment	B-5, Late Chincha I	Root 1949	>20	>20	0	0	0.01-1									Bowdoin College chemical laboratory
3709	silver colored dish	B-8, Late Chincha I	Root 1949	>20	>20	0.1-1	0	0.1-1									Bowdoin College chemical laboratory

Artifact ID	Description	Provenance	Reference	Wt. % Cu	Wt. % Ag	Wt. % Au	Wt. % Sn	Wt. % Pb	Wt. % As	Wt. % Fe	Wt. % Si	Wt. % Mg	Wt. % Bi	Wt. % Zn	Wt. % Ni	Wt. % Sb	Composition Analysis Method
3710F	copper colored plate fragment	B-8, Late Chincha I	Root 1949	>20	>20	0	0	0.1-1									Bowdoin College chemical laboratory
3741A	copper colored rings	C-5, Late Chincha II	Root 1949	>20	>20	0	0.01-1	0.01-1									Bowdoin College chemical laboratory
3744	silver colored earplug	C-5, Late Chincha II	Root 1949	>20	>20	0	0	0.01-1									Bowdoin College chemical laboratory
3844A	silver colored earplug	D, Inca (Chincha)	Root 1949	>20	>20	0	0	0.01-1									Bowdoin College chemical laboratory
3974A	silver colored jar	E-13, 2, Inca (Chincha)	Root 1949	>20	>20	0	0	0.01-1									Bowdoin College chemical laboratory
4488	copper colored earplug fragment	E-6, Early Ica	Root 1949	>20	>20	0.01-1	0	0									Bowdoin College chemical laboratory
4079B	copper colored sheet fragment	F-1, Late Chincha II	Root 1949	>20	>20	0.01-1	0	0.01-1									Bowdoin College chemical laboratory
4133	silver colored headband fragment	F-6, Late Chincha II	Root 1949	>20	>20	0	0	0.01-1									Bowdoin College chemical laboratory
4287	silver colored disc fragment	M, Middle Ica II	Root 1949	>20	>20	0.01-1	0	0.01-1									Bowdoin College chemical laboratory
5495A	copper colored mask	S-f, Middle Ica II	Root 1949	>20	>20	0	0.01-1	0.01-1									Bowdoin College chemical laboratory
4909A	silver colored beaker	T-a, Late Ica II	Root 1949	>20	>20	0	0	0.01-1									Bowdoin College chemical laboratory
3733A,B	copper colored earplugs (2)	C-4, Late Chincha II	Root 1949	>89	<10	0	0	0.01-1									Bowdoin College chemical laboratory
4108	silver colored disc	F-5, Late Chincha II	Root 1949	>89	<10	0	0	0.01-1									Bowdoin College chemical laboratory
3987	copper colored knife	E-13, 3, Inca (Chincha)	Root 1949	>90	<10	0	0	0									Bowdoin College chemical laboratory
4444A	copper colored club head	M, Middle Ica II	Root 1949	>90	<10	0	0	0									Bowdoin College chemical laboratory

13 Appendix B

Stern Leach / MIT Ag/Cu Bar Analysis

MIT ID No.	Melt #	Nominal Composition	Analysis Method *1 / Element / Assay Location	Assay # Number	TIAG Ag (%)	Diff Cu (%)	DCP Au (ppm)	DCP Ni (ppm)	DCP Zn (ppm)	DCP Cd (ppm)	DCP Fe (ppm)	DCP Pb (ppm)	DCP Pt (ppm)	DCP Pd (ppm)	DCP Sn (ppm)	DCP Al (ppm)	DCP In (ppm)	DCP Ir (ppm)	DCP Mg (ppm)	DCP Mn (ppm)	DCP Si **2 (ppm)	DCP As (ppm)	DCP Sb (ppm)	Total Impurities (ppm)	Total Composition (%)
5476	Bar 1	30 Cu / 70 Ag	Center Drill	239634	69.9252	30.0666	31	5	6	0	1	4	0	8	15	3	0	0	0	1	8			82	100
5476	Bar 1	30 Cu / 70 Ag	Pin	239460	69.9102	30.0816	32	3	3	1	0	4	0	8	1	3	0	3	0	0	24			82	100
5476	Bar 1	30 Cu / 70 Ag	Surface Drill	239459	69.9095	30.0786	35	0	6	2	2	4	0	8	2	6	0	0	1	0	53			119	100
5476	Bar 1		Average		69.9150	30.0756																		94	
5477	Bar2	60 Cu / 40 Ag	Center Drill	239635	39.9747	60.0141	13	5	0	5	2	11	8	7	14	5	2	13	1	1	25			112	100
5477	Bar2	60 Cu / 40 Ag	Pin	239462	40.0967	59.8891	13	4	0	6	2	9	8	6	13	6	2	12	1	1	59			142	100
5477	Bar2	60 Cu / 40 Ag	Surface Drill	239461	40.4430	59.5481	13	6	2	3	1	7	5	6	13	2	1	8	0	1	21			89	100
5477	Bar 2		Average		40.1715	59.8171																		114	
5478	Bar 3	70 Cu / 30 Ag	Center Drill	239636	30.0389	69.9455	10	14	4	8	4	12	13	7	21	6	2	22	1	2	30			156	100
5478	Bar 3	70 Cu / 30 Ag	Pin	239464	29.9355	70.0571	7	6	2	5	0	5	7	5	11	2	0	12	0	1	11			74	100
5478	Bar 3	70 Cu / 30 Ag	Surface Drill	239463	30.1329	69.8578	13	2	4	5	2	6	7	6	13	3	1	14	0	1	16			93	100
5478	Bar 3		Average		30.0358	69.9535																		108	
5479	Bar 4	80 Cu / 20 Ag	Center Drill	239637	20.1118	79.8839	8	0	0	0	0	8	1	0	3	5	2	0	0	0	16			43	100
5479	Bar 4	80 Cu / 20 Ag	Pin	239466	20.0340	79.9628	0	0	0	0	0	7	1	0	2	4	2	0	0	0	16			32	100
5479	Bar 4	80 Cu / 20 Ag	Surface Drill	239465	20.0976	79.8983	0	0	0	0	0	11	3	0	3	4	3	0	0	0	17			41	100
5479	Bar 4		Average		20.0811	79.9150																		39	
5480	Bar 5	95 Cu / 5 Ag	Center Drill	239638	4.9463	95.0397	6	12	55	8	8	0	17	6	3	3	0	8	1	3	10			140	100
5480	Bar 5	95 Cu / 5 Ag	Pin	239468	4.8975	95.0878	1	12	49	3	5	0	11	4	2	5	0	8	1	3	43			147	100
5480	Bar 5	95 Cu / 5 Ag	Surface Drill	239467	5.0110	94.9831	0	3	37	2	4	0	7	2	0	2	0	0	0	2	0			59	100
5480	Bar 5		Average		4.9516	95.0369																		115	
	Raw	Copper		239472	0.0000	99.9986	0	0	0	0	0	0	1	0	0	3	0	0	0	0	10			14	100
	Raw	Silver		239469	99.9516	0.0351	54	4	7	0	4	5	0	6	12	4	0	0	1	1	31	3	1	133	100

Analysis Method *1 TIAG - Computer Aided, Conductivity Based, End Point Titration
DCP - Direct-Coupled Plasma Spectrometry

**2 Some of the silicon numbers on the pin samples look high. Probably aas a result of glass from the pin tube remaining in the sample

For each of the alloy compositions, TIAG and DCP were performed on both the molten metal prior to casting and on the solidified ingot. To determine the composition of the melt, a glass pipette was inserted into the molten alloy before casting to retrieve a sample for analysis. This assay is referred to as “Pin.” To determine the compositions of the cast ingots, samples were drilled from two different locations on each ingot. The assay referred to as “Surface Drill” was drilled from the solid ingot to a depth that would include any surface enrichment. The assay referred to as “Center Drill” was drilled from the center of the ingot, but at a much greater depth.